Chemistry & Biochemistry Theses & Dissertations   Chemistry & Biochemistry

Fall 2016

Bioenergetics: Experimental Demonstration of Excess Protons and Related Features

Haitham A. Saeed
Old Dominion University

BIOENERGETICS: EXPERIMENTAL DEMONSTRATION OF EXCESS

PROTONS AND RELATED FEATURES

by

Haitham A. Saeed
B.S. August 2007, Alexandria University, Egypt
M.Sc. May 2015, Old Dominion University

A Dissertation Submitted to the Faculty of
Old Dominion University in Partial Fulfillment of the
Requirements for the degree of

DOCTOR OF PHILOSOPHY

CHEMISTRY

OLD DOMINION UNIVERSITY
December 2016

Approved By:

James W. Lee (Director)

Richard V. Gregory (Member)

Thomas Isenhour (Member)

Sandeep Kumar (Member)

ABSTRACT

BIOENERGETICS: EXPERIMENTAL DEMONSTRATION OF EXCESS PROTONS AND RELATED FEATURES

Haitham A. Saeed
Old Dominion University, 2016
Director: Dr. James W. Lee

Over the last 50 years, ever since the Nobel-prize work of Peter Mitchell's Chemiosmotic theory, the question whether bioenergetics energy transduction occurs through localized or delocalized protons has been a controversial issue among scientists. Recently, a proton-electrostatics localization hypothesis was formulated which may provide a new and clear understanding of localized and delocalized proton-coupling energy transduction in many biological systems. The aim of this dissertation was to test this new hypothesis.

To demonstrate the fundamental behavior of localized protons in a pure water-membrane-water system in relation to the newly derived pmf equation, excess protons and excess hydroxyl anions were generated and their distributions were tested using a proton-sensing aluminum membrane. The proton-sensing film placed at the membrane-water interface displayed dramatic localized proton activity while that placed into the bulk water phase showed no excess proton activity during the entire experiment. These observations clearly match with the prediction from the proton-electrostatics localization hypothesis that excess protons do not stay in water bulk phase; they localize at the water-membrane interface in a manner similar to the behavior of excess electrons in a conductor.

In addition, the effect of cations (Na^+ and K^+) on localized excess protons at the water-membrane interface was tested by measuring the exchange equilibrium constant of Na^+ and K^+ in

exchanging with the electrostatically localized protons at a series of cations concentrations. The equilibrium constant K_{PNa+} for sodium (Na$^+$) cations to exchange with the electrostatically localized protons was determined to be $(5.07 \pm 0.46) \times 10^{-8}$ while the equilibrium constant K_{PK+} for potassium (K$^+$) cations to exchange with localized protons was determined to be $(6.93 \pm 0.91) \times 10^{-8}$. These results mean that the localized protons at the water-membrane interface are so stable that it requires a ten millions more sodium (or potassium) cations than protons in the bulk liquid phase to even partially delocalize them at the water-membrane interface. This provides a logical experimental support of the proton electrostatic localization hypothesis.

One of the basic assumptions of proton-electrostatics localization hypothesis is that it treats liquid water as a proton conductor and that the proton conduction along the water-membrane interface might be a favored pathway for the proton energy coupling bioenergetics across biological membranes. In this study, experimental evidences discussing water acting as a proton conductor were discussed and the conductivity of water with respect to excess protons was estimated. Overall, these findings have significance not only in the science of bioenergetics but also in the fundamental understanding for the importance of water to life in serving as a proton conductor for energy transduction in living organisms.

This dissertation is dedicated to my parents, my wife and my little daughter Sarah.

ACKNOWLEDGMENTS

First and foremost, I thank God for equipping me to succeed in this endeavor. All praise and glory is to him. I would like to sincerely express my gratitude to everyone who has contributed to this work.

I would first like to thank my academic and research advisor Dr. James Lee for his mentorship. I am thankful to him for his academic guidance, patience, and encouragement throughout my research. He has spent countless hours reviewing my work and supporting me in my growth as a researcher. Without his dedication and advice, this dissertation wouldn't be possible. Secondly, I would like to thank the department of chemistry and biochemistry at ODU for accepting me in the program and providing me with the teaching assistantship during the past five years. I would also like to thank the other members of my dissertation committee, Dr. Isenhour, Dr. Gregory, and Dr. Kumar for their valuable comments and directions. I am grateful to Dr. Gregory for his advice, for allowing me using his equipments to conduct my experiments, and for making valuable contributions to my education at ODU. I would like also to thank Dr. Cooper for his valuable discussions and for providing me with several insights throughout my dissertation. I am exceptionally thankful to the staff members at department of chemistry and biochemistry. Their help and assistance are greatly appreciated. I would like to thank my friends and colleagues who worked closely with me and supported me when needed. I thank Matthew Huff and Cameron Smith for their help and support during these years.

Finally, I sincerely express my gratitude to my family members. I thank my parents who encouraged me since I was young to the pursuit of knowledge, investing all that they had to provide me with a good standard education. I also thank my sisters, my wife and my daughter for their faith, support and encouragement in all my endeavors, motives and academic pursuits.

TABLE OF CONTENTS

LIST OF TABLES

Table   Page

Table   Page

LIST OF FIGURES

Figure   Page

Figure   Page

CHAPTER 1

INTRODUCTION

1.1 BIOENERGETICS, ATP SYNTHESIS AND PROTON GRADIENT

Bioenergetics is a field in biochemistry and biophysics that is concerned with the study of energy conversion processes that occur within or across the biological membranes such as bacterial membranes, mitochondrial membranes, and thylakoid membranes in the chloroplast of plants (1, 2). Biological membranes play an important role in energy transduction and production of adenosine triphosphate (ATP) which is the main energy currency in any biological cell. Biological membranes have protein structures and components that catalyze the ATP synthesis and transport of ions and metabolites across them. In plants, for example, photosynthesis takes place in small organelles called chloroplasts. Chloroplasts have disc-like structures called thylakoids which consist of lipid bilayer membrane surrounding a liquid phase named the lumen. The thylakoid membrane has protein embedded structures called photosystem I (**PS I**) and photosystem II (**PS II**) -shown in Figure 1- that capture light during photosynthesis to drive the electron transport chain and generate the proton gradient across the membrane that drives the synthesis of ATP in cells (3, 4).

Across the thylakoid membrane, light-dependent reactions of photosynthesis take place as shown in Figure 1. It begins when a photon of light energizes the reaction center of photosystem (II) resulting in a primary charge separation event that vectorially release electrons from the reaction center to electron acceptors along the photosynthetic electron transport chain.

This dissertation was formatted based on *Proceedings of the National Academy of Sciences* journal.

The photochemically oxidized reaction centers are then reduced by the electrons that are acquired through the oxidation of water molecules that produces molecular oxygen and protons at the oxygen evolution complex of photosystem (II). The light energized electrons leaving photosystem (II) is transferred to Plastoquinone (**PQ**). The reduced Plastoquinone passes these electrons to a proton pump protein structure embedded in the thylakoid membrane named cytochrome b_6f complex causing it to pump protons from an external aqueous phase named stroma into the internal liquid lumen. At the same time, when photosystem (I) absorbs a photon of light its reaction center releases energetic electrons to a small protein structure called ferredoxin (**Fd**) that passes it to make NADPH from $NADP^+$ at the NADP reductase. Electrons lost from photosystem (I) are replaced by electrons generated from photosystem (II) as the electron carrier –Plastocyanin (**PC**)- carries the electrons from cytochrome b_6f complex to photosystem (I). During the process of electron transport chain, that takes place along the thylakoid membrane via a cascade of membrane proteins, protons are pumped into the lumen from the stroma. Consequently, a proton gradient is generated across the thylakoid membrane. The proton gradient is generated also from the release of two protons in the lumen for each water molecule which is photosynthetically oxidized at photosystem (II) and from the consumption of protons in the stroma to make NADPH from $NADP^+$ with the NADP reductase (1, 5-8).

The thylakoid membrane is mainly composed of phospholipids and galactolipids structure which are impermeable to ions including protons. Since the lipid bilayer structure of thylakoid membrane is considered as an osmotic barrier for ion diffusion, the protons must pass from high proton concentration in the lumen to low proton concentration in the stroma through specific channels embedded in the membrane called ATP synthase (9, 10). The diffusion force of protons from lumen into stroma due to concentration gradient generates a proton motive force

(pmf) that drive the synthesis of ATP molecule from adenosine diphosphate (ADP) and inorganic phosphate (Pi) in a process called photosynthetic phosphorylation (6, 11, 12). Each ATP molecule requires 3 protons to be synthesized (13). This process is a dynamic process in which ATP is continuously removed for stromal ATP-consuming reactions, while the proton gradient is continuously replenished by the photosynthetic electron-transfer chains. The overall photosynthetic phosphorylation equation (3, 14) for the light dependent reactions in green plants can be represented as:

$$2H_2O + 2NADP^+ + 3ADP + 3P_i + light \rightarrow 2NADPH + 2H^+ + 3ATP + O_2(g) \quad (1.1)$$
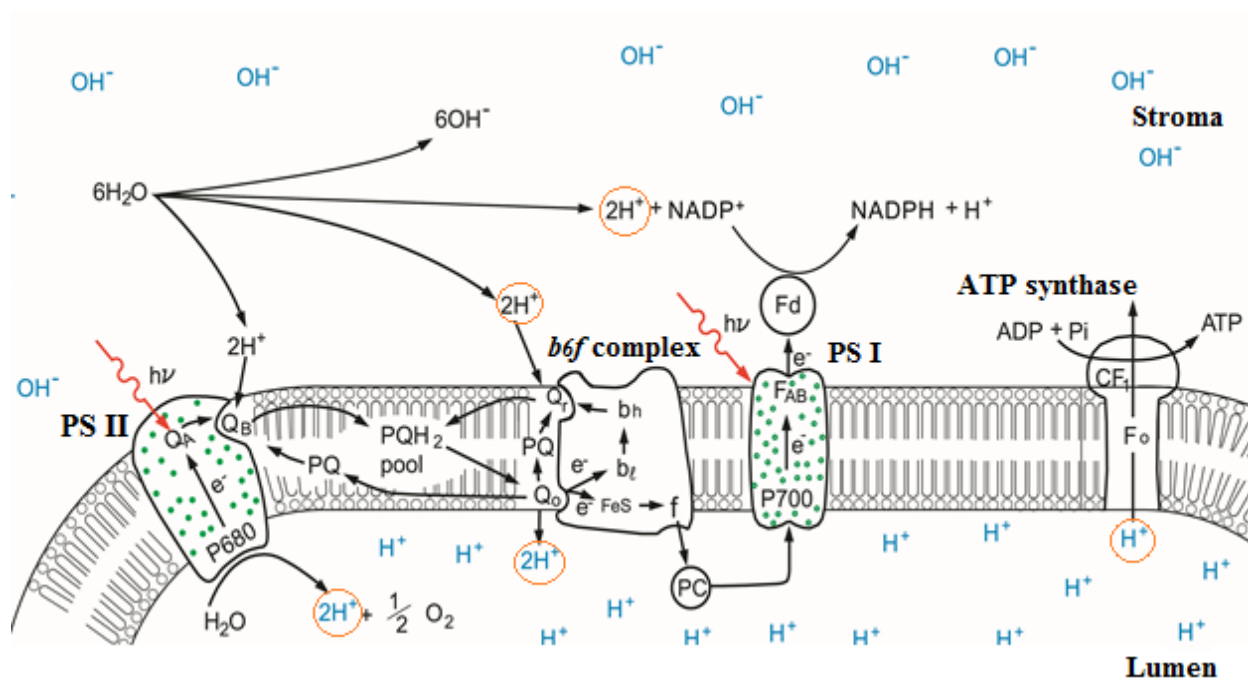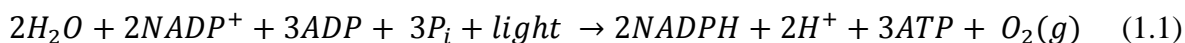
Figure 1. The mechanism of photophosphorylation at the thylakoid membrane showing the electron transport chain and the proton gradient across the photosynthetic membrane that drives the chemiosmotic ATP synthesis (15). (Modified with permissions from Lee 2012)

1.2 BACKGROUND INFORMATION

1.2.1 Peter Mitchell chemiosmotic theory and proton motive force

Back in the 1960s Peter Mitchell introduced the chemiosmotic theory which is a major milestone in the history of bioenergetics (12, 16). He put forward the idea that ATP synthesis is driven by a proton electrochemical gradient between two cellular compartments across the biological membrane. This proton electrochemical gradient ($\Delta\boldsymbol{\mu}_{\boldsymbol{H^+}}$), which is often expressed as proton motive force (pmf), is generated across biological membranes by electron-transport-linked proton translocation. Mitchell developed his famous proton motive force equation which is still being used in many biochemistry text books (1-3, 5, 17-19). It represents a quantitative thermodynamic measurement of the proton gradient across the biological membrane and can be expressed by

$$pmf = -\frac{\Delta\mu_{H^+}}{F} = \Delta\psi - \frac{2.3\,RT}{F} \times \Delta pH \qquad (1.2)$$

Where $\Delta\boldsymbol{\mu}_{\boldsymbol{H^+}}$ is the proton electrochemical gradient that has two components: an electrical component represented by $\Delta\psi$, which is the trans-membrane potential generated due to the difference in electrical potential across the membrane, and a chemical component represented by ΔpH which is the difference of protons concentration between the two bulk aqueous phases separated by the membrane. R is the gas constant, T is the absolute temperature, and F is the Faraday constant. It should be mentioned that the trans-membrane potential is the dominant component in mitochondria while the pH gradient is the dominant component in Thylakoids. In another words, chloroplasts rely more on the chemical potential (proton gradient) to generate the potential energy required for ATP synthesis (13).

In 1978, Peter Mitchell received the Nobel Prize for his chemiosmotic theory and his leading contribution to the field of bioenergetics. However, his conceptual scheme for proton coupling mechanism in the ATP formation has remained a controversial issue among biochemists till this day (15, 20-22).

1.2.2 The problem in Mitchell proton delocalization coupling mechanism

Mitchell's chemiosmotic theory was widely accepted as the best conceptual scheme to explain the formation of ATP in oxidative or photosynthetic phosphorylation. Nevertheless, his chemiosmotic theory couldn't explain many bioenergetics experimental observations due to his "delocalized" mechanism involving proton movements in the bulk aqueous phases (13, 15, 20). Mitchell has suggested that the ATP synthase is coupled to redox proton pumps via bulk phase-to-bulk phase delocalized proton electrochemical potential gradients that is generated across the biological membrane as shown in Figure 2. He assumed the membrane acts as an insulator between the two bulk phases that plays no role in the lateral transduction of the protons to the ATP synthase (15).

The most clear-cut observations that Mitchellian "delocalized" mechanism cannot explain are in alkalophilic bacteria (23-25) such as *Bacillus pseuodofirmus*. *B. pseuodofirmus* is a soil bacterium living in high alkaline environment and is intended to protect plant roots from nematode infestation. These bacteria keep their internal pH about 2.3 pH units more acidic than the ambient one, while $\Delta\psi$ is about 180 mV. The application of equation (1.2) with the experimentally measured membrane potential and pH values yields a pmf around 50 mV that is too small to drive the synthesis of ATP (23-34). Thus, it has remained an enigmatic problem for decades as how alkalophilic bacteria and similar organisms can carry out phosphorylation process with such low pmf value to synthesize ATP molecules (24, 29, 34).

Another piece of evidence was reported by Michel et al that the proton motive force was too small to account for the synthesis of ATP in the cells of *H. salinarium* (13, 35, 36). They concluded that "pumped protons can be used for ATP synthesis before they equilibrate with the protons in the extracellular bulk phase" (35). This contradicts with the basic premise of chemiosmotic theory and Mitchell's delocalization view. Moreover, Heberle et al. (37) reported that upon pumping of protons by the proton pumps across the membrane, protons diffuse along the membrane surface faster and more efficiently than proton exchange with bulk aqueous phase. In other words, protons might translocate from their source to the ATP synthase along the surface of the membrane without being equilibrated with the bulk aqueous phase. Their results showed that proton diffusion in the bulk phase has been significantly retarded by about eight-fold relative to proton translocation along the membrane surface. However, the physical basis for the retardation is not yet understood.

Dilley and Ort (20) observed some experimental observations that contradict with the classical chemiosmotic theory. They observed that photophosphorylation in chloroplasts happens even in the presence of permeable buffers that abolish the proton gradient between the two bulk aqueous phases across the thylakoid membrane. Also Boyer group observed that photophosphorylation begins before protons diffusion and before equilibration with the bulk phase take place (38).
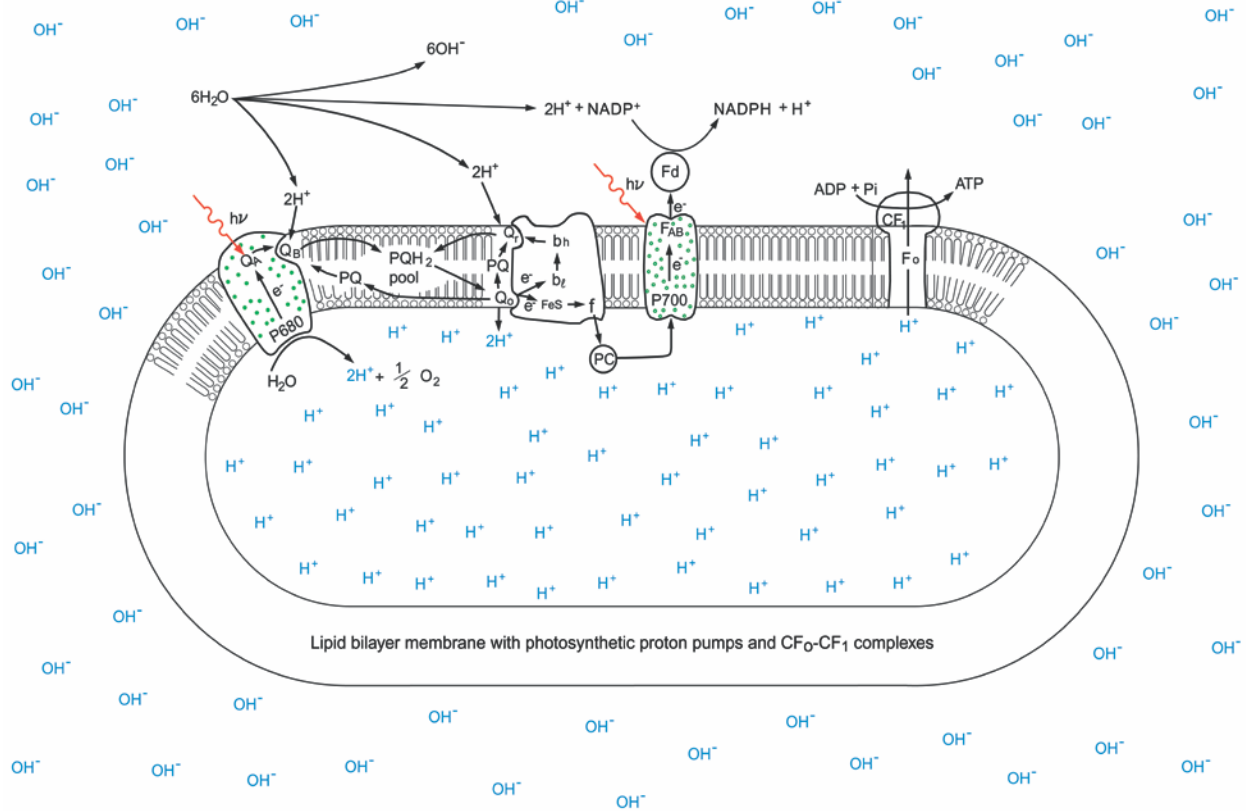
Figure 2. Description of the chemiosmotic theory that was proposed by Peter Mitchell showing delocalized proton (H$^+$) distribution and coupling (15). (Adapted with permissions from Lee, 2012)

1.2.3 Previous hypotheses for proton transfer pathway

There have been many hypotheses trying to explain the aforementioned long-standing bioenergetic conundrum. Williams (39-41) was the first one who thought that the pumped protons prefer a localized pathway through the membrane rather than being delocalized within the two bulk aqueous phases on each side of the membrane. He proposed proton sub-compartments that hinder protons from reaching the bulk aqueous phases (41). Kell has considered the probability that the ejected protons are spread on the surface of the membrane but are somehow prevented from prompt equilibration with the bulk aqueous phase, so that membrane surface pH might differ from the bulk phase pH at steady state (42, 43). He attributed the reason to the presence of Helmholtz layer that forms a kinetic (or thermodynamic) diffusion barrier which insulates the protons streaming on the membrane-water interface from diffusing into the bulk aqueous phase. Dilley proposed a protein structure with obstructed domains along the thylakoid membrane through which protons can diffuse laterally along the membrane surface from the source to the sink (ATP synthase) without entering into the aqueous bulk (44). However, after the advancement of electron microscopy, these occluded protein domains have never been found.

Recently, Cherepanov et al. proposed an interfacial proton barrier (45, 46). They suggested that there is an interfacial potential barrier that separates the membrane surface from the bulk aqueous phase. This barrier is formed as a result of water polarization at the negatively charged phospholipids of the membrane surface owing to the low dielectric permittivity (ε) of water. They argued that this potential barrier restricts the diffusion of protons from entering the bulk phase. Their model predicted a potential barrier of about 0.12 eV for the protons which located 0.5-1 nm away from the membrane surface (28, 47-49). This proposed interfacial

potential barrier might be true for pure water systems that lack the presence of other ions. However, this might not be satisfactory for explaining the complex energy transduction process that occurs in biological systems which has other non-protonic cations. Applying the potential barrier concept on biological systems will not only restrict protons but also restrict other ions (charged molecules) from reaching the bulk aqueous phase. In addition, based on their model one would expect a localized proton-coupling would take place whether the trans-membrane potential difference ($\Delta\psi$) is involved or not. In fact, Davenport-MaCarty et al (50) demonstrated that by eliminating the membrane potential $\Delta\psi$ (thylakoids in presence of valinomycin and 50 mM KCl), the imidazole permeable buffer resulted in a delay in the onset of photosynthetic phosphorylation indicating delocalized proton coupling. Moreover, their described interfacial proton barrier model might have a futile proton escape as fast as a microsecond/millisecond as reported by the authors (49). It is known that oxidative or photosynthetic phosphorylation is a recurring process that takes hours to synthesize sufficient amounts of ATP and other biomolecules for cell growth. Therefore, if protons escape through the barrier to the periplasmic bulk aqueous phase, it would be hard to explain the observed growth of alkalophilic bacteria.

Brändén et al proposed that the hydrophilic phospholipid head groups could act as a proton-collecting antenna that accelerate the proton uptake from the bulk water phase to the membrane surface which act as a proton acceptor (21, 51). The proposed proton-collecting antenna could be true in attracting protons and other cations to its surface forming electric double layer along the membrane negatively charged surface as expected by the Debye-Hückel theory (52). However, this double layer always exists at all time during light and dark conditions even when the proton motive force (pmf) is zero. This means that the protons and/or cations attracted to the membrane surface forming the double layer couldn't contribute to the proton motive force

that drives the flow of protons across the membrane for two reasons: first, the protons forming the double layer are not dynamic. Second, there would be no need for light (photosynthetic) and/or chemical (respiratory) energy to create excess protons and establish the proton gradient across the membrane as it would violate the fundamental principles of thermodynamics by driving work without requiring external energy (53).

There have been some simulation modeling efforts using ab initio and classical molecular dynamics simulations for water with solvated H_3O^+ and OH^- ions (54, 55). These models predicted that the surface of pure water has lower pH (pH<4.8) than its bulk phase. They attributed the reason due to stabilization of protons at the surface (56, 57). However, to our knowledge experimental demonstration of the distribution excess protons in pure water-membrane system hasn't been studied.

1.2.4 Water at membrane interface

In an effort to investigate the physical properties of water adjacent to solid surfaces, Pollack reported a new phase of water that he considered it a fourth phase of water and he named it "the exclusion zone" (58). The exclusion zone is a large zone of water 10 to 100 μm wide that forms adjacent to hydrophilic surfaces such as Nafion which has Teflon like backbone that contains negatively charged sulfonic acids groups. It was named Exclusion Zone (EZ zone) because it excludes practically anything suspended or dissolved in water like suspended microsphere in pure water or red blood cells in blood vessels (58, 59). The EZ has more ordered hexagonal structured water molecules and contains lots of negative charges due to high oxygen to hydrogen ratio which is 2:3. Consequently, it exhibits different properties than that of the bulk water. Pollack reported experimental data that even conflict with the concept of electric double layer. In

his experiments, suspended microsphere particles were observed distancing themselves away from the hydrophilic surface by 100,000 times the Debye length (Debye length $= 10^{-9}$ meter). He found that hydrophilic surfaces impact the nearby water in a way that makes it different in properties from bulk water. For example, the water adjacent to hydrophilic surfaces (EZ water) was more viscous, more stable, and more structurally ordered than bulk water. Its IR spectra and UV-visible light absorption spectra were higher than the bulk water. It has a higher refractive index than bulk water. Overall, Pollack has reported results showing that EZ water hardly resembles liquid water at all (60, 61).

Gilbert Ling proposed that water adjacent to hydrophilic membrane would have a stacked dipole arrangement of water ordering. This arrangement begins at the surface where water dipoles would stack one upon another to a certain distance away from the surface until ordered growth is limited by disruptive forces of thermally induced motion (62). Lippincott et al had proposed a hexagonal structure for the water adjacent to the surface. They stated that the substance is built of oxygen and hydrogen in a hexagonal lattice arrangement. This substance resembles water but its properties are not like water. Water to this substance is like ethylene gas to poly-ethylene polymer. They found that the ratio of hydrogen atoms to oxygen atoms in this hexagonal structure is 3:2 unlike bulk water which is 2:1 ratio (63).

Researchers reported that water adjacent to many diverse surfaces including quartz, proteins subunits and metals has a hexagonal arrangement of atoms (64-67). They confirmed the hexagonal structure using a scanning electron microscope, a transmission electron microscope, and UV absorption spectra. The EZ water absorbs at 270 nm (UV region) which is expected when electrons are delocalized as in the case of the hexagonal benzene ring (58, 59, 68-70).

What's interesting is that it was found that water adjacent to certain polymers and metals had a positively charged Exclusion Zone (61).

1.2.5 Revised proton motive force equation (Proton-electrostatics localization hypothesis)

It is important to be skeptical about hypotheses in sciences, because it helps moving the field forward and encourages others to develop critical tests to investigate and sometimes alter the conventional generally accepted schemes.

J. W. Lee recently published a new hypothesis named proton-electrostatics localization hypothesis (15). This hypothesis provides a possibly unified explanation of the proton localization and/or delocalization in all bioenergetics systems within bacteria, mitochondria and thylakoid structure in the chloroplast of plants without requiring any proton sub-compartments or interfacial proton barrier. The proton-electrostatics localization hypothesis is based on two assumptions: The first assumption is that excess protons in aqueous phase can quickly transfer among water molecules throughout the hydrogen bond network by "hops and turns" mechanism which was first outlined by Grotthuss two centuries ago (71, 72). The second assumption is that liquid water can be considered as a proton conductor. Since the excess protons mobility in water is very fast, excess protons in liquid water can be treated like the excess electric charges in a metallic conductor where Gauss law can be applied on them. According to Gauss law, for electrostatic charge distribution in a general conductor, excess electric charge in a conductor at equilibrium will reside on the surface of the conductor body and not in the bulk. This is expected because the freely moving excess electrons repel one another and arrange themselves on the surface to suffer the minimum possible repulsion. Similarly, applying Gauss law on excess protonic charge in the aqueous proton conductor will lead to electrostatic localization of excess

protons on the water surface along the water-lumenal interface of the thylakoid membrane as shown in the Figure 3.

According to the proton-electrostatics localization hypothesis (15, 22), Mitchell's proton motive force equation (Equation 1.2) should be revised by adding a new term in the equation accounting for the effective concentration of the localized protons at the membrane-water interface $[H^+]^L_{eff}$ as follows:

$$pmf\ (\Delta p) = \Delta\psi + \frac{2.3\ RT}{F}\ \left(pH_{nB} + Log\big([H^+]^L_{eff} + [H^+]_{pB}\big)\right) \qquad (1.3)$$

Where $\Delta\psi$ is the transmembrane electrical potential difference; pH_{nB} is the stroma bulk phase pH; $[H^+]^L_{eff}$ is the effective concentration of the localized protons at the membrane-water interface; $[H^+]_{pB}$ is the proton concentration in the lumen bulk aqueous phase inside the thylakoid structure; F is the Faraday constant; R the gas constant; and T the temperature.
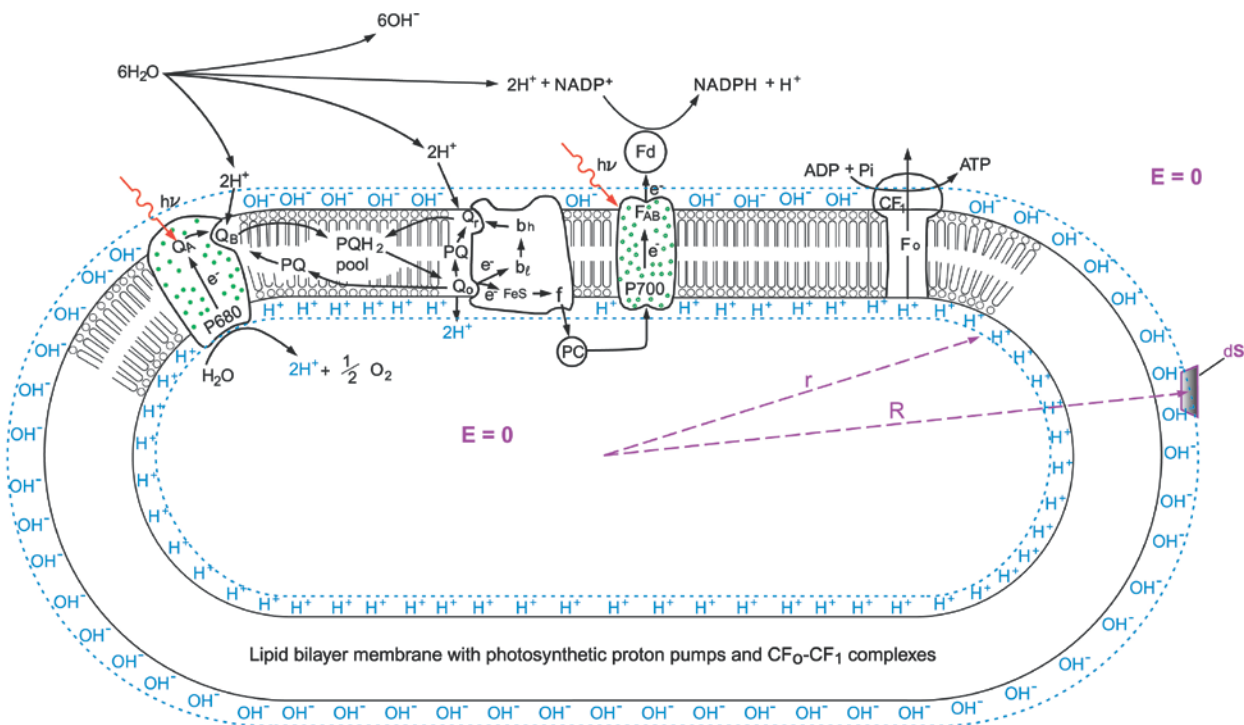
Figure 3. Proton-electrostatics model illustrating the electrostatic localization of excess protons (H$^+$) and hydroxyl ions (OH$^-$) ions at the water-membrane interface along the two sides of the thylakoid membrane in a theoretically pure water-membrane system forming a proton capacitor (15). (Adapted with permissions from Lee 2012)

As mentioned previously, according to the proton-electrostatics localization hypothesis (15, 22), when excess protons are created in the lumen due to the photosynthetic proton pump from the stroma into the lumen, the excess protons in the lumen will not stay in the bulk water phase because of their mutual repulsion. However, they distribute themselves to the water-membrane interface at the lumenal side of the membrane where they attract electrostatically the excess hydroxyl anions at the stromal side of the membrane, forming an "excess protons-membrane-excess anions" capacitor-like system as shown in Figure 3. Therefore, a proton capacitor concept can be used to determine the effective localized proton concentrations $[H_L^+]^0$ at the membrane-water interface. By assuming a pure water-membrane-water system and a

reasonable thickness (l) for the localized proton layer, the effective localized proton concentrations in absence of other cations $[H_L^+]^0$ can be calculated using the following equation:

$$[H_L^+]^0 = \frac{C}{S} \cdot \frac{\Delta\psi}{l \cdot F} = \frac{\Delta\psi \cdot \kappa \cdot \varepsilon_o}{d \cdot l \cdot F} \qquad (1.4)$$

Where C/S is the membrane capacitance per unit surface area; $\Delta\psi$ is the electrical potential difference across the membrane; F is the Faraday constant; κ is the dielectric constant of the membrane; ε_o is the dielectric permittivity; d is the thickness of the membrane; and l is the thickness of the localized proton layer.

In a pure water membrane system, the effective localized proton concentrations $[H_L^+]^0$ can be calculated using equation (1.4). However, multiple non-proton cations in the bulk aqueous phase could exchange and compete with the protons at the localized proton layer as shown in Figure 4. Therefore, Lee[22] further pointed out that the effective concentration of the electrostatically localized protons at equilibrium with non-proton cations $[H^+]_{eff}^L$ can be expressed as:

$$[H^+]_{eff}^L = \frac{[H_L^+]^0}{\prod_{i=1}^{n} \left(K_{Pi} \left(\frac{[M_{pB}^{i+}]}{[H_{pB}^+]} \right) + 1 \right)} \qquad (1.5)$$

Where, $[H_L^+]^0$ is the effective concentration of localized protons without cation exchange, as expressed in equation (1.4); the K_{Pi} is the equilibrium constant for non-proton cations (M^{i+}) to exchange with the localized protons at the water-membrane interface; $[M_{pB}^{i+}]$ is the concentration of the non-proton cations in the liquid culture medium; and $[H_{pB}^+]$ is the concentration of protons in the bulk phase of the liquid culture medium. Since protons can transfer so quickly among

water molecules (72), their conduction is much faster than that of any other cations. In addition, being so small in size, protons may be distributed electrostatically at the water-membrane interface faster than any other large cations such as Mg^{++}, K^+, or Na^+. Therefore, it is expected that the equilibrium constant K_{Pi} for non-proton cations such as Na^+ or K^+ to delocalize the localized protons from the membrane-water interface should be far much less than one.
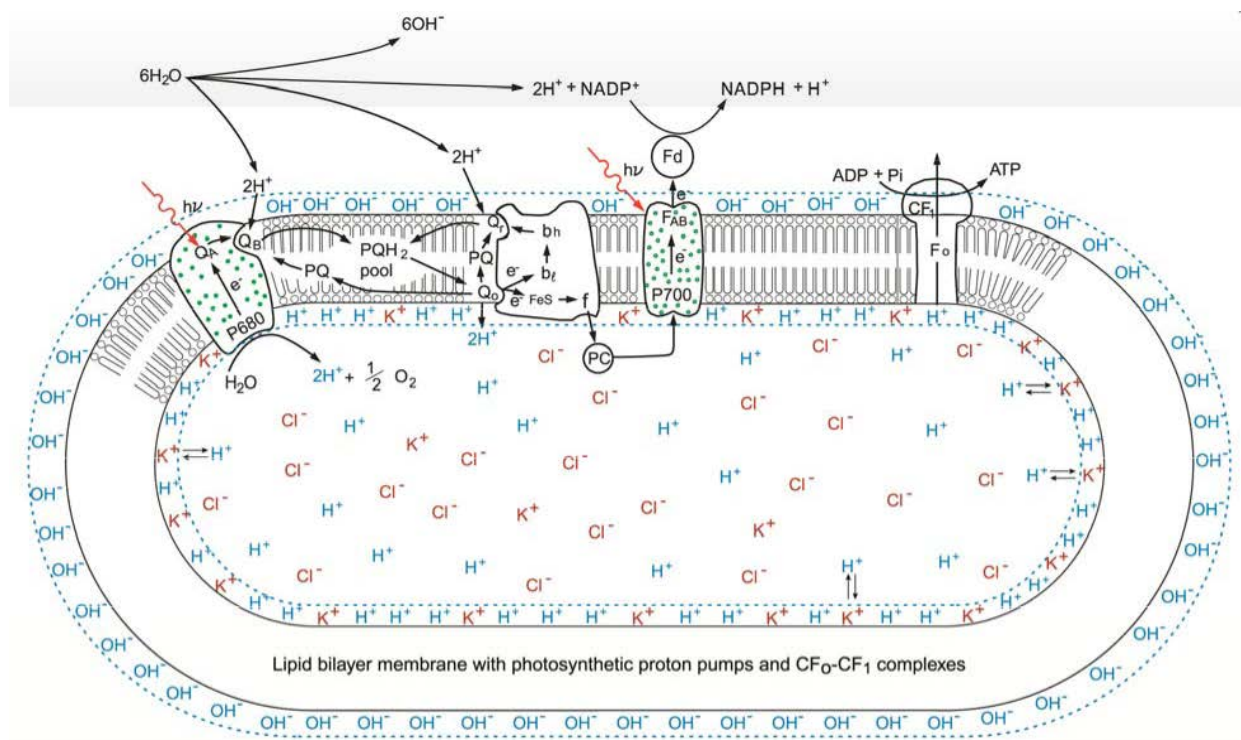
Figure 4. Proton-electrostatics model elucidating the effect of high salt treatment: High concentration of K^+ cations could partially delocalize via cation exchange the electrostatically localized protons at the water-membrane interface of the thylakoid membrane (15). (Copied with permissions from Lee 2012)

Consequently, according to the proton-electrostatics localization hypothesis (15, 22), Mitchell's pmf equation (1.2) should now be modified to account for the effective localized

proton concentrations at the membrane-water interface and that is by substituting equation (1.4) in equation (1.5) then substituting equation (1.5) in equation (1.3). The revised new pmf equation(22) has now been written as:

$$\text{pmf}\ (\Delta p) = \Delta\psi + \frac{2.3\ \text{RT}}{\text{F}}\left(pH_{nB} + \log_{10}\left(\frac{C}{S} \cdot \frac{\Delta\psi}{l \cdot F\left(\prod_{i=1}^{n}(K_{Pi}\left(\frac{[M_{pB}^{i+}]}{[H_{pB}^{+}]}\right) + 1)\right)} + [H_{pB}^{+}]\right)\right) \tag{1.6}$$

Where $\Delta\psi$ is the electrical potential difference across the membrane; pH_{nB} is pH of the stromal bulk phase; $[H^{+}_{pB}]$ is the proton concentration in the lumenal bulk aqueous phase; C/S is the specific membrane capacitance; l is the thickness for localized proton layer; K_{Pi} is the equilibrium constant for non-proton cations (M^{i+}_{pB}) to exchange for localized protons; and $[M^{i+}_{pB}]$ is the concentration of non-proton cations in liquid culture medium.

The modified pmf equation (1.6) agrees perfectly with the Mitchellian pmf equation (1.2) when the membrane potential $\Delta\psi$ is zero. This means that Mitchell's chemiosmotic theory is not entirely wrong and is still a significant milestone in the history of bioenergetics (22). However, Mitchell's pmf equation (1.2) underestimates the true transmembrane proton motive force (pmf) which is due to the delocalization view of excess protons that was postulated by Mitchell in his theory. Furthermore, Mitchell's chemiosmotic theory does not clearly explain what really define or contribute to the membrane potential $\Delta\psi$. On the other hand, according to Lee's equations (1.4) and (1.5) as shown above, it is now quite clear that there is a close relationship between the localized excess proton concentrations $[H_{L}^{+}]^{0}$ and the membrane potential $\Delta\psi$: it is the localized excess protons, the thickness for localized proton layer and the membrane capacitance that define

the membrane potential $\Delta\psi$. Therefore, the proton-electrostatics localization hypothesis can be considered as a significant development over the chemiosmotic theory.

1.2.6 Proton-electrostatics localization predictions (Bioenergetics explanation using Lee's hypothesis)

The implications from the proton-electrostatics localization hypothesis may have significance to the fundamentals of bioenergetics. For example, the new pmf equation (Equation 1.6) could now help solve the enigmatic problems in the bioenergetics of alkalophilic bacteria which is shown in Figure 5. Its application (22) has recently yielded an overall pmf (Δp) value (215~233 mV) that is nearly 4 times more than that (50 mV) calculated from the Mitchellian equation (equation 1.2) for the alkalophilic bacteria growing at pH 10.5. This pmf value (215~233 mV) is sufficient to drive the synthesis of ATP in alkalophilic bacteria and hence elucidates the 30-year-longstanding bioenergetics conundrum in alkalophilic bacteria as how they are able to synthesize ATP (22).
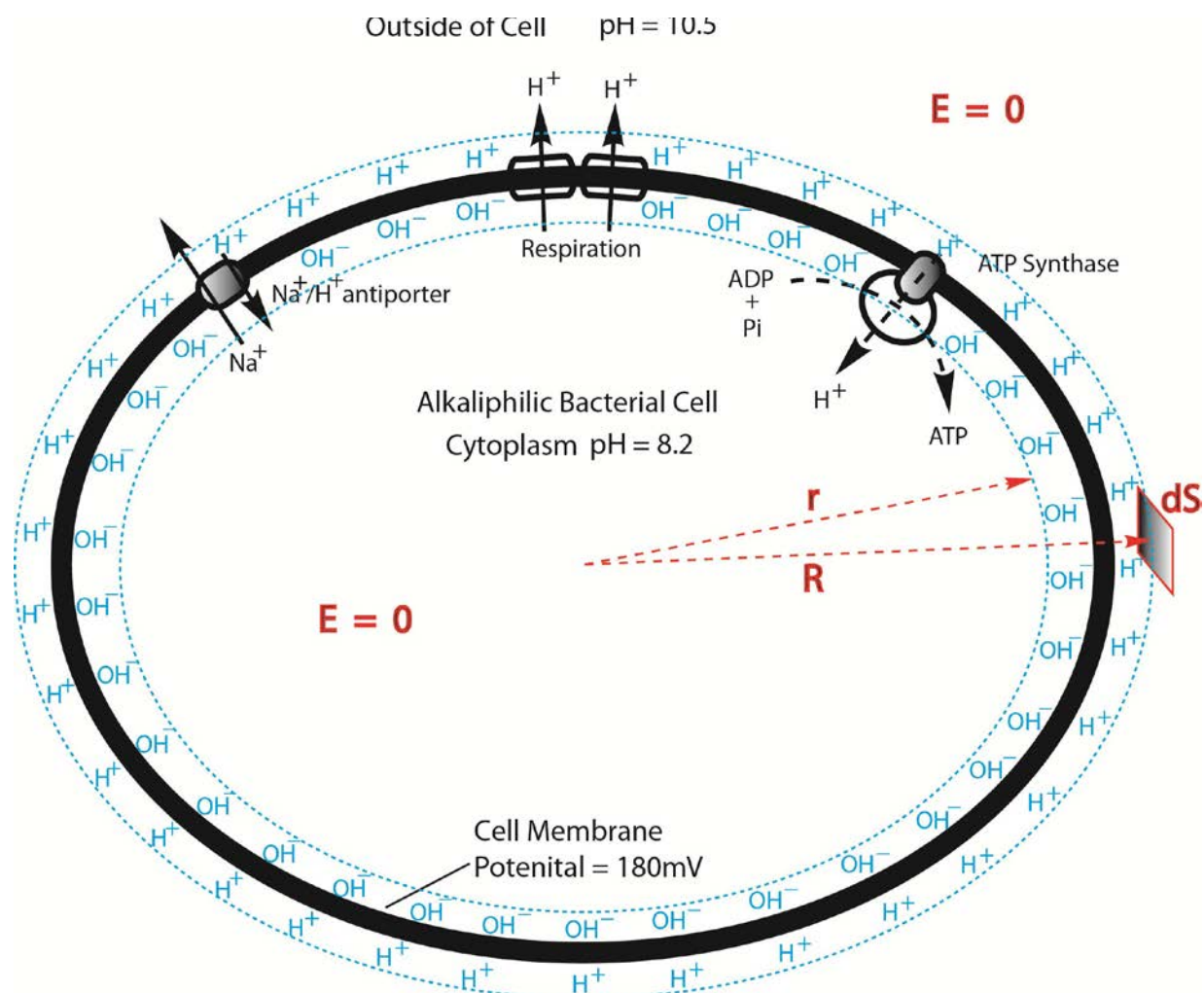
Figure 5. Proton-electrostatics model for Alkaliphilic bacterial cell showing the electrostatic localization of excess protons (H^+) and hydroxyl ions (OH^-) at the water-membrane interface along the two sides of the bacterial cell membrane in a theoretically pure water-membrane-water system (22). (Copied with permissions from Lee, 2015)

The proton-electrostatics localization hypothesis also predicts that high concentration of other cations (in form of salt with high ionic strength) could partially delocalize via cation exchange the electrostatically localized protons at the water-membrane interface (15). This is because the cation (K^+) from the added salt could replace some of the protons along the water-membrane interface as illustrated in Figure 4. As a result, some of the protons could stay in the

bulky water phase in the lumen. The hypothesis predicts that the cation exchange equilibrium constant for other cations to delocalize the localized excess protons from the water-membrane interface would be far less than one. In addition, introducing high salt concentration (such as 100 mM KCl) could enhance the movement of some ions including, but not limited to, Cl^- and K^+ across the thylakoid membrane. This ion migration would neutralize the electrostatic protons charges and thus cause proton delocalization. The hypothesis further explains Dilley's experimental observation (73) that the illumination time required for the onset of ATP synthesis is longer for thylakoids in the presence of high salt concentration (KCl salt solution) than that with low salt concentration. This is because at high salt concentration, K^+ cations could exchange with some of the localized protons resulting partial proton delocalization (15).

1.2.7 Comparison of electrochemical and protochemical circuits

Nicholls presented a good simple analogy for the protochemical cells and the proton motive force which he named it "a proton circuit" (1, 74). He mentioned that there is an analogy between the electrical circuits and the proton circuits (Figure 6). Both can be used to provide power (lighting the bulb in electric circuit is equivalent to making ATP in proton circuit). Both have an applied voltage (potential difference (V) of power source in electric circuit is equivalent to pmf in proton circuit), both have current (electric current (I) is equivalent to proton flux), and both can have a conductance which is reciprocal of resistance (electrical conductance through electrical wires is equivalent to proton conductance in aqueous phase). Both can produce useful work (illuminating the light bulb in electrical circuit and ATP synthesis in proton circuit). Both can be short circuited where short circuit in electrical circuit is equivalent to proton leak in proton circuit. Accordingly, for a closed functional circuit, insulation is needed in electrical circuit. Similarly, the lipid bilayer membrane in the proton circuit can be considered as an

insulator of high resistance between positive and negative charges to prevent short circuit of protons (proton leak). Overall, the laws govern the energy flow around both circuits are similar.
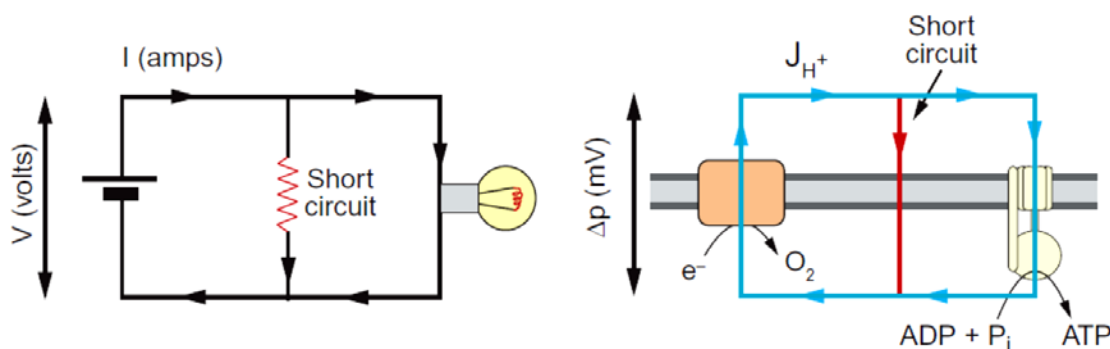
Figure 6. Comparison of electric circuit and proton circuit. Proton circuits (on right) is analogous to electric circuit (on left) in terms of voltage (pmf is equivalent to potential), current (proton flux is equivalent to electric current (I)), and conductance (proton conductance in water is equivalent to electrical conductance in metallic wire). (Copied with permissions from Nicholls et al, *Bioenergetics*. 2013)

1.3 DISSERTATION HYPOTHESES

a) In this dissertation the proton-electrostatics localization hypothesis will be tested in relation to the revised pmf equation (Equation 1.6) and the fundamental knowledge of proton energy coupling over Mitchell's classic Chemiosmotic theory described above. The proton-electrostatics localization hypothesis (15) predicts that excess protons do not stay in water bulk phase; they localize at the water-membrane interface in a manner similar to the behavior of excess electrons in a conductor.

b) The proton-electrostatics localization model would predict that the addition of a higher ionic strength (such as 100 mM Potassium salt solution) may partially delocalize protons from the water-membrane interface via cation exchange with protons as shown in Figure 4. This would result that some protons could stay in the bulky water phase in the thylakoid lumen. Since protons can transfer so quickly among water molecules via Grotthuss mechanism (72), their conduction is much faster than that of any other cations. In addition, being so small in size protons as part of water molecules may be distributed electrostatically at the water-membrane interface faster than any other large cations such as K^+, or Na^+. Therefore, it is expected that the equilibrium constant K_{Pi} for non-proton cations such as Na^+ to delocalize the localized protons from the membrane-water interface should be far much less than one.

c) **Water is a proton conductor**. Excess proton in water usually forms a weak chemical bond with an adjacent water molecule to make a hydronium ion (H_3O^+). The transfer of proton across water molecule is much faster compared to other cations. There have been many efforts describing the mechanism of proton kinetics in water (75-78). In fact protons may move by mechanisms not available to other cations such as sodium ion and potassium ion. It has been simulated via computer simulations (Ab intio) that excess protons mobility is five to seven times higher than that of similarly sized cations. The reason of the high mobility of excess protons is attributed to a chemical transfer mechanism rather than hydrodynamic diffusion. Excess protons shuttle quickly through the water molecules via hops and turns mechanism that involve an exchange of hydrogen and covalent bonds. This structural diffusion process of excess protons among water molecules is known as Grötthus mechanism. Zundel et al (79) have described that the

excess proton tunnels so quickly between two water molecules through the hydrogen bond forming a complex named Zundel cation ($H_5O_2^+$). However, Eigen considered that hydrated excess proton is coordinated to three water molecules forming a complex named Eigen cation ($H_9O_4^+$). It was found that there is a rapid inter-conversion between the Zundel ($H_5O_2^+$) and the Eigen cations ($H_9O_4^+$) in solutions (80, 81).

1.4 GOALS AND OBJECTIVES OF STUDY

The primary goal of this thesis study is to test the proton-electrostatics localization hypothesis in relation to the revised pmf equation (Equation 1.6) and the fundamental knowledge of proton energy coupling over Mitchell's classic Chemiosmotic theory described above. The following are the specific goals and objectives of the thesis study:

Goal 1: Experimental demonstration of localized excess protons at a water-membrane interface

As discussed above that proton motive force and proton movements in cells is analogous to electric current in electric circuits. So, the first goal of this dissertation is to create excess protons in pure water via electrolysis process then track their distribution pattern within the bulk aqueous phase and on the water surface. According to the proton electrostatic effect, the excess protons should be distributed along the outer surface of the water body. Also when two aqueous phases are separated by a membrane, the excess protons are expected to distribute themselves at the water-membrane interface at the P side. Therefore, by tracking the distribution of the excess protons, we should be able to test the proton-electrostatics localization hypothesis. With the assumption that excess protons are localized on the surface and not equilibrated with the bulk aqueous phase, the conventional pH potentiometric electrode measurements will not be capable

of detecting the surface protons. Consequently, the best way to detect and track the distribution of excess protons would be by using a solid state proton indicator. The work of Chapter 2 in this dissertation has for the first time experimentally demonstrated the localized excess protons at a water-membrane interface with a pure water-membrane-water system in relation to equation (1.6) to test the proton-electrostatics localization hypothesis.

Goal 2: Testing the effect of cations (Na^+ and K^+) on localized excess protons at a water-membrane interface

The proton-electrostatics localization hypothesis further predicts that high concentration of other cations (in form of salt solutions with high ionic strength) could partially delocalize via cation exchange the electrostatically localized protons at the water-membrane interface (15). Our goal is to test the effect of cations (Na^+ and K^+) on localized excess protons at the water-membrane interface by measuring the exchange equilibrium constant of Na^+ and K^+ cations in exchanging with the electrostatically localized protons with a series of cation concentrations. Determination of the cation exchange equilibrium constant is another significant way to test and validate the proton-electrostatics localization hypothesis. The work presented in Chapter 3 details the effect of cations (Na^+ and K^+) on localized excess protons at the water-membrane interface.

Goal 3: Measuring the conductivity of water with respect to excess protons

It is well known that pure water (free of any dissolved ionic salt) is nonconductive with respect to electrons. How about the proton conduction in pure (deionized) water with respect to excess protons? Is it conductive to protons? And if it is, how could the proton conductivity be measured knowing that neither the conventional conductivity probe nor the pH meter could detect the excess protons? Chapter 4 of this dissertation will experimentally answer these questions by

innovatively measuring proton conduction through a water column. In addition, certain related evidences from literature will be also discussed. In brief, measurement of the proton conduction was done by joining two separate chambers containing ultrapure water by a water column contained in a silicon tube with series of different lengths. This silicon tube that was filled with a continuous column of water constituted the water proton-conduction wire. The experiment was performed under Direct Current (DC) by sweeping voltage starting with low non water-electrolyzing potential and ending with high water-electrolyzing potential. By this setup, we were able to measure the proton conductivity of water with respect to excess protons. The experimental current and resistance were measured, compared to the theoretical value and the DC proton conductivity was determined.

CHAPTER 2

EXPERIMENTAL DEMONSTRATION OF LOCALIZED EXCESS

PROTONS AT A WATER-MEMBRANE INTERFACE

Preface

The contents of this chapter were published in 2015 in Bioenergetics journal and are reformatted

to fit this thesis. Below is the full citation.

Saeed HA, Lee JW (2015) Experimental Demonstration of Localized Excess Protons at a Water-

Membrane Interface. Bioenergetics 4: 127. doi:10.4172/2167-7662.1000127

2.1 INTRODUCTION

Peter Mitchell's work on his chemiosmotic theory (16, 82, 83) won the 1978 Nobel prize in

chemistry and his bioenergetics (proton motive force) equation since then was introduced in

many textbooks (3, 5, 84). One of the forms of the Mitchellian bioenergetics equation is

expressed as free energy difference $\Delta\tilde{\mu}H^+$ (also known as the Gibbs energy change (ΔG)) for

protons across a biological membrane including a term for the concentration difference and a

term for the electrical potential:

$$\Delta\tilde{\mu}H^+ = \Delta G = RT\ln\frac{[C_2]}{[C_1]} + ZF\Delta\psi \qquad (2.1)$$

Where C_1 and C_2 are the proton concentrations on the two sides of the membrane, Z is the charge

on a proton (1 for a proton), F is the Faraday's constant, $\Delta\psi$ is the electrical potential difference

across the membrane, R is the gas constant, and T is the absolute temperature.

This Mitchellian equation (2.1), sometimes, is written also as the equation for the proton motive force (pmf) Δp that drives the protons through the ATP synthase:

$$\text{pmf}\,(\Delta p) = -\Delta\tilde{\mu}_H{}^+ / F = \Delta\psi - 2.3RT/F \times \Delta pH \qquad\qquad (2.2)$$

Where ΔpH is the pH difference between the two bulk aqueous phases separated by the membrane.

From equation (2.1), one can clearly see that Mitchell treated the protons as solutes such as sugar molecules that are delocalized and can stay everywhere in the bulk aqueous phase. Consequently, the Mitchellian delocalized proton-coupling view is that the ATP synthase is coupled to the redox proton pumps via bulk phase-to-bulk phase proton electrochemical potential gradients generated across the biological membrane; while the membrane is regarded as an insulator between the two bulk phases that plays no role in the lateral transduction of the protons to the ATP synthase.

The chemiosmotic theory was a major milestone in the history of bioenergetics when the early bioenergeticists including the "metabolic enzymologists" were still using substrate-level phosphorylation as a model to seek some kind of "chemical coupling" for "phosphorylated intermediate" with "energy-rich" squiggle (~) bonds (11, 83). The chemiosmotic theory provided a revolutionary concept that the enigmatic link between electrogenic proton pumps and a proton-translocating ATP synthase is a proton gradient across the membrane (85). Its revolutionary significance or influence to the field of bioenergetics could be hardly overstated, which is almost something like the Schrodinger equation to the modern quantum mechanics. It generated continuous discussions and sometimes heated debates that energized the entire field of

bioenergetics. As a result, biochemists can now understand the biological energy transduction processes far better than before the era of the chemiosmotic theory (85).

However, the question of whether the proton pathway is delocalized throughout the bulk aqueous volume or is localized at its membrane surface has remained open to discussion since it was first raised in 1961 by Williams (20, 38, 44, 86, 87). He rightly pointed out the deficiency of the Mitchellian delocalized proton-coupling view by stating (39): "If charge is thrown out into the medium, as in osmotic theories, then we face the problem of equilibration of the energy of single cell on its outside with the whole of the volume in which it is suspended, say the Pacific Ocean."

This statement made by Williams 40 years ago remains as a valid criticism to the Mitchellian chemiosmotic theory even of today. Unfortunately, probably because of the "Storm and Stress" period in the history of bioenergetics where the debates among disjunctive factions of bioenergeticists were so fiercely that the opposing parties with such deep emotions apparently lost the ability to objectively consider other's points including Williams′ "Pacific Ocean" arguments (88). Hopefully, our new generation of scientists who are not emotionally attached with any of the opposing factions and bear none of the historical baggage will be able to restore the scientific civility and help move the field forward. Let's think about a bacterial cell growing in liquid culture medium in a flask. It is known that bacterial cell membrane is energized by pumping protons across the cellular membrane from the inside to the outside of the cell, which creates a proton motive force across the membrane. However, according to the Mitchellian equation (2.1 or 2.2) to create a proton motive force across the membrane, the bacterial cell in a liquid culture flask would have to cause a bulk-phase pH change in the entire volume of its liquid culture medium, which physically is impossible. From here, we can also understand that there is

something missing in the Mitchellian equation (2.1 and 2.2) since it does not fit with the known physical reality here.

Perhaps, the most well-established scientific observations that showed the failure of the Mitchellian delocalized proton view are in alkalophilic bacteria, such as *Bacillus pseuodofirmus* (23-25). These bacteria keep their internal pH about 2.3 pH units more acidic than the ambient bulk pH 10.5, while $\Delta\psi$ is about 180 mV in the direction from outside across the cellular membrane to the cytoplasm (26, 27, 31). The application of equation (2.2) in this case would yield a pmf (Δp) value so small (44.3 mV at T = 298K) that it has remained as a mystery for the last three decades as to how these organisms can synthesize ATP (29, 30, 34).

This long-standing unresolved energetic conundrum (32, 33) can now be explained by the proton-electrostatics localization hypothesis (15). Recently, we elaborated the proton-electrostatics localization hypothesis and derived the following new proton motive force (pmf) equation:

$$\text{pmf}\,(\Delta p) = \Delta\psi + \frac{2.3\,RT}{F}\left(pH_{nB} + \log_{10}\left(\frac{C}{S}\cdot\frac{\Delta\psi}{l\cdot F\left(\prod_{i=1}^{n}[K_{Pi}\left(\frac{[M_{pB}^{i+}]}{[H_{pB}^{+}]}\right)+1]\right)} + [H_{pB}^{+}]\right)\right) \quad (2.3)$$

Where $\Delta\psi$ is the electrical potential difference across the membrane; pH_{nB} is pH of the cytoplasmic bulk phase; $[H_{pB}^{+}]$ is the proton concentration in the periplasmic bulk aqueous phase; C/S is the specific membrane capacitance; l is the thickness for localized proton layer; K_{Pi} is the equilibrium constant for non-proton cations (M_{pB}^{i+}) to exchange for localized protons; and $[M_{pB}^{i+}]$ is the concentration of non-proton cations in liquid culture medium.

The use of this newly derived equation has recently yielded an overall pmf (Δp) value (215~233 mV) that is 4 times more than that (44.3 mV) calculated from the Mitchellian equation

for the alkalophilic bacteria growing at pH 10.5 (22). This newly calculated value is sufficient to overcome the observed phosphorylation potential ΔGp of −478 mV to synthesize ATP in the bacteria. Therefore, we have explained the 30-year-longstanding bioenergetics conundrum in alkalophilic bacteria as how they are able to synthesize ATP.

The core concept of the proton-electrostatics localization hypothesis is built on the premise that a water body, such as the water within a bacterial cell, can act as a proton conductor in a manner similar to an electric conductor with respect to the electrostatic behavior and charge conduction. This is consistent with the well-established knowledge that protons can quickly transfer among water molecules by the "hops and turns" mechanism that has been first outlined by Grotthuss two centuries ago (76, 89, 90). By applying Gauss Law equation to a water-membrane-water system, it was found mathematically that the excess protons are localized at the water-membrane interface, forming a proton-capacitor-like structure: the localized excess protons-membrane-anions system (22). Therefore, we may use the proton capacitor concept to calculate the effective concentration of the localized protons $[H_L^+]^0$ at the membrane-water interface in a pure water-membrane-water system assuming a reasonable thickness (l) for the localized proton layer using the following equation:

$$[H_L^+]^0 = \frac{C}{S} \cdot \frac{\Delta\psi}{l \cdot F} = \frac{\Delta\psi \cdot \kappa \cdot \varepsilon_o}{d \cdot l \cdot F} \qquad (2.4)$$

where C/S is the membrane capacitance per unit surface area; F is the Faraday constant; κ is the dielectric constant of the membrane; ε_o is the electric permittivity; d is the thickness of the membrane; and l is the thickness of the localized proton layer.

This proton-capacitor equation (2.4) is the foundation for the revised pmf equation (2.3), which has an additional term that accounts for the effect of non-proton cations exchanging with the localized protons. An experimental demonstration of the proton capacitor concept with a pure

water-membrane-water system in relation to equation (2.4) is fundamentally important to testing the proton-electrostatics localization hypothesis. In this chapter, recent experimental study is reported in which the distribution of localized excess protons at a water-membrane interface was demonstrated for the first time.

2.2 MATERIALS AND METHODS

2.2.1 Excess protons generation

Two ElectroPrep electrolysis systems (Cat no. 741196) purchased from Harvard Apparatus Inc. were used with one of them as a control. Each of these ElectroPrep electrolysis systems (Figure 7.) comprised a cathode chamber, a small Teflon center chamber and an anode chamber. The small Teflon center chamber was inserted to the middle of the inter-chamber wall with O-ring fitting (and with silicon-seal when necessary) that separates the cathode and anode water chambers. To test the proton capacitor concept predicted by the proton-electrostatics localization hypothesis, a 25-µm thick aluminum membrane (Al) was sandwiched in between two pieces of impermeable 75-µm thick Teflon (Tf) membrane (all with a diameter of 2.35 cm), forming a Tf-Al-Tf membrane as shown in Figure 8. Membrane thickness measurements were performed using a Mitutoyo micrometer. Unlike the conventional water electrolysis application, the objective of our experiments was to determine whether the excess protons (created by the electrolytic water oxidation) in the anode chamber would behave like solutes, such as sugar molecules, and stay in the bulk phase as in the Mitchellian delocalized view or would distribute themselves only to the water-membrane interface as predicted by the proton-electrostatics localization hypothesis. Therefore, in many of our experiments, excess protons and excess hydroxyl anions were generated in two water bodies separated by a membrane through the use of "open-circuit" water-electrolysis. When the proton capacitor across the membrane was charged

up by the excess protons generated in the anode chamber and excess hydroxyl anions in the cathode chamber, the electric current of the water electrolysis process would approach zero, which can be analogous to a respiratory membrane system such as mitochondria with a fully charged membrane potential at its respiratory "state 4" resting stage (91).
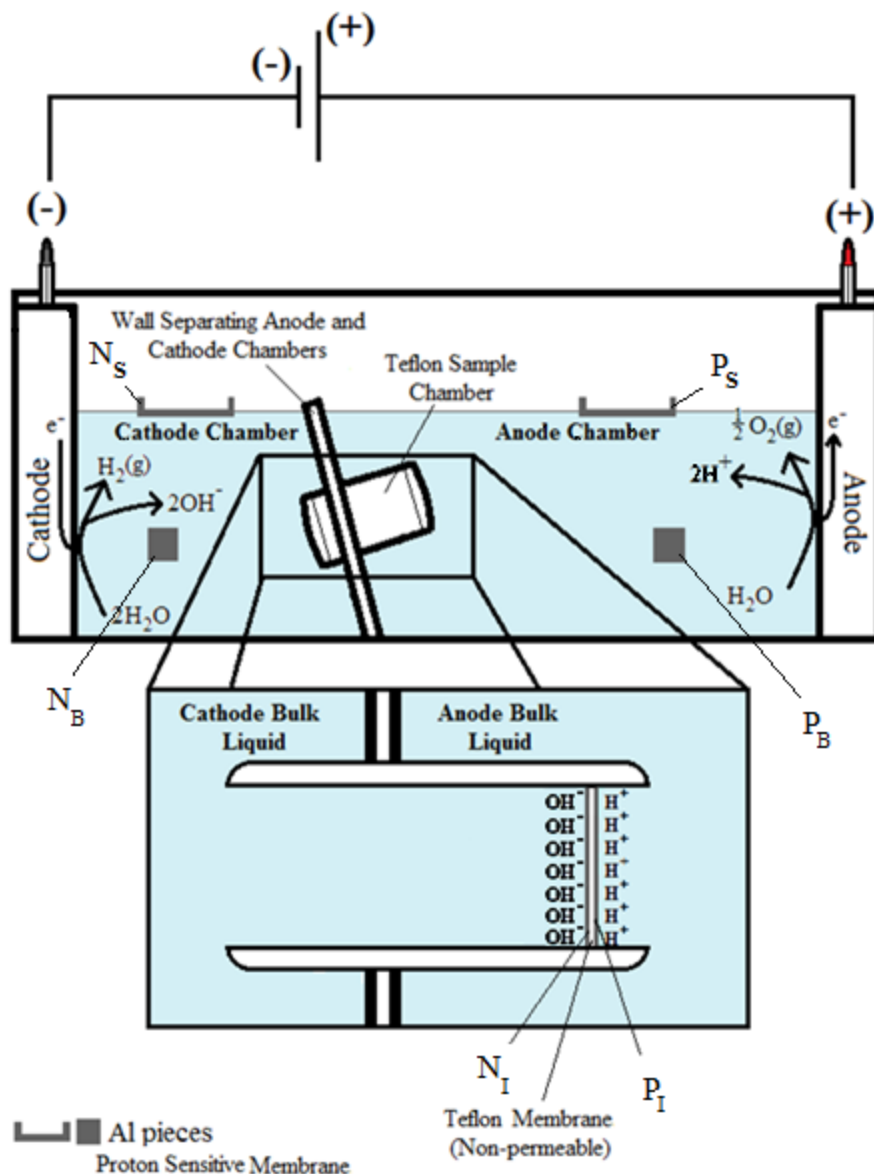
Figure 7. Illustration on how excess protons and excess hydroxyl anions were generated by utilizing an ElectroPrep "open-circuit" water-electrolysis system comprising a cathode chamber, a Teflon center chamber assembly, and an anode chamber. The excess protons in the anode water were electrostatically localized at water-membrane interface (P_I) along the membrane surface while the excess hydroxyl anions in the cathode water chamber (at the left) were electrostatically attracted to the water-membrane interface (N_I) on the other side of membrane, forming a "hydroxyl anions-membrane-excess protons" capacitor-like system (see Inset). Pieces of proton-sensitive Al films were applied on the anode water surface (P_S), the cathode water surface (N_S), in the middle of the anode chamber water bulk phase (P_B) and in the middle of the cathode chamber water bulk phase (N_B).
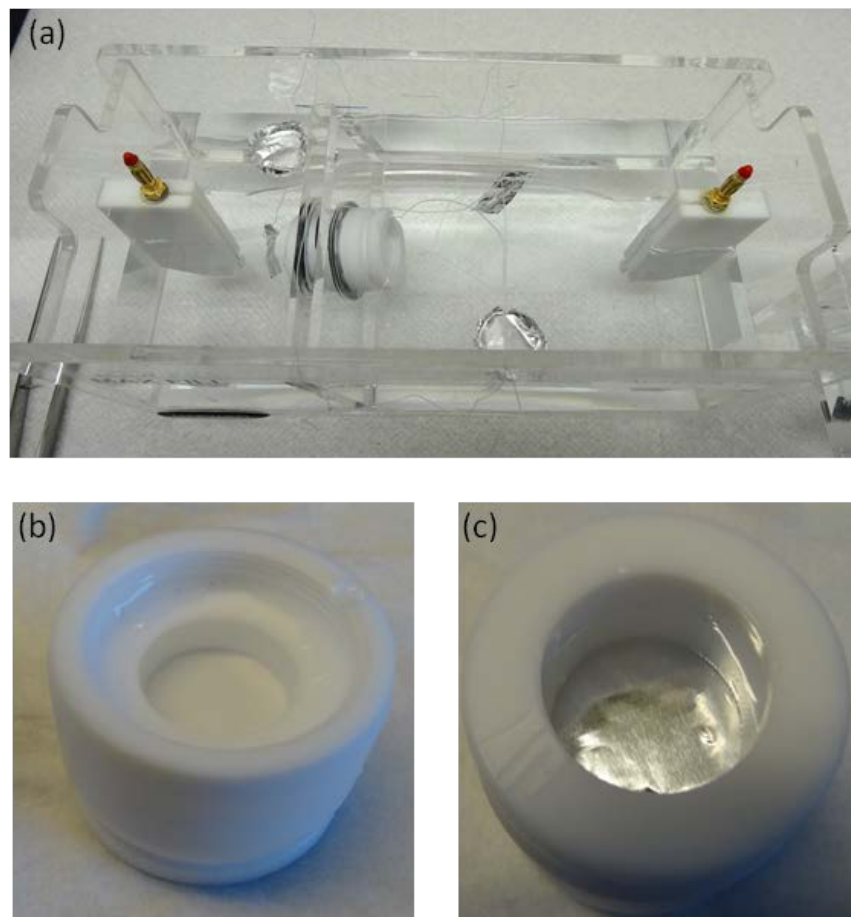
Figure 8. (a) A top view photograph showing the ElectroPrep apparatus. Pieces of proton-sensitive films were applied on the water surface and in the middle (bulk phase) of both the anode and cathode water chambers. Nylon strings were used to anchor the pieces of proton-sensitive films that were suspended in the middle of both the anode and cathode water chambers. (b) Teflon center chamber assembly with a Tf-Al-Tf membrane. (c) Teflon center chamber assembly with a proton-sensing Al-Tf-Al membrane.

2.2.2 Bulk-phase water pH measurement

The proton-electrostatics localization hypothesis predicts that the excess protons could not be detected by a bulk-phase pH measurement with a pH meter; whereas the Mitchellian delocalized view would predict the opposite. Therefore, water bulk-phase pH was measured to test the predictions. In each experiment, about 2 liters of ultrapure MilliQ-deionized water (Millipore, 18.2 MΩ.cm at 22.5 ºC) were generated through a Millipore NanoPure Water filtration system (Model SYNS00000) and collected in a 4-L beaker. To ensure the quality of the ultrapure MilliQ-deionized water, the pH of the deionized water source was checked separately by pouring a small fraction of the water into two separate 50-ml beakers (in duplicate) and measuring the water pH (recording 6 stable pH readings per replicate water sample) using Inlab pure pro ISM pH probe (Mettler Toledo) integrated with IQ scientific Instruments handheld pH meter designed to measure pH for aqueous samples with very low ionic strength, including ultra-pure water. In this way, the deionized water that was used to fill the anode and cathode chambers had never been contacted with any pH electrode to eliminate any possible contamination of Cl⁻ ions from the glass pH electrode. We have noticed that Cl⁻ ions could interfere with the proton-sensing Al film activity.

After the Teflon center chamber was placed into the inter-chamber wall, the two compartments of each ElectroPrep electrolysis system were filled with ultrapure MilliQ-deionized water (Millipore, 18.2 MΩ.cm at 22.5 ºC): 300 ml in the cathode chamber and about 600 ml in the anode chamber rendering an equal water level in both chambers (Figure 7). The bulk phase pH values in the anode and cathode chambers were measured at the end of each 10-hour experiment by inserting the glass pH electrode into the bulk water phase in each of the

water chambers and recording at least 6 stable pH readings for each of the water bulk aqueous phase.

2.2.3 Detection of localized excess protons with a proton-sensing film

In our preliminary experiment, it was discovered that aluminum metal can be used as a sensor to detect the excess protons by its corrosion-associated color change. Therefore, extra heavy duty aluminum membrane purchased from VWR was cut into round disks with a diameter of 2.35 cm. A Teflon membrane disk (Tf) was sandwiched in between a pair of aluminum (Al) membrane disks with an equal-diameter of 2.35 cm, forming a proton-sensing Al-Tf-Al membrane assembly. This assembly was then fit with the small Teflon center chamber (Figure 8c). In addition, pieces of proton-sensing Al film were placed on the water surfaces (P_S and N_S), and more importantly into the water bulk-water phase (P_B and N_B) near the middle of both the anode and cathode water chambers (Figure 7 and Figure 8) to track the distribution of the created excess protons.

After the apparatus was set up as shown in (Figure 7), 200 V of electrolysis voltage was applied to the system for 10 hours using a Source Voltage/digital multi-meter system (Keithley instruments series 2400S-903-01 Rev E). The resulting electric current was measured as a function of time using the digital multi-meter interfaced with a PC computer using LabVIEW software. The area under the current versus time curve was integrated using Originpro 8.6 and LabVIEW program to calculate the amount of the total charges (coulombs) that passed through the electrolysis process in relation to the production of excess protons.

2.3 RESULTS AND DISCUSSION

2.3.1 Localized excess protons demonstrated with a proton-sensing film

During the open-circuit electrolysis of ultrapure water, excess protons were produced in the anode (P) chamber while excess hydroxyl anions were generated in the cathode (N) chamber (Figure 7). According to the proton-electrostatics localization hypothesis, the free excess protons in the anode water body would not stay in the bulk liquid phase; they would localize to the water-membrane (Teflon) interface (the P_I site) in the anode (P) chamber and attract the excess hydroxyl ions of the cathode water body to the N_I site at the other side of the membrane, forming an "excess anions-membrane-excess protons" capacitor-like system (as shown in the inset of Figure 7). According to this prediction, the bulk pH in either the anode water body or the cathode water body would not be affected by the excess protons or the excess hydroxyl ions created by the water electrolysis process. These predicted features were indeed observed in this experimental study. It is known that aluminum surface can begin to be corroded by protons when the effective proton concentration is above 0.1 mM (equivalent to a pH value below 4) as shown in (Appendix B, Figure S2) (92, 93). This property was therefore employed as a proton-sensing mechanism in combination with the bulk phase pH electrode measurement to determine the distribution of excess protons in the water-membrane-water system (Figure 7). In the first set of experiments (performed in triplicate), small pieces of aluminum film were employed as a proton sensor at a number of locations in both of the water chambers to serve as an indicator for the excess protons. As illustrated in Figure 7 and Figure 8c, a Teflon membrane (Tf) was sandwiched in between two pieces of aluminum film (Al), forming a proton-sensing Al-Tf-Al membrane system that separate the two water bodies: the cathode water body on the left and the anode water body on the right. The result of the "cathode water Al-Tf-Al water anode" experiment showed that only the proton-sensing film placed at the P_I site facing the anode liquid showed proton-associated corrosion (see the dark brownish grey on the exposed part of the

proton-sensing film in Figure 9) while the proton-sensing film placed in the bulk liquid phase (P_B) of the anode chamber or floated on the top surface (P_S) of the anode water body showed no proton-associated corrosion activity. This is a significant observation since it indicates that excess protons are localized primarily along the water-membrane interface at the P_I site, but not in the bulk liquid phase (P_B). This observation agrees with the proton-electrostatics localization hypothesis perfectly. Also as expected, all pieces of proton-sensing film placed at the N_I, N_B, and N_S sites of the cathode liquid showed no-proton-associated corrosion activity as well.
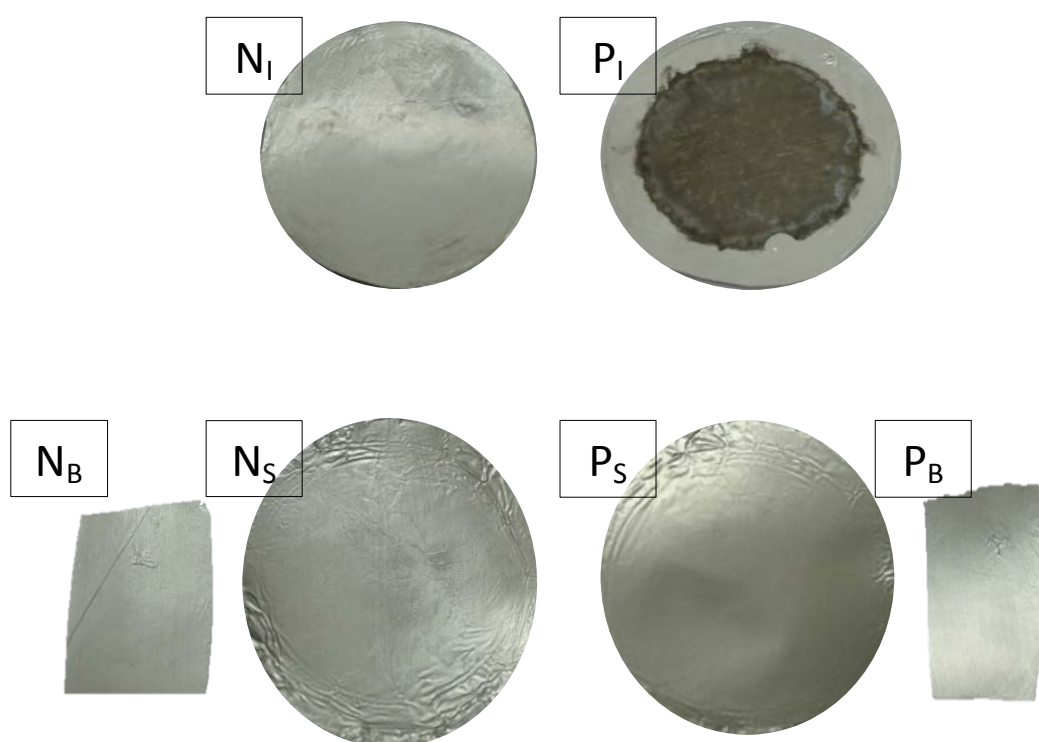
Figure 9. Observations of proton-sensing Al films after 10 hours of "cathode water Al-Tf-Al water anode" experiment with water electrolysis (200 V). N_I: proton-sensing film at the N side of Teflon membrane detected no proton activity. P_I: proton-sensing film at the P side of Teflon membrane detected dramatic activity of localized protons (dark grey color). N_B: proton-sensing film suspended inside the water of the cathode chamber. N_S: proton-sensing film floating on the water surface of cathode chamber. P_S: proton-sensing film floating on the water surface of anode chamber. P_B: proton-sensing film suspended inside the water of the anode chamber.

According to the Mitchellian proton delocalized view, the excess protons in a water body would behave like a solute such as a sugar molecule which can stay anywhere in the liquid including its bulk liquid phase. Certain commonly heard arguments in favor of the Mitchellian proton delocalized view even as of today seem still believe that the excess protons would behave like solutes that could delocalize into the bulk liquid phase somehow by "proton solvation" or "electro diffusion". If that delocalized view is true, it would predict that all the proton-sensing films in the anode water chamber including the one placed in the bulk liquid (P_B) should be able to detect the excess protons. The observation that the proton sensor placed into the anode chamber bulk water phase (P_B) could not detect any excess protons while the proton sensor placed at the P_I site showed proton-associated aluminum corrosion activity clearly rejects the Mitchellian proton delocalized view.

2.3.2 Result of bulk-phase pH measurements

During a 10-hour experiment with 200V-driven water electrolysis, it was noticed, as expected, the formation of small gas bubbles at both the anode and cathode platinum electrodes. This observation is consistent with the well-known water electrolysis process in which water is electrolytically oxidized to molecular oxygen (gas) producing protons in the anode water compartment while protons are reduced to molecular hydrogen (gas) leaving more hydroxyl anions in the cathode water compartment. If the Mitchellian proton delocalized view is true, it would predict that the production of excess protons in the anode water compartment would result in a lower pH value for the bulk water body while the generation of excess hydroxyl anions in the cathode water body would result in a higher pH in its bulk water body. That is, if the proton delocalized view is true, it would predict a significant bulk-phase pH difference (ΔpH) between

the anode and the cathode water bodies. Our experimental result with the bulk-phase pH measurements demonstrated that the Mitchellian proton delocalized view is not true. As shown in Table 1, after the 10-hour experiment with the water Al-Tf-Al (membrane) water system, the measured pH value in the anode bulk water body (5.76 ± 0.09) remained essentially the same as that of the cathode bulk water phase (5.78 ± 0.14). These bulk water phase pH values averaged from 3 replication experiments (each replication experiment with at least 6 reading of pH measurement in each chamber water, n= 3 x 6 = 18 as shown in Appendix C, Table S1-Table S4) were statistically also the same as those (5.78 ± 0.04 and 5.76 ± 0.02) in the control experiments in absence of the water electrolysis process. This is a significant experimental observation since it confirmed the prediction of the proton-electrostatics localization hypothesis that the excess protons do not stay in the bulk water phase and thus cannot be measured by a pH electrode in the bulk phase.

Table 1. Averaged pH values that were measured in bulk water phase before and after 10 hours experimental run with "cathode water membrane water anode" systems.

Experiments		pH of Cathode Water	pH of Anode Water
With (Al-Tf-Al) 200 V	Before	6.89± 0.03	6.89± 0.03
	After	5.78± 0.14	5.76± 0.09
With (Tf-Al-Tf) 200 V	Before	6.71± 0.10	6.71± 0.10
	After	5.81± 0.04	5.76± 0.03
With (Al-Tf-Al) control (0V)	Before	6.89± 0.03	6.89± 0.03
	After	5.68± 0.06	5.78± 0.02
With (Tf-Al-Tf) control (0V)	Before	6.71± 0.10	6.71± 0.10
	After	5.76± 0.02	5.78± 0.04

*The averaged pH values and standard deviation (± sign) were calculated from the original data of bulk water phase.

pH measurements presented in detail in the Appendix C (Table S1-Table S6).

This observation can also explain why in certain bioenergetic system such as thylakoids where ATP synthesis through photophosphorylation sometimes can occur without measurable ΔpH across the thylakoid membrane between the two bulk aqueous phases (38). As shown in the present study, although the bulk-phase pH difference (ΔpH) between the anode chamber water and the cathode chamber water is zero, the excess protons were localized at the water-membrane interface as demonstrated by the dramatic proton activity on the proton-sensing film placed at the P_I site (Figure 9). This indicated that the concentration of localized excess protons was much higher than 0.1 mM.

Furthermore, the measured pH value of 5.76± 0.09 in the anode bulk water phase was also consistent with the observation that the piece of proton-sensing film placed in the anode bulk water phase (P_B) showed no sign of proton-associated corrosion activity while the proton-sensing film placed at P_I site had dramatic proton-associated corrosion (Figure 9). This indicated that the generated excess protons are localized primarily at the water-membrane interface at the P_I site resulting in a proton surface density that is high enough (pH < 4) to cause the aluminum corrosion there.

The pH measurements also showed that the freshly deionized water had an average pH value of 6.89± 0.03 before being used in the experiments (Table 1). Since the experiments were conducted with the laboratory ambient air conditions, the gradual dissolution of atmospheric CO_2 into the deionized water during a 10-hour experiment period resulted in water pH change from 6.89± 0.03 to 5.68± 0.06, which was observed in the control experiment with the same "cathode water Al-Tf-Al water anode" setup except without turning on the electrolysis voltage (0 V). Therefore, this bulk water pH change had little to do with the 200V-driven water electrolysis process. The same magnitude of bulk water pH change before and after the experiment was observed for the deionized water in both the anode and cathode chambers, which also supports the understanding that this bulk water pH change from the beginning to the end of the experiment was due to the gradual dissolution of atmospheric CO_2 into the deionized water during the 10-hour experiment period. There was no difference between the bulk-phase pH of anode chamber water (pH 5.76± 0.09) and that of the cathode chamber water (5.78± 0.14) at the end of the experiment. This result also points to the same underline understanding that the excess protons do not behave like typical solute molecules. Excess protons do not stay in the water bulk

phase; they localize at the water-membrane interface at the P_I site so that they cannot be detected by the bulk-phase pH measurement.

A further set of experiments with the setup of "cathode water Tf-Al-Tf water anode" was also conducted in triplicate. In this set of experiments, Tf-Al-Tf membrane system was used instead of the Al-Tf-Al membrane system. Since the Teflon membrane is chemically inert to protons, the use of the Tf-Al-Tf membrane system eliminated the consumption of excess protons by the aluminum corrosion process at the P_I site that was demonstrated above. In this set of the experiments, no bulk-phase pH difference (ΔpH) between the anode and cathode water bodies was observed as well. As shown in Table 1, after 10 hours run at 200V with the "cathode water Tf-Al-Tf water anode" system, the measured pH value in the anode bulk water phase (5.76± 0.03) was essentially the same as that of the cathode bulk water phase (5.81± 0.04). This experimental observation again indicated that the excess protons do not stay in the bulk water phase and thus cannot be measured by the bulk liquid phase pH measurement. Since liquid water is an effective proton conductor as discussed above, the excess protons produced in the anode water compartment electrostatically localize to the water-membrane interface at the P_I site.

2.3.3 Excess protons assessed with water electrolysis electric current

The proton-charging-up process in this "excess hydroxyl anions Tf-Al-Tf excess protons" capacitor system was monitored by measuring the electric current of the 200V-driven water electrolysis process as a function of time during the entire 10-hour experimental run. The data in the inset of Figure 10 showed that the electric current of the water electrolysis process decreased with time as expected. That is, when the excess protons were generated in the anode water compartment (while the excess hydroxyl anions were generated in the cathode water compartment), this "excess hydroxyl anions Tf-Al-Tf excess protons" capacitor is being charged

up by localization of the excess protons at the P_I site and the excess hydroxyl anions at N_I site (Figure 7). According to our analysis, this process reached thermodynamic equilibrium after about 1500 seconds (shown in the inset of Figure 10) under this experimental condition where the curve of the water electrolysis current quickly became flat indicating the completion of the water electrolysis-coupled proton-charging-up process.
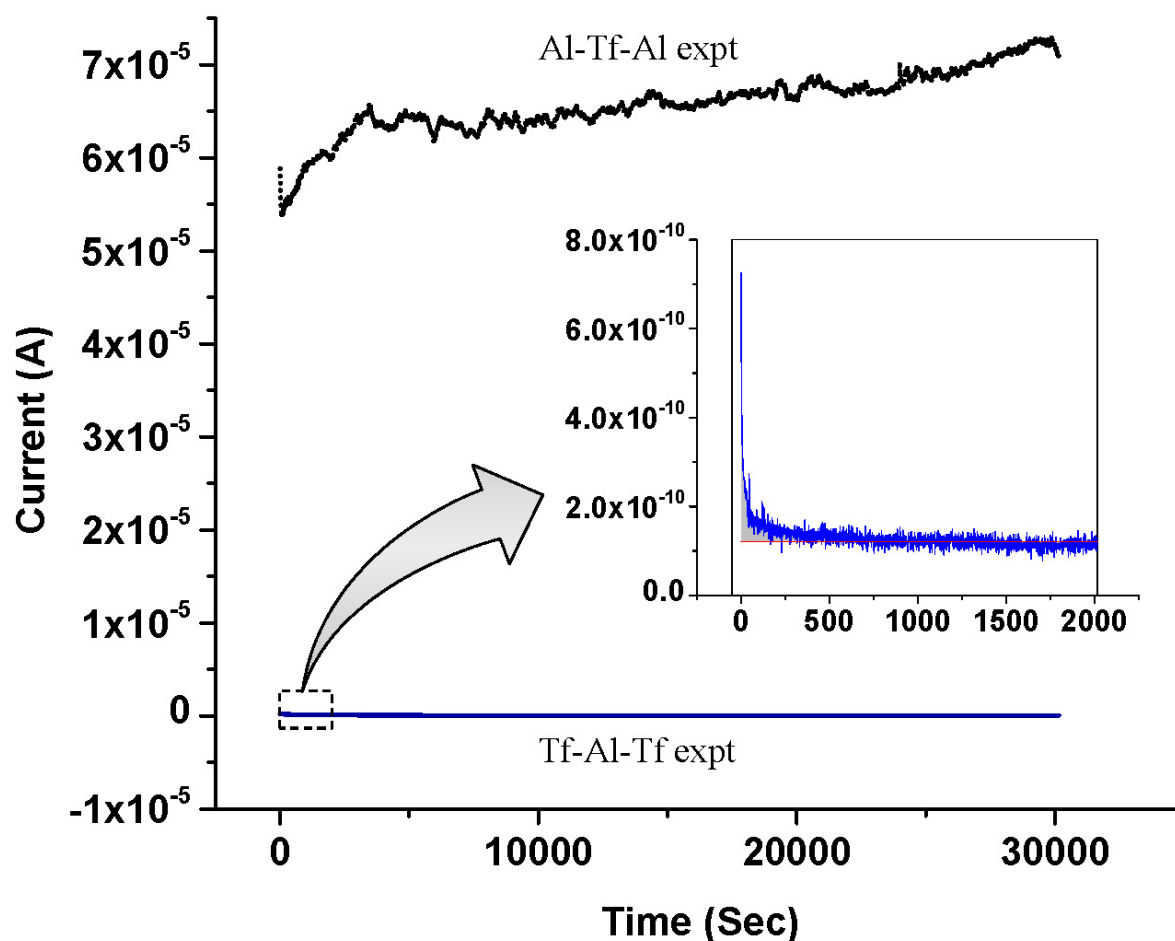
Figure 10. The electric current of water electrolysis measured as a function of time with 200 V during 10 hours experimental run. The black curve shows average of three experiments with "cathode water Al-Tf-Al water anode". The blue line shows average of three experiments with "cathode water Tf-Al-Tf water anode"; and its initial part within the first 2000 seconds is plotted in an expanded scale showing the integration for the area under the curve (Inset). More detailed data is shown in (Appendix B, Figure S1).

By calculating the area under the water-electrolysis current curve above the flat baseline as shown in the inset of Figure 10, the amount of excess protons loaded onto the "excess hydroxyl anions Tf-Al-Tf excess protons" capacitor was estimated to be 2.98 x 10^{-13} moles

(Table 2). The area of the Teflon membrane surface exposed to the anode water at the P_I site was measured to be 2.55 cm^2. If that amount of excess protons were loaded at the P_I site onto the Teflon membrane surface exposed to the anode water, the maximal localized excess proton density per unit area was estimated to be 1.19 nanomoles H$^+$/m^2. Although the exact thickness of the localized excess proton layer at the P_I site is yet to be determined, our recent study (22) indicated that the effective thickness for this type of the electrostatically localized excess proton layer may be about 1±0.5 nm. If that is the case, then the localized excess proton density of 1.19 nanomoles H$^+$/m^2 would translate to a localized excess proton concentration of 1.19 mM H$^+$ (equivalent to a localized pH value of 2.92 as calculated in Table 2) at the P_I site, which can explain why they can be detected by the proton-sensing Al film there.

Table 2. Calculation of localized proton density per unit area in "cathode water Tf-Al-Tf water anode" experiment.

	Area under the curve **(Coulombs)**	**Moles of excess protons H$^+$** **(mol)**	**Localized proton density per unit area** **(mole H$^+$/m^2)**	**pH at P_I of the Tf-Al-Tf**
Replicate 1	3.03 x 10^{-8}	3.14 x 10^{-13}	1.25 x 10^{-9}	2.90
Replicate 2	2.25 x 10^{-8}	2.33 x 10^{-13}	9.33 x 10^{-10}	3.03
Replicate 3	3.35 x 10^{-8}	3.47 x 10^{-13}	1.38 x 10^{-9}	2.85
Average	2.88 x 10^{-8}	2.98 x 10^{-13}	1.19 x 10^{-9}	2.92 ± 0.09

The water electrolysis current in the "cathode water Al-Tf-Al water anode" experiment was also monitored. As shown Figure 10, after about 5000 seconds, the water electrolysis electric current at the steady state of this experiment reached around 6.5×10^{-5} A, which was much bigger than that (below 1×10^{-10} A) of the "cathode water Tf-Al-Tf water anode" experiment. This large water electrolysis electric current can be attributed to the consumption of excess protons by the proton-sensing Al film at the P_I site. As the proton-sensing film at the P_I site consumes the excess protons, more excess protons can then be produced at the anode electrode, resulting in a significant water-electrolysis electric current. The high concentration of the electrostatically localized excess protons at the P_I site thermodynamically drives the aluminum corrosion reaction in which aluminum atoms are oxidized by protons resulting in evolution of molecular hydrogen gas. During the experiment, we indeed noticed the formation of gas bubbles on the aluminum membrane surface at the P_I site (Figure 11).

Figure 11. Teflon center chamber (with Al-Tf-Al membrane) after 10 hours electrolysis. Formation of gas bubbles and significant proton activity was noticed on the aluminum film surface at the P_I site.

By calculating the area under the water-electrolysis current curve from the "cathode water Al-Tf-Al water anode" experiment and subtracting that of the "cathode water Tf-Al-Tf water anode" experiment, we were able to calculate the amount of excess protons that were generated by the anode and consumed by the proton-sensing film at the P_I site. As shown in Table 3, during the 10-hr "cathode water Al-Tf-Al water anode" experiment, a total of 2.11×10^{-5} moles of excess protons were generated by the anode platinum electrode. These excess protons were apparently translocated to the proton sensing film surface at the P_I site and consumed there by the corrosion reaction as shown in Figure 9. The amount of protons consumed per unit area was calculated to be 8.29×10^{-6} moles per cm^2 as shown in Table 3.

Table 3. Calculation* of the amount of protons consumed in proton-sensing-associated corrosion process in the "cathode Al-Tf-Al water anode" experiment. The surface area of Al exposed to the localized proton attack was $\Pi r^2 = 2.545$ cm$^2 = 2.5 \times 10^{-4}$ m^2.

	Area under the curve (Coulombs)	Moles of excess protons H$^+$ = (mol)	Observance of corrosion	Amount of protons consumed (moles H$^+$ /m^2)
Replicate 1	2.01	2.07×10^{-05}	Yes	0.0833
Replicate 2	2.10	2.17×10^{-05}	Yes	0.0871
Replicate 3	2.01	2.08×10^{-05}	Yes	0.0833
Average	2.04 ± 0.05	2.11×10^{-05}	Yes	0.0846 ± 0.0022

*Moles of excess protons $H^+ = \dfrac{Area\ under\ curve}{96485}$

2.4 CONCLUSION

The experimental results reported above clearly demonstrated that excess protons were localized at the water-membrane interface in the anode water-membrane-water cathode system. The most remarkable evidence for the localized excess protons came from the observation that the proton-sensing film placed at the P_I site of Teflon membrane showed dramatic excess proton activity (corrosion) while the proton-sensing film placed into the anode chamber water bulk phase (P_B) showed no proton activity during the entire experiment. The density of localized excess protons created in this experiment was estimated to be about 1.19 mM H^+ (pH value of 2.92) at the water-membrane interface (P_I site), which explains why it can be sensed by the proton-sensing Al membrane. Furthermore, the bulk-phase pH measurements in both anodic and cathodic water chambers also confirmed that excess protons do not stay in the bulk aqueous phase, which clearly rejects the Mitchellian proton delocalized view. These observations clearly match with the predictions from the proton-electrostatics localization hypothesis: excess protons do not stay in the water bulk phase; they localize at the water-membrane interface in a manner similar to the behavior of excess electrons in a conductor. This finding has significance not only in the science of bioenergetics but also in the fundamental understanding for the importance of water to life. It is now quite clear that water serves not only as a solvent and substrate but also as a proton conductor for proton coupling energy transduction in living organisms.

Furthermore, the localized excess protons that have now been demonstrated for the first time through this research may have practical implications as well. For example, the utilization of localized excess protons that can be created in pure water may lead to clean "green chemistry" technologies for industrial applications such as metal acid washing and/or protonation of certain micro/nanometer materials without requiring the usage of conventional acid chemicals such as nitric and sulfuric acids.

CHAPTER 3

THE EFFECT OF CATIONS (Na$^+$ AND K$^+$) ON LOCALIZED EXCESS

PROTONS AT A WATER-MEMBRANE INTERFACE

Preface

This chapter is the basis of the paper which is in preparation to be submitted to physical

chemistry B journal. The title of the paper will be as follows:

Saeed HA, Lee JW. The Effect of Cations (Na$^+$ and K$^+$) on Localized Excess Protons at a Water-

Membrane Interface.

3.1 INTRODUCTION

Peter Mitchell's work on chemiosmotic theory (16, 82, 83) won him the 1978 Nobel prize in

chemistry, and its central bioenergetics equation has been incorporated into many textbooks (3,

5, 84). In one of its forms, this equation is expressed as the proton motive force across a

biological membrane that drives protons through the ATP synthase:

$$\text{pmf} = \Delta\psi + \frac{2.3\,RT}{F}\,\Delta\text{pH} \qquad (3.1)$$

Where $\Delta\psi$ is the electrical potential difference across the membrane, R is the gas constant, T is

the absolute temperature, and ΔpH is the pH difference between the two bulk aqueous phases

separated by the membrane. In this framework, the protons are considered to be solutes, similar

to sugar molecules, that are delocalized, existing everywhere in the bulk aqueous phases.

Consequently, the Mitchellian view of bioenergetics is that the ATP synthase is coupled to the

redox proton pumps via bulk phase-to-bulk phase proton electrochemical potential gradients

generated across the biological membrane. The chemiosmotic theory was a major milestone in

the history of bioenergetics; its significance to the field could hardly be overstated.

However, the question as to what extent the proton coupling pathway for producing ATP is delocalized throughout the bulk aqueous volume or localized at the membrane surface has remained under discussion since it was first raised in 1961 by Williams (20, 38, 44, 86, 87). He (39) pointed out a deficiency of the delocalized proton-coupling view by stating: "If charge is thrown out into the medium, as in osmotic theories, then we face the problem of equilibration of the energy of a single cell on its outside with the whole of the volume in which it is suspended, say the Pacific Ocean." Perhaps the most well-established observations that disagree with the Mitchellian equation (3.1) are in alkalophilic bacteria, such as *Bacillus pseuodofirmus* (23-25). These bacteria keep their internal pH about 2.3 units more acidic than the ambient bulk pH of 10.5, while its membrane potential is about 180 mV (26, 27, 31). The use of the Mitchellian equation (3.1) in this case would yield a pmf value so small (44 mV at T = 298K) that it has remained a mystery for the last three decades as how these organisms are able to synthesize ATP (29, 30, 34). Also notable are the elegant measurements on thylakoids by Dilley et al. (73), who measured photosynthetic ATP production in the presence of a bulk proton permeable buffer (pyridine) and found that protons in the bulk phase were not governing the ATP synthesis process in thylakoids under low salt conditions. Dilley et al. (44, 73, 94) conjectured that a hypothetical proteins-occluded space along the membrane surface could provide a localized proton pathway to the ATP synthase, but no evidence for such a protein system has been found. Similarly, other conjectured explanations for protons being localized at membrane surfaces have not gained acceptance.

Biological membranes are made of phospholipids which have negatively-charged phosphate groups. The presence of a net negative charge on the biological membrane

surfaces produce an electrical potential that attracts the counter-ions (of opposite charges) and repels ions carrying the same charge as that of the surface. Several theories have been introduced in an attempt to determine the surface potential of charged surfaces and to describe the electrical phenomena at the surfaces of the biological membranes. Helmholtz recognized that the charges that are fixed on a solid surface immersed in an electrolyte solution attract counter-ions via the Coulomb force from the aqueous phase (95). He said that both the fixed charges and the counter-ions form what he named an electrical double layer. Unfortunately, the Helmholtz electrical double layer model does not adequately explain all the features, since it hypothesizes rigid layers of opposite charges.

In order to describe the electrostatic attraction of the counter-ions to the charged solid surface such as the phospholipid membrane, Gouy and Chapman have used the Poisson equation (96, 97). Unlike the earlier considerations of Helmholtz, Gouy suggested that counter ions are not rigidly held, but tend to diffuse into the liquid phase. As a result, the thickness of the resulting diffused double layer will be affected by the kinetic energy of the counter ions. Gouy and Chapman developed the diffuse double layer theory in which the change in concentration of the counter ions near a charged surface and the charge distribution of ions as a function of distance from the charged surface follow the Boltzmann distribution. They have used Boltzmann equation to describe the statistical tendency of the counter-ions to diffuse away from a region of high concentration. However, since the Boltzmann distribution assumes that activity is equal to molar concentration there would be an error in evaluating and describing the effective charge distribution near the biological membrane surface. It was found experimentally that the thickness of the double layer that reflects the extensiveness of the counter-ion clouds is always greater than the calculated one (58). The Gouy-Chapman theory is not entirely accurate as it assumes that

ions behave as point charges and that there is no physical limits for the ions in their approach to the surface (98). Clearly, it is known that ions have a finite size which is determined by their ionic radius and degree of hydration. Also the Gouy-Chapman model assumes that the rigid charged surface has planar surface which cannot be applied for the biological membranes because they are not smooth due to the presence of integral proteins protruding from their surfaces (99, 100). Stern, therefore, modified the Gouy-Chapman diffuse double layer (99). He considered that ions have a finite size and cannot approach the surface closer than few nanometer which was described by Debye length. Stern also assumed that there is a possibility for some ions and dipolar molecules to be specifically adsorbed by the surface, and this layer has become known as the Stern Layer (101). Electrochemists have highlighted for many years the short comings of the Gouy- Chapman theory as it ignored some important effects such as specific ion binding, ionic sizes, oriented dipoles, and hydration effects (99-101).

For solutions adjacent to charged surfaces like electrodes, the potential of the electrode becomes proportional to the surface charge density which is similar to a capacitor whose plates has specific charge densities and separated by a distance (r_D). As mentioned before that the diffuse electric double-layer presented by Gouy-Chapman is currently the model being used for describing the ionic atmosphere near a charged surface whose thickness is estimated as the Debye length (r_D). The magnitude of the Debye length ─which appears as the characteristic decay length of the surface potential─ depends only on the properties of the solution not on the properties of the charged surface (102). For example, a monovalent electrolyte like NaCl solution at 25 ℃, the Debye length is 30.4 nm at 10^{-4} M, 0.96 nm at 0.1 M and 0.3 nm at 1 M. This means that the Debye length decreases by increasing the concentration of the electrolytes (103).

Unfortunately, the Debye length cannot be used to estimate the thickness of the localized excess protons because the equations used in calculating the Debye length can be applied only to charge-balanced solutions including 1:1 electrolyte solutions such as NaCl, 2:1 electrolytes such as $CaCl_2$ and 1:2 electrolytes such as Na_2SO_4 (104). That is, the Debye length equations cannot be applied to estimate the thickness of the localized excess protons (layer) that does not have counter ions. Consequently, it is necessary to develop more appropriate equations to describe the nature and the thickness of localized excess protons on the charged and the uncharged membrane interface.

Recently, Lee has put forward the proton electrostatic localization hypothesis for a natural mechanism to produce surface membrane localized protons (15, 105), which is built on the premise that a water body acts as a proton conductor. This premise is consistent with the well-established knowledge that protons quickly transfer among water molecules by the "hops and turns" mechanism first outlined by Grotthuss two centuries ago (76, 89, 90). Considering a conceptualized system consisting of an impermeable membrane immersed in pure water with an excess number of free protons (H^+) inside and an equal number of free hydroxyl ions (OH^-) outside, and given that pure water acts as a proton conductor, it follows mathematically from applying the Gauss Law of electrostatics that the excess protons and ions are localized at the water-membrane interface, forming a capacitor-like structure (105). For an idealized proton capacitor, the concentration of the localized protons $[H_L^+]^0$ at the membrane-water interface is related to the membrane electric potential difference by

$$[H_L^+]^0 = \frac{C}{S} \cdot \frac{\Delta \psi}{l \cdot F} = \frac{\Delta \psi \cdot \kappa \cdot \varepsilon_o}{d \cdot l \cdot F} \qquad (3.2)$$

Where *C/S* is the specific membrane capacitance per unit surface area, *l* is the thickness of the

localized proton layer, κ is the dielectric constant of the membrane, ε_o is the electric permittivity, and d is the membrane thickness.

Considering biological systems, it is important to note that non-proton cations in the aqueous media may exchange with protons localized at the membrane surface and thereby reduce their concentration. According to the proton electrostatic localization hypothesis (22), such exchange effects can be expressed by augmenting equation (3.2) for the concentration of surface localized protons as

$$[H_L^+] = \frac{[H_L^+]^0}{\prod_{i=1}^{n} \left(K_{Pi}\left(\frac{[M_{pB}^{i+}]}{[H_{pB}^+]}\right) + 1\right)} \qquad (3.3)$$

Where $[H^+{}_{pB}]$ is the proton concentration in the bulk aqueous phase, $[M_{pB}^{i+}]$ is the concentration of non-proton cations, and K_{Pi} is the equilibrium constant for non-proton cations to exchange with the localized protons. Thus, it is to be expected that the non-proton cation concentrations that occur in biological systems may play a significant role in modulating the proton motive force for varieties of biological functions including the production of ATP.

Furthermore, according to the proton electrostatic localization hypothesis (22) the proton motive force in equation (3.1) must be revised by combining the concentration of surface localized protons with the concentration of bulk phase protons; explicitly,

$$\text{pmf} = \Delta\psi + \frac{2.3\,RT}{F}\log_{10}\left(\left([H_L^+] + [H_{pB}^+]\right)/[H_{nB}^+]\right) \qquad (3.4)$$

Here, as in equation (3.3), $[H_{pB}^+]$ is the proton concentration in the periplasmic bulk aqueous phase while $[H_{nB}^+]$ is the proton concentration in the cytoplasmic bulk phase. This pmf equation also adds clarification beyond equation (3.1) in which the electrical potential difference term

$\Delta\psi$ in equation (3.4) that helps to drive protons through the ATP synthase is the same factor (in equation (3.2)) that determines the concentration of surface localized protons which are available to the ATP synthase. Indeed, $\Delta\psi$ exists precisely because of the excess cations (including H^+) and the excess anions (such as OH^-) charge layers localized on either sides of the membrane. Moreover, it is expected that the surface localized protons would make a very significant contribution to the protons available for driving ATP synthesis. In fact, applying equation (3.4) to the alkalophilic bacteria case noted above, using reasonable estimates for the quantities in equations (3.2) and (3.3), yields a pmf value of ~225 mV, which is 5 times larger than the value obtained from equation (3.1) and is sufficient to overcome the observed phosphorylation potential in order to synthesize ATP (105).

The Lee proton electrostatic theoretical model which has a characteristic localized proton coupling feature does not necessarily contradict with the electric double layer theoretical model. These two models represent two different processes: the former describes the proton motive force with electrostatically localized excess proton coupling bioenergetics while the later belongs to the classic electric double layer phenomenon. For example, the negatively-charged phosphate groups of the biological membrane could attract protons and other cations to its surface forming an electric double layer along the membrane negatively charged surface as expected by the Gouy-Chapman theory (52). However, this double layer always exists at all time during light and dark conditions even when the proton motive force (pmf) is zero. This means that the protons and/or cations attracted to the membrane surface's fixed charge forming the double layer couldn't contribute to the proton motive force that drives the flow of protons across the membrane for two reasons: first, the protons forming the double layer are not dynamic. Second, there would be no need for light (photosynthetic) and/or chemical (respiratory) to create excess

protons and establish the proton gradient across the membrane as it would violate the fundamental principles of thermodynamics by driving work without requiring external energy (53). In fact, as described by the Lee proton electrostatic theoretical model, it is the free excess protons that have the dynamic ability to be coupled to the ATP synthase and are relevant to the proton motive force.

As illustrated in Figure 12, our experimental work in Chapter 2 clearly demonstrated the formation of a localized excess protons layer at the water-membrane interface in an anode water-membrane-water cathode system (106), where excess protons were generated by water electrolysis in an anode electrode chamber while excess hydroxyl anions were created in a cathode chamber. When a positive voltage is applied to the anode electrode in water, it first attracts the hydroxyl anions to anode electrode surface and then counter ions (protons) distribute themselves near the anions layer, forming a typical "electric double layer" on the anode surface (Figure 12a, right side). When significant number of excess protons are produced by water electrolysis (in mimicking a biological proton production process such as the respiratory proton pumping system and the photosynthetic water-splitting process) in the anode chamber, the excess protons electrostatically distribute themselves at the water-surface (including the membrane surface) interface around the water body including a part of the "electric double layer" at the anode surface. From here, it can be seen that the excess proton layer at the water-membrane is apparently extended from the secondary (proton) layer of the "electric double layer" at the anode. The excess proton layer at the water-membrane interface attracts electrostatically the excess hydroxyl anions in the cathode chamber at the other side of the membrane, forming an "excess anions-membrane-excess proton" capacitor-like structure.

Since the membrane is just an insulator layer (not an electrode), the excess proton layer at the water-membrane interface is likely to be a special monolayer (with a thickness probably of about 1 nm), but definitely not an "electric double layer" as that of a typical electrode. The conclusion of excess proton monolayer is also consistent with the known "electric double layer" phenomenon since the excess proton layer can be treated as an extension from the second (proton) layer of the anode's "electric double layer" (Figure 12a, right side) around the proton-conductive water body.

When the electrolysis voltage is turned off, the electric polarization at both anode and cathode disappears and so does the "electric double layer", leaving only the excess proton layer around the anode chamber water body and the similarly formed excess hydroxyl (anions) layer around the cathode chamber water body as illustrated in Figure 12b. The excess anions-membrane-excess proton capacitor (shown in the middle of Figure 12b) may represent a proof-of-principle mimicking an energized biological membrane such as a mitochondrial membrane system at its energized resting state.
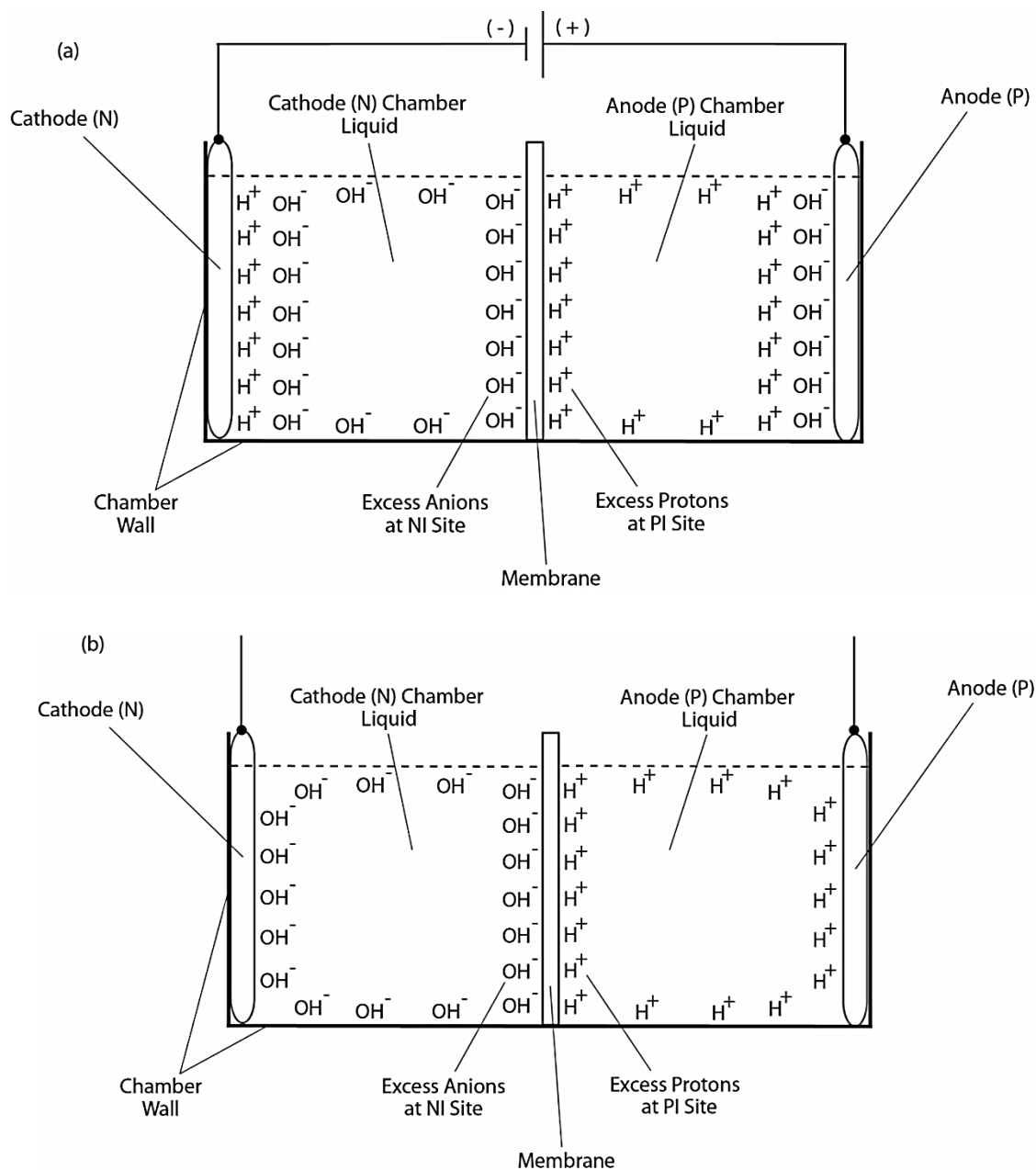
Figure 12. Schematic diagram showing experimental demonstration of a localized excess protons layer at the water-membrane interface in an "anode water-membrane-water cathode" system. Top (a): showing the excess proton monolayer is extended from a secondary proton layer of the "electric double layer" that covers the anode surface when electrolysis voltage is applied; Bottom (b): showing the likely distribution of excess protons and excess hydroxyl anions in the two water chambers separated by a membrane when electrolysis voltage is turned off.

The electrostatic localization conceptualization is quite general. It does not depend on biological scales or processes. Therefore, to provide a first proof-of-principle study (106), we have carried out laboratory bench experiments to create excess protons using an electrolysis set-up with cathode and anode water chambers separated by an impermeable membrane.

In Chapter 2, we experimentally demonstrated using a proton-sensing film that excess protons do not stay in water bulk phase; instead they localize at the water-membrane in a manner similar to the behavior of excess electrons in a metallic conductor (106). These observations clearly support the proton-electrostatics localization hypothesis (15, 105) which is a significant contribution in understanding the biological energy transduction processes and the distribution of protons across a biological membrane.

In this Chapter, we report the effect of cations (Na^+ and K^+) on localized excess protons at the water-membrane interface by measuring the exchange equilibrium constant of Na^+ and K^+ cations in exchanging with the electrostatically localized protons at a series of cations concentrations. The experimental determination of the cation exchange equilibrium constant with the localized protons reported here will provide a logical support for the electrostatic localized proton hypothesis and gain more fundamental understanding for the effect of non-proton cations on localized proton population density.

3.2 MATERIALS AND METHODS

Two ElectroPrep electrolysis systems (Cat no. 741196) purchased from Harvard Apparatus Inc. were used in this experimental study with one of them as a control. Each system comprised a cathode chamber, a small Teflon center chamber and an anode chamber as illustrated in Figure 13. The small Teflon center chamber was inserted to the middle O-ring fitting channel of the

inter-chamber wall that separates the cathode and anode water chambers. The ElectroPrep electrolysis system was made of Teflon, a completely inert material that is unreactive under high power voltage.
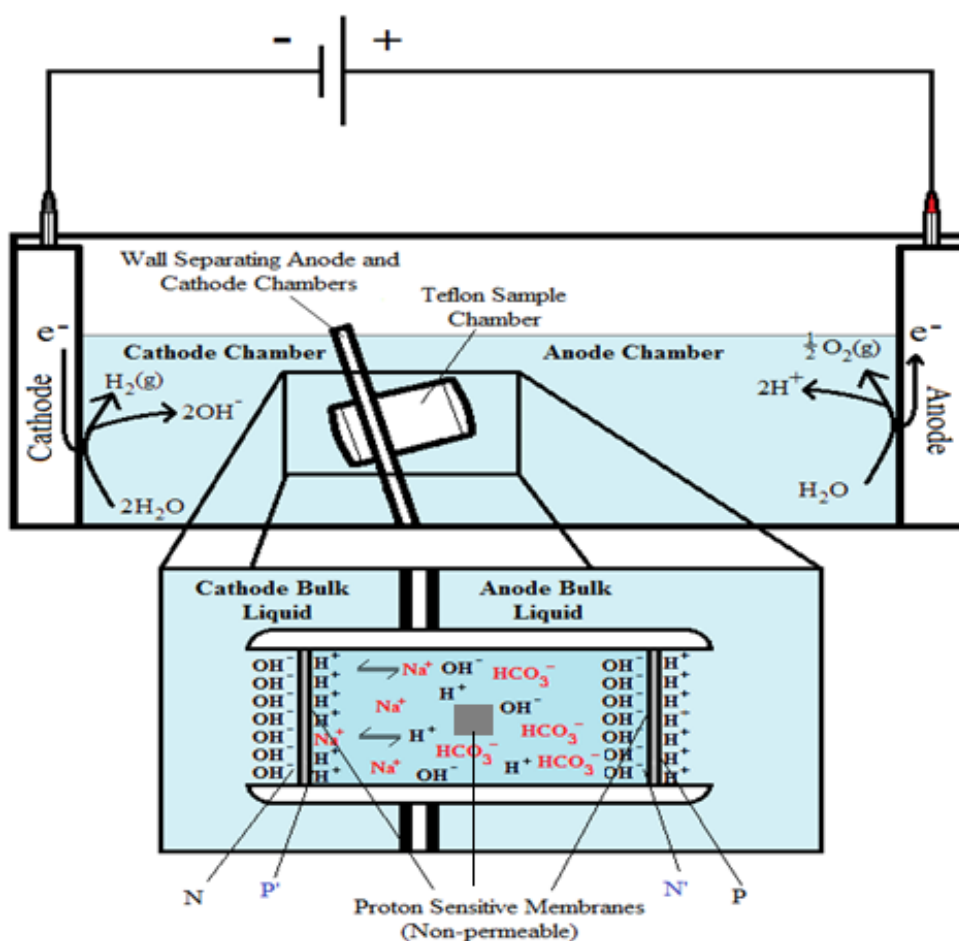
Figure 13. Schematic diagram of the system testing the effect of sodium cations on localized protons at the P′ side in the Teflon center chamber. The inset shows the exchange of the added sodium (Na^+) cations with the electrostatically localized protons at the P′ side. A small piece of proton-sensing Al film was placed into the bulk liquid phase (the C_B site) of the center chamber.

To test the effect of (K^+ and/or Na^+) salt concentration on localized excess protons, 1.5 ml of pure water or salt solution was placed inside a 1500 µl Teflon center chamber (Harvard Apparatus) as shown in Figure 13. The Teflon center chamber was sealed at each of its two ends by Al-Tf-Al membrane assembly that is formed by sandwiching an impermeable 75-µm thick Teflon (Tf) membrane with two pieces of 25-µm proton-sensing aluminum (Al) films (having equal-diameter of 2.35 cm) placed at the two side ends of the Teflon center chamber (internal diameter 1.5 cm and length 0.9 cm). In addition, a small piece of aluminum was inserted in the middle liquid bulk phase of the Teflon center chamber. The small Teflon center chamber was then placed in between the anode and the cathode compartments of the apparatus as in Figure 13 so that one end of the center chamber was in contact with cathode bulk liquid (denoted N side), while the other end was in contact with anode bulk liquid (denoted P side).

The ultrapure MilliQ-deionized water (Millipore, 18.2 MΩ.cm at 22.5 ℃) used in this study was degased by boiling the water in an autoclave (Yamato, Model SM510) and then it was cooled down to room temperature before using. The two compartments were then filled with ultrapure MilliQ-deionized water (Millipore, 18.2 MΩ.cm at 22.5 ℃): 300 ml in small compartment where the cathode electrode resides (cathodic compartment) and about 600 ml in large compartment where the anode electrode resides (anodic compartment), rendering an equal water level in both compartments (Figure 13 shows the schematic diagram of the system and a detailed description of the electrolysis process). This effectively created a "cathode water membrane (Al-Tf-Al) water membrane (Al-Tf-Al) water anode" system.

The pH of the deionized water was measured separately in a small beaker using Orion™ ROSS Ultra™ pH Electrode (Thermo Scientific, Cat No. 8102BNUWP) that is designed to measure pH for aqueous samples with very low ionic strength, including ultra-pure water. Two

point calibrations were performed using a buffer of pH 7.00, and a buffer of pH 4.01, according to manufacturer instructions.

Series of experiments with the above settings were performed comparatively in the presence (and absence) of $NaHCO_3$ or $KHCO_3$ solution at a series of the ionic salt concentrations (0, 10, 50, 100, 150, 200 & 400 mM) that was placed into the Teflon center chamber (Figure 13, inset bottom). These experiments were performed to test the effect of sodium (or potassium) cations on the electrostatically localized protons at the induced P′ side in the center chamber, in comparison with the unperturbed P side facing the anode water. After sealing one end of the Teflon center chamber with (Al-Tf-Al) membrane, 1.6 ml of liquid water or the ionic salt solution was introduced into the Teflon center chamber through the other end, which was then sealed with another (Al-Tf-Al) membrane. The ultrapure MilliQ-deionized water used in all experiments was pre-degassed to remove the excess dissolved air gases from the liquid water. The Teflon center chamber assembly was then fitted into the O-ring channel within the inter-chamber wall that separates the cathode and anode water chambers. The apparatus was then rinsed with ultrapure MilliQ-deionized water to remove any possible salt contamination before loading ultrapure MilliQ-deionized water into cathode chamber (300 ml) and the anode chamber (600 ml). This setup created a "cathode water membrane (Al-Tf-Al) –salt solution−membrane (Al-Tf-Al) water anode" system.

After the apparatus was set up as shown in Figure 13, an electrolysis voltage of 200 V was applied to the system for 10 hours using a digital multimeter system (Keithley instruments series 2400S-903-01 Rev E). To ensure safety, all experiments were performed inside a fume hood that has a built-in air-fan driven ventilation system to disperse the small amount of potentially explosive H_2 and O_2 gases generated from the water electrolysis process through the

fume hood ducts into the outside atmosphere. A second apparatus with the exactly same setup and liquid samples except without the 200 V electrolysis voltage was used as a control. The liquid pH was measured for the salt solution inside the Teflon center chamber after the 10-hour period for both the experiment and the control (recording 6 stable pH readings for each sample) using Orion™ ROSS Ultra™ pH Electrode (Thermo Scientific, Cat No. 8102BNUWP). Also the conductivity measurement for the water in each of the anode chamber and the cathode chamber at the end of the experiment was performed (recording 6 stable conductivity readings for each sample) using a Beckman coulter conductivity probe (Model 16 x 120 mm, item no. A57201).

3.3 RESULTS AND DISCUSSION

3.3.1 Demonstration of electrostatically localized protons at the P and P′ interfaces in a "water-membrane-water-membrane-water" system

In the system described above, water in the Electroprep apparatus was electrolyzed at 200 V, forming excess protons / O_2 gas in the anode chamber (P) and excess hydroxyl anions / H_2 gas in the cathode (N) chamber (Figure 13). Based on the proton-electrostatics localization hypothesis (15), it is predicted that the free excess protons in the anode chamber would migrate and localize themselves primarily at the water-membrane interface (the P site) in the anode (P) chamber. The excess protons localized at the P side would induce an electrostatic localization of hydroxide ions at the other side of the membrane (the N′ site) forming an "excess anions-membrane-excess protons" capacitor-like system (as shown in Figure 14 and on the right of the inset of Figure 13). Similarly, the excess hydroxide ions generated in the cathode chamber would migrate and localize primarily at the water-membrane interface (the N site) in the cathode (N) chamber. It is

predicted that this hydroxide ions localization at the N side would induce electrostatic localization of protons at the other side of the membrane (the P′ site) forming an "excess anions-membrane-excess protons" capacitor-like system (as shown in Figure 14 and on the left of the inset of Figure 13).
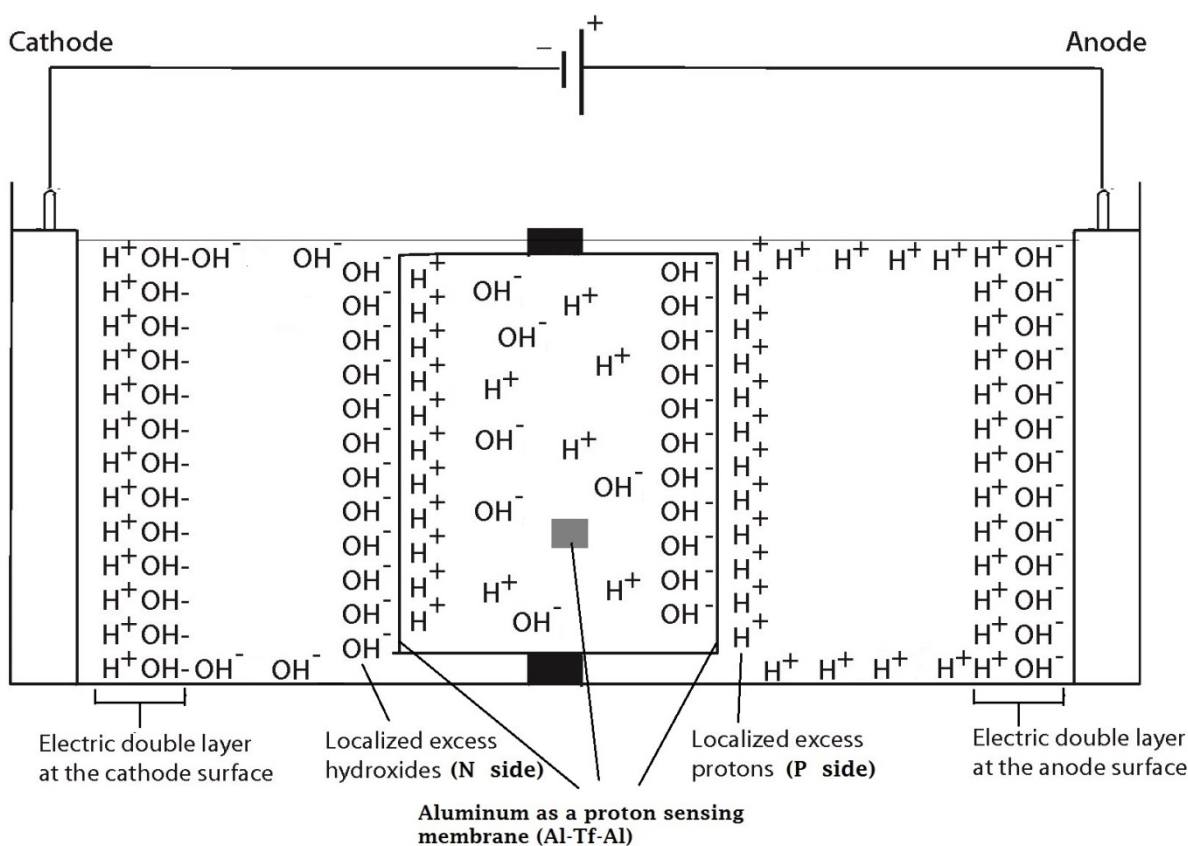
Figure 14. Schematic diagram showing the distribution of protons and hydroxide ions in the cathode, center and the anode water chambers under the influence of applying 200V when the electrodes are polarized. The inset shows the electrostatic distributions of protons and hydroxide ions on P′ and N′ sites respectively in a "water-membrane-water-membrane-water" system.

These predicted features were indeed demonstrated through observation of localized proton activity on Al films at the P and P′ sites while there were no observable proton activity at the N and N′ sites, and no observable excess proton activity in the bulk liquid phase at the P_B, C_B, and N_B sites in the three liquid chambers (Figure 15). As predicted by the hypothesis, it was noticed that the proton sensing films (Al-Tf-Al) at the two ends of the Teflon sample chamber had detection of protons on P and P′ sites that were adjacent to pure water (in absence of any salt) as shown in Figure 15. The proton-sensing detection employed here was in the form of Al surface corrosion (Equations 3.5 and 3.6) when the effective proton concentration was above 0.1 mM (equivalent to a pH value below 4) as explained in (Appendix B, Figure S2) (92, 93). While the proton-sensing film placed at the N and/or N′ side of the Teflon membrane detected no significant proton activity so that its color remained unchanged (Figure 15).

$$Al_2O_3 + 6H^+(localzied) \leftrightarrow 2Al^{3+} + 3H_2O \qquad (3.5)$$

$$2Al\,(s) + 6H^+(localized) + 6OH^- \rightarrow 2Al(OH)_3 + 3H_2(g) \qquad (3.6)$$
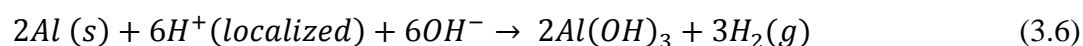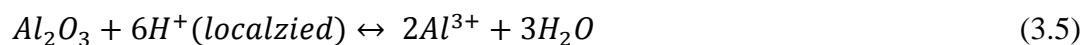
It is worth to mention that the Al film in the Al-Tf-Al membrane does not serve as an electrode since the Al membrane itself was not connected to any external voltage source. It acted as part of an insulating membrane where excess protons accumulate at the surface on the P site while excess hydroxides are localized at the N side as shown in the middle of Figure 14. Therefore, as discussed previously, there is a monolayer of protons localized at the Al membrane surface but there is no double layer formation as expected by Gouy-Chapman double layer theory due to the absence of counter-ions in the anode chamber. However, an electric double

layer is expected to be established on the charged electrode surfaces as illustrated in Figure 14. In this three-water-chambers system, we also demonstrated an induced proton layer at the membrane-water interface (the P′ site) in the center liquid chamber with the evidence of proton-sensing film at the P′ site showing intense localized proton activity while those at C_B and N′ sites showing no protonic activity (Figure 15).

Proton-sensing film placed at cathode (**N**) site.
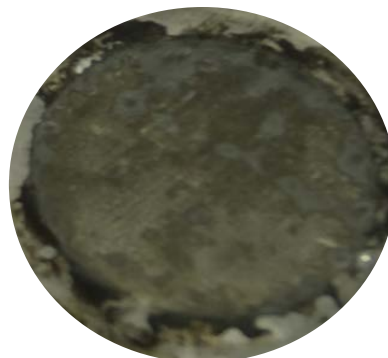
Proton-sensing film placed at cathode facing the solution in the center Teflon chamber (**P′**) site.

Proton-sensing film placed at anode facing the solution in the center Teflon chamber (**N′**) site.

Proton-sensing film placed at anode (**P**) site.

Proton-sensing film suspended inside the cathode bulk water phase (**N$_B$**)

Proton-sensing film suspended inside the anode bulk water phase (**P$_B$**)

Proton-sensing film was placed into the bulk liquid phase of the center chamber (**C$_B$**)

Figure 15. Observation of proton-sensing films after 10 hours electrolysis (200 V) for the cathode water *Al-Tf-Al-DI water- Al-Tf-Al* water anode experiment. Images show proton-sensing films that were placed at N, P, N′, P′, N$_B$, P$_B$ and C$_B$ sites.

Table 4. Three replicates of final pH measurements for experiments with arrangement "cathode water-Al-Tf-Al-DI water- Al-Tf-Al- water anode "after 10 hours electrolysis (see Appendix C, Table S7-Table S8).

Replicates	Experiment (200v)			Control (0V)		
	Cathode chamber pH	Center chamber pH	Anode chamber pH	Cathode chamber pH	Center chamber pH	Anode chamber pH
Replicate 1	5.88 ± 0.13	7.28 ± 0.18	5.82 ± 0.09	5.78 ± 0.14	5.91 ± 0.06	5.70 ± 0.08
Replicate 2	6.01 ± 0.09	7.04 ± 0.08	5.80 ± 0.01	5.75 ± 0.04	6.11 ± 0.05	5.89 ± 0.34
Replicate 3	5.85 ± 0.10	7.27 ± 0.14	5.79 ± 0.08	5.71 ± 0.03	6.17 ± 0.03	5.72 ± 0.10
Average	5.92 ± 0.12	7.20 ± 0.17	5.81 ± 0.07	5.75 ± 0.08	6.07 ± 0.13	5.77 ± 0.21

Our bulk-phase pH measurements (Table 4) demonstrated that the Mitchellian proton delocalization view is not true. After the 10-hour water electrolysis, the measured pH value in the anode bulk water body (5.92 ± 0.12) remained nearly the same as that of the cathode bulk water phase (5.81 ± 0.07). If the Mitchellian proton delocalized view is true, there should be significant bulk-phase pH difference (ΔpH) between the anode and the cathode water chambers; In contrast, the measured bulk pH data demonstrated again that the Mitchellian proton delocalized view is not true. These bulk water phase pH values averaged from 3 replication experiments (each replication experiment with at least 6 reading of pH measurement in each chamber water, n= 3 x 6 = 18) were statistically also the same as those (5.75± 0.08 and 5.77± 0.21) in the control experiments in absence of the water electrolysis process. Notably, these results again show that excess protons do not stay in the water bulk phase; they localize at the

water-membrane interface at the P and P′ sites so that they cannot be detected by the bulk-phase pH measurement.

These are significant observations, since both the proton-sensing film detection and bulk liquid pH measurement have now demonstrated, for the first time, that protons can be localized at a water-membrane interface through electrostatic induction at the P′ site in a "cathode water membrane (Al-Tf-Al) water membrane (Al-Tf-Al) water anode" system where the third water body (the center water chamber) was placed in between an anode water chamber and a cathode water chamber interacting in series (Figure 14). The operation of this setup resulted in the formation of two proton capacitors interacting in series: a proton capacitor across the membrane (Al-Tf-Al) with the N and P′ sites and another one across the other membrane (Al-Tf-Al) with the N′ and P sites as illustrated in (Figure 13 and Figure 14). This result again shows that liquid water bodies are proton conductors; the behavior of excess protons in proton conductors appears to be similar to that of excess electrons in electric conductors in forming capacitors across insulating membrane barriers.

3.3.2 Equilibrium constant of sodium cation (Na$^+$) in exchanging with electrostatically localized protons

Demonstration of the localized protons at P′ site in the center chamber enabled us to evaluate the cation exchange of other cations with the localized protons by using salt solutions only in the center chamber without requiring the use of salts in the anode and cathode chambers (Figure 13 and Figure 16). Use of salts in the anode and the cathode chambers which have large volumes would not only cost much more chemical materials but also might interfere with the electrolysis process complicating the interpretation of the experimental results. Therefore, the utilization of the localized protons demonstrated previously at P′ site with the use of salt solutions in the center

chamber provided an advantage for us to perform quite clean experiments in measuring the effect of other cations on localized protons including the determination of the cation exchange equilibrium constants with the localized proton population without requiring the use of any salt in the anode or the cathode chambers.
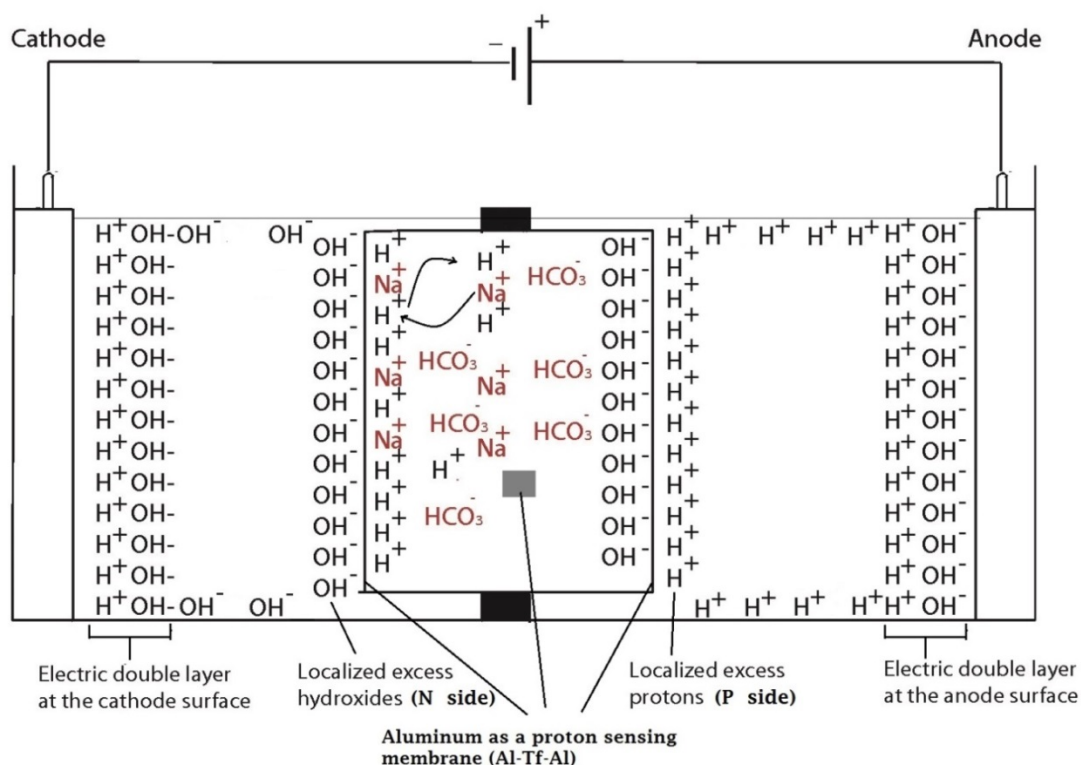
Figure 16. Schematic diagram after introducing salt into Teflon center chamber showing the distribution of different ions in the cathode, center and the anode water chambers under the influence of applying 200V when the electrodes are polarized. The inset shows the exchange of the added sodium (Na^+) cations with the electrostatically localized protons at the P′ side in a "water-membrane-sodium bicarbonate-membrane-water" system.

Our experimental results (Table 5) showed that the addition of 10 mM and/or 25 mM sodium ions (sodium bicarbonate solution) in the center chamber had no significant effect on the electrostatically localized protons at the P′ side facing the sodium salt solution. While the use of 75 mM sodium ions (in the center chamber) led to the reduction of electrostatically localized protons populations at the P′ site by about 50%, which was monitored by the color change of the proton-sensing film at the P′ side in comparison with that of the proton-sensing film placed at the positive controls (0 mM sodium ions i.e.: water with no salt) P′ side site and the P site facing the anode liquid (also no salt). It required the use of 200 mM or higher sodium ion solution in Teflon center chamber to exchange out the localized protons at the P′ side to a level that could not be detected by the proton-sensing film (Table 5, row 7). Based on our analysis, this effect of sodium salt ($NaHCO_3$) solution on the localized protons at the P′ side is probably owing to the sodium cations at higher concentrations (75 mM or above) that may partially exchange with the electrostatically localized protons at the P′ site.

Table 5. Observation of proton-sensing films after 10 hours electrolysis (200 V) for the "cathode water Al-Tf-Al- bicarbonate solution - Al-Tf-Al water anode" experiment. Images show proton-sensing films that were placed at P′ sites for both sodium and potassium bicarbonate solutions. (See Appendix C, Table S9–S14 for more detailed data)
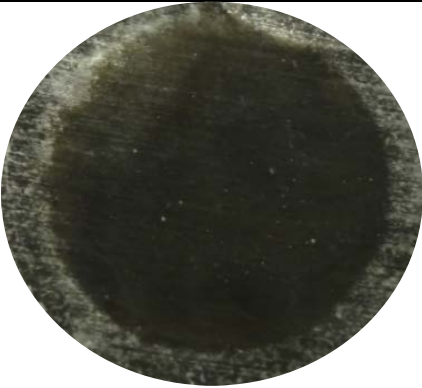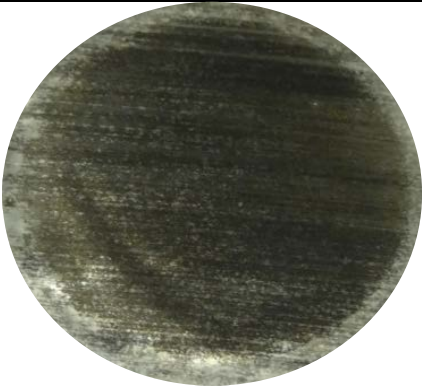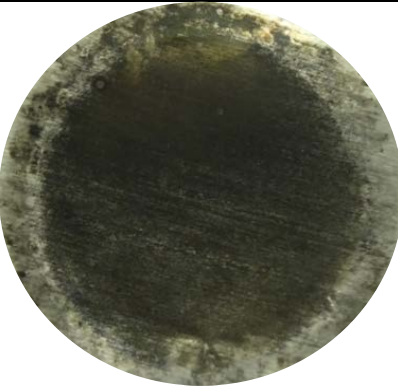
Concentration of Salt solution	Proton-sensing film placed at cathode (**P′**) site in contact with **sodium** bicarbonate solution	Proton-sensing film placed at cathode (**P′**) site in contact with **potassium** bicarbonate solution
0 mM		
10 mM		
25 mM		

Table 5. Continued.
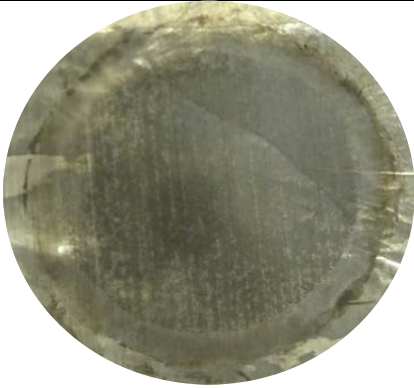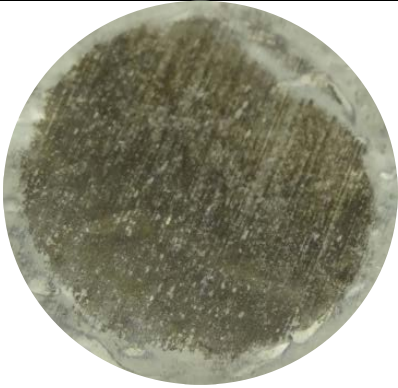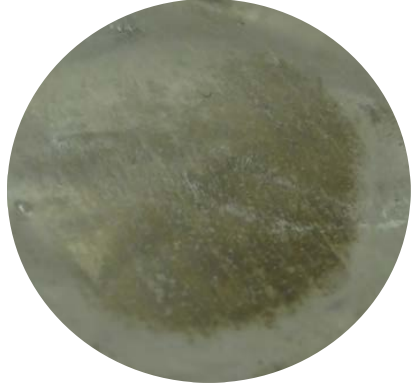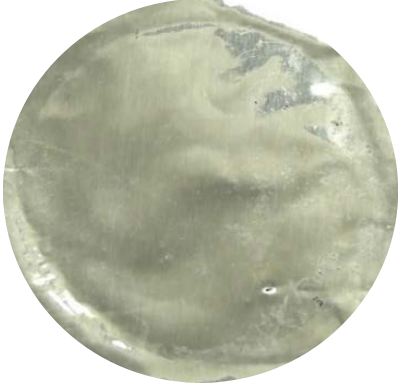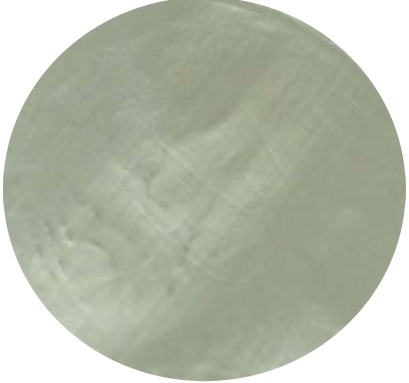
Concentration of Salt solution	Proton-sensing film placed at cathode (**P′**) site in contact with **sodium** bicarbonate solution	Proton-sensing film placed at cathode (**P′**) site in contact with **potassium** bicarbonate solution
50 mM		
75 mM		
100 mM		

Table 5. Continued.

Concentration of Salt solution	Proton-sensing film placed at cathode (**P′**) site in contact with **sodium** bicarbonate solution	Proton-sensing film placed at cathode (**P′**) site in contact with **potassium** bicarbonate solution
200 mM		
500 mM		

One may think that the observed effect may be due to the bicarbonate anion not due to the sodium cation, so the cation exchange experiments (of different concentrations) were repeated again but with other cations such as K^+ which showed the same effect on P′ side. But interestingly, in K^+ salt solution, the 50% color change at the P′ site was observed at 50 mM (Table 5, row 4) instead of 75 mM. This additional observation further supports that the observed

effect was due to cation exchange and not due to a bicarbonate effect. It is well known that the size of potassium cation is bigger than sodium cation. However, in aqueous solution as a free ion, the small sodium ion attracts more water molecules giving it a larger effective diameter compared to the hydrated potassium ion. Since the hydrated radius of potassium ion is smaller than the hydrated radius of sodium ion; its diffusion mobility is faster compared to sodium. It was determined that the mobility of sodium ions under the influence of unit potential gradient is (0.53 x 10^{-3} cm^2 V^{-1} s^{-1}) which is slower than potassium ion mobility (0.76 x 10^{-3} cm^2 V^{-1} s^{-1}) under the influence of unit potential gradient (107). That's probably why it required higher concentration of sodium ions (75 mM) to delocalize 50% of the electrostatically localized protons on P′ site and 200 mM Na$^+$ for nearly complete proton delocalization at the P′ site. Moreover, it was reported that fresh solutions of bicarbonate have practically no action on aluminum corrosion (108-111).

The cation exchange equilibrium constant (K_p) can be expressed as:

$$K_p = \frac{[Na_L^+] \cdot [H^+]}{[H_L^+] \cdot [Na^+]} \qquad (3.7)$$

Where $[Na_L^+]$ is the localized sodium ions concentration on the water-membrane interface (P′ site); [H$^+$] is the concentration of free delocalized protons in the bulk liquid phase; $[H_L^+]$ is the localized protons concentration on the water-membrane interface (P′ site); and [Na$^+$] is the free sodium ions concentration in the bulk liquid phase.

At the midpoint with 50-50% cation/proton exchange at the localized proton layer, the concentration of the localized non-proton cation would be equal to the concentration of the localized protons. This means that when $[Na_L^+]$ =$[H_L^+]$, the cation exchange equilibrium constant (K_P) would be

$$K_{pNa^+} = \frac{[H^+]}{[Na^+]} \qquad (3.8)$$

We observed that the 50-50% cation/proton exchange was achieved when the sodium ion concentration was 75 mM as shown in Table 5 (and Appendix C, Table S13). At 75 mM of sodium ion concentration (the midpoint), the amount of localized protons on the proton sensitive membrane was decreased to half compared to that of the positive control in the absence of sodium ion. The pH of the sodium salt solution (75 mM) inside the Teflon center chamber before the sodium/proton exchange process was found to be (8.37 ± 0.09) as shown in Table 6 (and Appendix C, Table S23). By using this pH value for the bulk proton concentration $[H^+]$ and the known sodium ion concentration (75 mM) in equation (3.8), the sodium/proton cation exchange equilibrium constant was calculated to be $10^{-(8.37 \pm 0.09)}$ M /0.075 M= (5.86 ± 1.2) x 10^{-8}.

We noticed that the pH of the sodium ion solution (75 mM) was slightly changed during the cation-proton exchange experiment using the Al film-based proton sensor (Equations 3.5 and 3.6) at P′ site. The final pH value of the bulk sodium bicarbonate solution after 10 hours experimental run at 200V was 8.48 ± 0.07. Using this final pH value (8.48 ± 0.07) for the bulk proton concentration $[H^+]$ and the known sodium ion concentration (75 mM) in equation (3.7), the K_{pNa^+} value was calculated to be $10^{-(8.48 \pm 0.07)}$ M /0.075 M= (4.45 ± 0.73) x 10^{-8}, which is slightly smaller than that calculated using the initial pH (8.37 ± 0.09). The true K_{pNa^+} value is likely to be in between with an average of (5.07 ± 0.46) x 10^{-8}.

Table 6. pH measurements for a series of concentrations of freshly prepared sodium salt solution inside the Teflon center chamber after 10 hours open-circuit electrolysis at 200V.

Concentration of sodium salt solutions (mM)	pH after 10 hours experiment at 200V	pH after 10 hours experiment at 0V (control)
0 mM	7.52 ± 0.02	6.41 ± 0.03
10 mM	8.81 ± 0.05	8.42 ± 0.01
25 mM	8.76 ± 0.11	8.61 ± 0.24
50 mM	8.45 ± 0.02	8.39 ± 0.02
75 mM*	8.48 ± 0.07	8.37 ± 0.09
100 mM	8.30 ± 0.01	8.22 ± 0.02
200 mM	8.19 ± 0.03	8.16 ± 0.01
500 mM	8.14 ± 0.01	8.11 ± 0.02

*pH measurement for 75 mM Sodium bicarbonate (midpoint with 50-50% sodium/proton exchange) is average of 4 replications while the rest of pH measurements are averages of 2 replications. See Appendix C Tables S15-S18, S23 for more detailed information.

3.3.3 Equilibrium constant of potassium cation (K^+) in exchanging with electrostatically localized protons

Similarly, at 50 mM potassium ion concentration (the midpoint), the amount of localized protons on the proton sensitive membrane was decreased to half compared to that of the positive control in the absence of potassium ion (Table 5 and Appendix C, Table S14). The pH of the potassium salt solution (50 mM) inside the Teflon center chamber before the potassium/proton exchange process (Table 7 and Appendix C, Table S24) was determined to be 8.45 ± 0.03. By using this pH value for the bulk proton concentration $[H^+]$ and the known potassium ion

concentration (50 mM) in $K_{pK^+} = \frac{[H^+]}{[K^+]}$, the potassium/proton cation exchange equilibrium constant was calculated to be $10^{-(8.45 \pm 0.03)}$ M /0.050 M= $(7.20 \pm 0.59) \times 10^{-8}$.

The final pH value of the bulk potassium bicarbonate solution after 10 hours experimental run at 200V was 8.48 ± 0.13. Using this final pH value (8.48 ± 0.13) for the bulk proton concentration $[H^+]$ and the known potassium ion concentration (50 mM) in $K_{pK^+} = \frac{[H^+]}{[K^+]}$, the K_{pK^+} value was calculated to be $10^{-(8.48 \pm 0.13)}$ M /0.050 M= $(6.85 \pm 1.99) \times 10^{-8}$, which is slightly smaller than that calculated using the initial pH (8.45 ± 0.03). The true K_{pK^+} value is likely to be in between with an average of $(6.93 \pm 0.91) \times 10^{-8}$.

The bulk concentration of potassium ions after the potassium/proton exchange process used in determining the potassium cation exchange equilibrium constant was the concentration that resulted in 50-50% cation/proton exchange at the localized proton layer (ie: 50 mM K^+). This is because the amount of localized protons that was exchanged out by the potassium ions was likely so small that it would not significantly reduce the 50 mM K^+ concentration. In Chapter 2 we have determined the amount of localized proton density at the P_I site that has an effective area 2.55 cm^2 to be 1.19×10^{-9} mol/m^2 which is equivalent to a localized pH value of 2.92 assuming a 1 nm proton layer thickness. However, after 50-50% cation/proton exchange, the remaining amount of localized proton density on the P' site would be 6.01×10^{-4} M. The remaining of the proton populations would be delocalized in the bulk salt solution (1.5 ml) rising the concentration of bulk protons by 1.02×10^{-7} mM which is so small compared to the K^+ concentration (50 mM).

Table 7. pH measurements for a series of concentrations of freshly prepared potassium salt solution inside the Teflon center chamber after 10 hours open-circuit electrolysis at 200V.

Concentration of potassium salt solutions (mM)	pH after 10 hours experiment at 200V	pH after 10 hours experiment at 0V (control)
0 mM	7.86 ± 0.16	6.79 ± 0.07
10 mM	8.85 ± 0.08	8.47 ± 0.05
25 mM	8.61 ± 0.11	8.42 ± 0.03
50 mM*	8.48 ± 0.13	8.45 ± 0.03
75 mM	8.56 ± 0.03	8.37 ± 0.03
100 mM	8.26 ± 0.03	8.30 ± 0.01
200 mM	8.36 ± 0.01	8.26 ± 0.01
500 mM	8.23 ± 0.03	8.19 ± 0.01

*pH measurement for 50 mM potassium bicarbonate (midpoint with 50-50% potassium/proton exchange) is average of 4 replications while the rest of pH measurements are averages of 2 replications. See Appendix C, Tables (S19-S22, S24) for more detailed information.

3.3.4 Other related observations with electrostatically localized protons

During the experiments, we noticed the importance of using ultrapure Millipore water that does not contain too much dissolved gases. For example, during the winter season when the laboratory temperature (typically about 22 ºC) is significantly higher than the outside water supply, the Millipore water supplied from a cold air-saturated water source often contains too much dissolved air gases that may slowly release the excess gases due to gas solubility change in response to slight temperature changes, forming numerous tiny gas bubbles on the surfaces of the water chambers including the Al-Tf-Al membrane surface. These tiny gas bubbles can sometime be so problematic that they could negatively affect the formation and detection of localized protons on the Al-Tf-Al membrane surface because the gas bubbles apparently reside at the

water-membrane interface and form an air-gap barrier between the membrane and the liquid water phase. To eliminate this problem for improved reproducibility of experiments, a special effort was made to the laboratory water source: the Millipore water was degased by boiling the water through autoclave and then it was cooled down to room temperature before the experimental use.

As part of the effort in tracking the integrity of the center chamber assembly's fitting with the middle O-ring fitting channel of the inter-chamber wall and the sealing at the two ends of the center chamber with the Al-Tf-Al membranes, the conductivity of the water in each of the anode chamber and the cathode chamber was measured after each experiment (Appendix C, Table S17, S18, S21 and S22). The conductivity measurements for both the anode and the cathode water chambers were in the range from (1.004 ± 0.057) to (2.961 ± 1.130) µS which are acceptable values for pure water conductivity after equilibration with atmospheric carbon dioxide. This means that the salt leakage from the Teflon center chamber was negligible in our experiments and that the sealant was tight enough to keep the salt solutions trapped within the Teflon center chamber. Electrolytic current was also monitored to ensure no significant salt leakage from the Teflon center chamber. The observed current in the given set up was in the range from 50 to 70 µA. The experiments were redone again if any leakage was observed i.e.: if the current measurement in a magnitude of over 100 µA.

The reason of using bicarbonate salt solutions in our cation exchange experiments was because it was noticed that proton-sensing film material (aluminum membrane) was sensitive not only to protons but also to a number of other chemical species including Cl^-, NO_3^-, SO_4^{-2}, and CH_3COO^-. For example, it was reported that chloride ions have a high penetration power into the passive aluminum oxide film that protects the aluminum from corrosion (112, 113). This was

attributed to its small size that is close to the oxygen atoms in the oxide layer and its high mobility that makes it capable to substitute the oxygen atoms in the alumina network. Eventually, this may lead to a decrease in the film's resistivity and hence the corrosion of the aluminum atoms that is beneath the protective layer (114). Similarly, it was reported that aggressive anions like chlorides, thiocyanate, hydroxide, sulfide, nitrate, formate and acetate are highly corrosive for aluminum (115).

It is also important to use freshly prepared sodium bicarbonate solution because the pH of bicarbonate solution differs based on the concentration and temperature as well as its exposure to air. Increasing the concentration of the bicarbonate results in a decrease in the pH of the solution from 8.40 ± 0.00 (10 mM of sodium bicarbonate) to 8.21 ± 0.01 (700 mM of sodium bicarbonate). Moreover, exposure to atmospheric air, or excessive stirring, or being at relatively higher temperature (as in summer season) enhance the losing of CO_2 content from the bicarbonate solution to the air. When the sodium bicarbonate solution loses its CO_2 content, the solution becomes more alkaline and its pH increases (110).

In our experiments, the sodium bicarbonate was trapped inside the Teflon center chamber where there was no contact with the atmospheric air. This was to ensure that the only factor that affects the corrosive activity on the aluminum surface is the electrostatic localized proton attack on P′ site in the center chamber and not the change in the pH of the solution due to the loss of its carbon dioxide content. A control experiment was performed to evaluate the effect of exposure of bicarbonate solution to the atmospheric air by introducing the bicarbonate solution in an open beaker. The bicarbonate solution (10 mM $NaHCO_3$) that was in contact with atmosphere lost some of its carbon dioxide content and accordingly its pH changed from an initial pH of (8.40 ± 0.00) to (8.86 ± 0.00) after 10 hours.

Another control experiment was performed to evaluate the effect of exposure of bicarbonate solution to the atmospheric air by introducing 10 mM of sodium bicarbonate that was freshly prepared (had initial pH (8.40 ± 0.00)) in the following and left for 10 hours: 1) Inside the Teflon center chamber that was sealed at both ends with Al along with a small piece of Al that was suspended inside, and 2) In a small glass beaker where pieces of Al were placed on the surface and suspended in the bulk of the solution. After 10 hours, the sodium bicarbonate solution that was trapped inside the Teflon center chamber had a pH (8.42 ± 0.01) which is nearly similar to the initial pH, while the pH of sodium bicarbonate solution in the open beaker rose to pH (8.78 ± 0.00). It was also observed that the aluminum pieces inside the Teflon center chamber had no change, while all the aluminum pieces with sodium bicarbonate solution exposed to the air in the open beaker had observable corrosion on their surfaces (Appendix B, Figure S3). This observation indicates that sodium bicarbonate solution which is enclosed in a chamber or a bottle preserves its pH and accordingly no Al corrosion will be observed while sodium bicarbonate solution which is exposed to air for hours loses its carbon dioxide content and accordingly its pH rises to a higher value that could enable Al corrosion.

It was also observed that the temperature has an effect on the pH of the bicarbonate solution (116-118). Sodium bicarbonate solution (10 mM) that was kept in a beaker at 16 °C had a slight pH change (8.66 ± 0.00) from the freshly prepared solution (pH 8.40 ± 0.00) and a slight corrosive effect on the aluminum pieces compared to the pH (8.86 ± 0.00) of sodium bicarbonate solution that was kept in a beaker at room temperature 26 °C (Appendix B, Figure S3).

Under our experimental conditions we have observed a slight change in the pH of the bicarbonate salt solutions due to different concentrations (Table 6 and Table 7). Using a pH glass electrode would only detect the pH of the bulk medium without detecting the pH changes that

may have occurred at the membrane surface. Based on our results in absence of salt, the surface pH of the Al membrane was way below pH 4 as it was observed by the corrosion activity on P′ side (Table 5, row 1-6). However, salt addition into the center chamber induced an increase in the surface pH at the P′ site which is directly proportional to the concentrations of the cations added through cation exchange with the localized protons as discussed above. Consequently, altering the electrolyte composition and/or concentration of the bulk medium would cause significant changes in the local pH at the membrane surface with only minimum alteration in the bulk-phase pH of the bulk solution. These observations may have implications also in understanding the salinity tolerance in biological systems in relation to localized proton coupling bioenergetics.

3.4 CONCLUSION

The electrostatically localized excess protons are distinctly different from the fixed-charge-attracted electric double layer phenomenon. The proton electrostatic localization hypothesis predicts that the localized excess protons are likely to be in a monolayer at the water-membrane interface that may be exchanged with the non-proton cations in the liquid. Our experimental results showed that there is an inverse proportionality between the concentration of the salt solution and the corrosion activity of the proton sensing film placed at P′ site. By increasing the salt concentration inside the small Teflon center chamber, the proton-sensing corrosion activity of the aluminum membrane placed at P′ site would decrease till showing no proton associated corrosion activity when the salt concentrations are above 200 mM for both sodium and potassium salt solutions. This was attributed to the delocalization of the localized protons at the membrane water interface through cation exchange by the added cations of the salt solution.

According to the proton electrostatic localization hypothesis (15, 22), the equilibrium constant for protons to electrostatically occupy the cation sites at the water-membrane interface (in any possible competition with any other cations) is likely to be extremely larger than one. Conversely, the equilibrium constant K_{Pi} for non-proton cations such as Na^+ to delocalize the localized protons from the membrane-water interface is expected to be extremely smaller than one. Through our experiments mentioned above, we have now determined experimentally for the first time that the equilibrium constant for non-proton monovalent cations to exchange with the electrostatically localized protons is indeed much less than one (likely on the order of 10^{-8}). The equilibrium constant K_{PNa^+} for sodium (Na^+) cations to exchange with the electrostatically localized protons was determined to be $(5.07 \pm 0.46) \times 10^{-8}$. Similarly, the equilibrium constant K_{PK^+} for potassium (K^+) cations to exchange with the electrostatically localized protons was determined to be $(6.93 \pm 0.91) \times 10^{-8}$. These results mean that the localized protons at the water-membrane interface are so stable that it requires ten millions more sodium (or potassium) cations than protons in the bulk liquid phase to even partially delocalize the localized protons at the water-membrane interface. This provides a logical experimental support of the proton electrostatic localization hypothesis. It may also have fundamental implications in understanding the salinity tolerance in biological systems in relation to localized proton coupling bioenergetics.

CHAPTER 4

EXCESS PROTON CONDUCTION IN PURE WATER

4.1 INTRODUCTION

4.1.1 Nature of excess protons

Excess proton in water usually forms a weak chemical bond with an adjacent water molecule to form what is named a hydronium ion (H_3O^+) with C_{3v} symmetry (119). The transfer of proton across water molecule is so fast compared to other cations. It has been simulated via computer simulations (Ab intio and MS-EVB) (120) that excess protons mobility is five to seven times higher than that of similarly sized cations. The reason of the high mobility of excess protons is attributed to a chemical transfer mechanism rather than hydrodynamic diffusion (121, 122). Excess protons shuttle through the water molecules via hops and turns mechanism that involve an exchange of hydrogen and covalent bonds. This structural diffusion process of excess protons among water molecules is known as a "hop-turn" mechanism or Grötthus mechanism for Von Grötthus who first suggested proton transfer mechanism in pure water systems (71, 72, 123). Contrary to what is taught in many textbooks, the hydrated excess proton does not exist as a simple hydronium cation (H_3O^+) (124). Zundel et al (79) have described that the excess proton tunnels so quickly between two water molecules through the hydrogen bond forming a complex named Zundel cation ($H_5O_2^+$) (125). However, Eigen considered that hydrated excess proton (H_3O^+) is coordinated to three water molecules forming a complex named Eigen cation ($H_9O_4^+$) (107, 126, 127). It was found that there is a rapid inter-conversion between the Zundel ($H_5O_2^+$) and the Eigen cations ($H_9O_4^+$) in solutions which is governed by the dynamics of the local solvent structure in the second solvation shell of the hydronium cation (H_3O^+) (76, 80, 128).

Using the multistate empirical valence bond (MS-EVB) methodology in a reactive molecular dynamics simulations, Mark et al found that excess proton is a dynamic electrical charge defect that is delocalized over several water molecules (76).

4.1.2 Evidences that water is a proton conductor

It is well known that ultrapure water that is free of ions is electronically nonconductive since it is lacking the charge carriers for electrons. However, Fuchs et al (129, 130) have reported an unusual effect of liquid water when exposed to a Direct Current (DC) electric field. They noticed that when a high voltage (~15 kV cm^{-1}) is applied to two beakers filled with ultrapure liquid water, a horizontal bridge of semi liquid water forms between the two beakers. They named this bridge "the floating water bridge". The floating water bridge is a special case of an electrohydrodynamic (EHD) liquid bridge which was first discovered in 1893 by Sir William Armstrong (131).

This water bridge has unique properties that are different from liquid water and solid ice (132, 133). When the pH in both beakers was measured after applying the high voltage it was found to be nearly the same (134). It was also observed that the level of water in the cathode beaker was higher than that in the anode beaker due to a mass transfer from the anolyte to the catholyte (134, 135). It was reported that only solutions with low conductivities can form this floating water bridge, while water solutions with high conductivities due to different ions in it will not form the floating water bridge.

It has been simulated that water can conduct protons due to the nature of protons that can transfer via an interchange of chemical and hydrogen bonds across water molecules (136). Lee (15) suggested that water with excess protonic charges is a good conductor of protons and this makes water has a unique physiological properties. Contrary to Mitchell's delocalized proton

view, Lee postulated that excess protons may electrostatically localize at the water-membrane interface instead of staying in the bulk aqueous phase due to electrostatic repulsion effect and the fast mobility of excess protons through the hydrogen bond network. It was suggested that the proton conduction along the water-membrane interface might be a favored pathway for the proton energy coupling bioenergetics across biological membranes (15, 22, 53). Furthermore, it has been experimentally demonstrated in Chapter 2 that excess protons indeed do not stay in water bulk phase; they localize at the water-membrane interface in a manner similar to the behavior of excess electrons in a conductor (106). This experimental finding supported Lee's proton-electrostatic localization model that excess protons do not stay in the water bulk phase; they localize at the water-membrane interface.

Conductance is the reciprocal of electric resistance (ohm) and its units is in Siemen. When dealing with bulk material it is convenient to measure its specific conductance rather than just conductance. Specific conductance of a substance is commonly known as conductivity which is the electrically measured conductance of the material of 1 cm length having 1 square cm as area of cross section. Conductivity of water can be defined as the ability of water to conduct electric current. It increases with increasing the amount of mobile ions in water which are the electric charge carriers. Its unit is in microsiemen per centimeter and it is the reciprocal of resistivity (Ω-cm). For example, fresh ultrapure water has a conductivity of 0.055 µS/cm which can also be expressed as $(1/ (0.055 \times 10^{-6} \ Scm^{-1}))$ that is 18.2 $\times 10^{-6}$ ohms-cm (18.2 MΩ-cm).

It is worthwhile to note that the conventional electrical resistivity of water is measured typically with non-electrolytic high frequency AC probing voltage which does not drive water electrolysis process. Because of the use of non-electrolytic high-frequency AC probing voltage that does not electrolyze water; no excess protons are generated in the water body during

conventional electrical resistivity measurement. Therefore, the conventional water electrical resistivity measurement would not accurately measure the conductivity of water with respect to excess protons.

The purpose of this work is to further demonstrate the behavior of excess protons in a pair (anodic and cathodic) of separated water bodies and then to measure the DC conductivity of water with respect to excess protons using a water column inside a silicon tube that connects two chambers of pure deionized water. The conductivity of any conducting material can be determined by measuring the resistance of the material (or solution) in a cell of predefined length and cross sectional area. Therefore, measurement of the proton conduction in ultrapure water was performed by joining two separate chambers containing pure water by a bridge (silicon tube) of variable predefined lengths and diameter. This silicon tube had a continuous column of water that was free from any gas bubbles. The experiment was performed under Direct Current (DC) by sweeping voltage starting with low non water-electrolyzing potential (voltages) and ending with high water-electrolyzing potential. By this setup, we were able to measure the DC conductivity of water with respect to excess protons. The experimental current and resistance were measured, compared to the theoretical value and the DC proton conductivity was estimated.

4.2 MATERIALS AND METHODS

4.2.1 Demonstration of localized excess protons on proton sensing film using two isolated water chambers

Two Teflon chambers (Hoefer®, ElectroPrep SP-741196) were placed 30 cm apart and filled with 550 ml of ultrapure de-ionized water (Figure 17). Proton sensitive membrane (Al) were applied in both chambers on the chamber side and suspended in the middle bulk aqueous phase. In the anode chamber small amount of sodium bicarbonate salt was added every hour to reach

(50 mM, 100 mM, 200 mM, 300 mM, 400 mM, 500 mM, 600 mM and 700 mM) concentrations. After each addition, 200V was applied to the two isolated water chambers.

The initial pH of the deionized water was measured separately in a small beaker using Inlab pure pro ISM pH probe (Mettler Toledo Cat. No. 51344172) designed to measure pH for aqueous samples with very low ionic strength, including ultra-pure water. The final pHs of the solutions in both chambers were measured at the end of experiment by recording 6 pH readings for each sample and averaging them to minimize uncertainty.

Figure 17. Schematic diagram of experimental apparatus, consisting of two Teflon chambers that were placed 30 cm apart, filled with 550 ml of ultrapure water showing distribution of excess protons and excess hydroxides in both the anode and the cathode chambers under the influence of applying electrolyzing potential when the electrodes are polarized.

4.2.2 Evaluating the conductivity of water with respect to excess protons

Two chambers made of Teflon were filled with 600 ml of ultrapure de-ionized water (MilliQ, Millipore Corporation, USA) at room temperature 22.5 ºC. The initial conductivity of the ultrapure deionized water was measured with an AC conductivity meter integrated within the Millipore synergy water system and was determined to be 0.055 μS cm^{-1} (resistivity 18.2 MΩ.Cm at 22.5 ºC). This conductivity increased to 0.75 – 0.80 μS cm^{-1} due to equilibration with the atmospheric carbon dioxide (137). The two water chambers were positioned 30 cm apart (away from one another with 30 cm air gap) and were connected together through a tube (made of silicon) that has a continuous column of water (Appendix B, Figure S4). Tube lengths of (50, 100, 150, 200, 275, 350 cm) and of diameter (0.3 cm) were used as shown in Figure 18. The opening of each of these tubes was immersed in the liquid water at a distance 5 cm away from the electrode surface. The experiment was performed under Direct Current (DC) by sweeping voltage using digital multimeter system (Keithley instruments series 2400S-903-01 Rev E). Different voltages were applied, starting with low non water-electrolyzing potential 0.2 V, and ending with high water-electrolyzing potential 210V. In all experiments, the resulting electric current (I) and resistance (R) were measured using the same digital electrometer integrated -via GPIB cable - with KickStart (version 1.8.0) software. The voltages applied were (0.2, 0.3, 0.6, 1, 1.3, 1.5, 3, 6, 12, 25, 50, 100, 120, 150, 175, 200, and 210V) with 217 measurements (I and R) each and 0.5 second time delay between each measurement. The electric current and the resistance measurement were recorded for a period of 120 seconds. When the measurement reached equilibrium state (usually happens after 20 sec), the measured current/resistance in the steady state region (from time 20s to 120s) were averaged and this was done for each applied voltage.
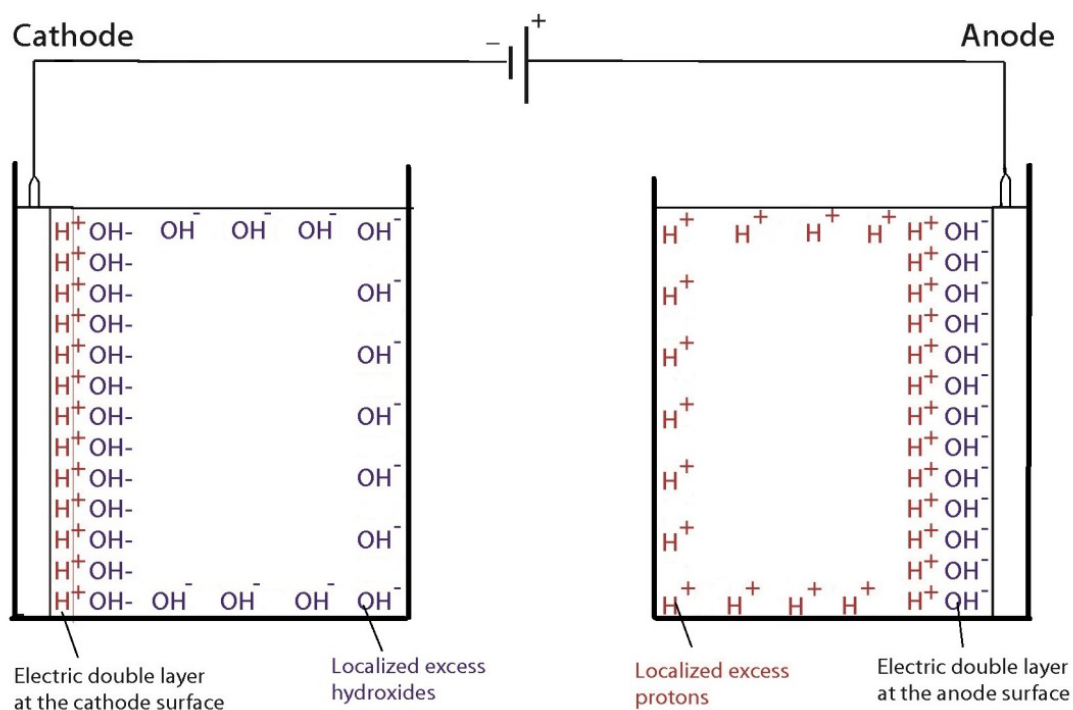
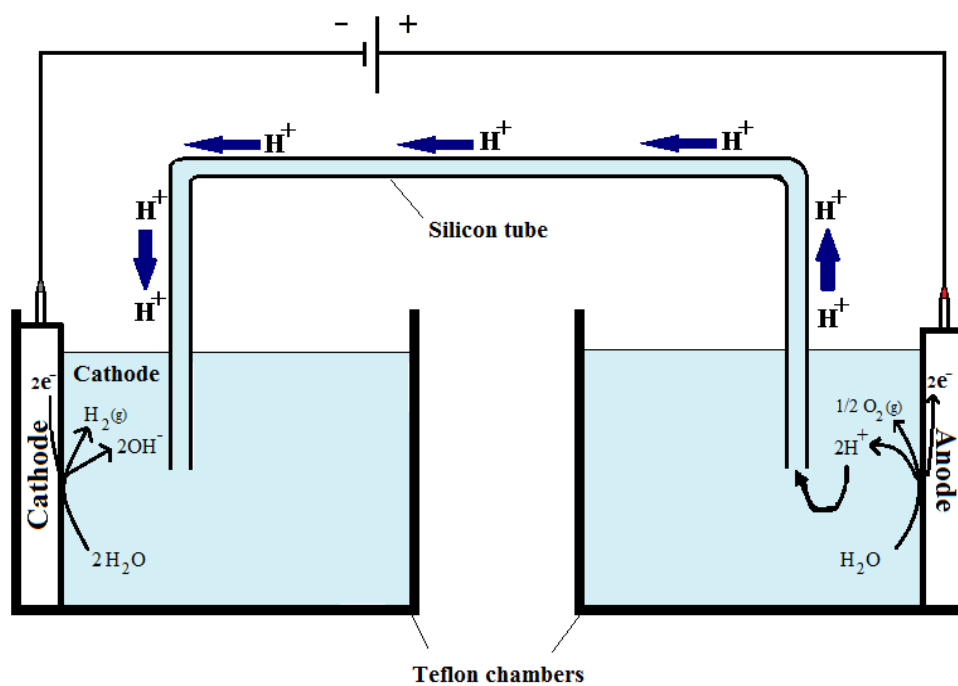**Figure 18.** Schematic diagram of experimental apparatus, consisting of two Teflon chambers that were placed 30 cm apart, filled with 600 ml of ultrapure water. The figure shows the protonic movement from the anode to the cathode to maintain electro-neutrality under the influence of applying electrolyzing potential when the two Teflon chambers are connected with a continuous column of water in a silicon tube bridge of 0.3 cm diameter.

The conventional conductivity measurement for the liquid water samples was performed using a Beckman coulter conductivity probe (Model 16 x 120 mm, item no. A57201). To ensure the quality of the ultrapure MilliQ-deionized water, the pH of the source deionized water was checked separately by pouring a small fraction of it into a separate 50-ml beaker and measuring its pH using Inlab pure pro ISM pH probe (Mettler Toledo Cat. No. 51344172). This pH electrode is mainly designed to measure pH for aqueous samples with very low ionic strength, including ultra-pure water. In addition, since pure water have very low ionic strength, pHISA pH ionic strength adjustor (Cat. No. 700003 Thermo Fisher Scientific Chelmsford, MA 01824 USA) was added to the small fraction of water in order to get a rapid, stable and precise pH measurement. The sample was prepared by adding 0.5 ml of pHISA pH ionic strength adjustor to 50 ml water sample. Two point calibrations were performed using a buffer of pH 7.00, and a buffer of pH 4.01, according to manufacturer instructions. Also the bulk phase pH of the deionized water was measured in the anode and cathode chambers at the end of each experiment. Six pH readings were recorded and the averages were taken to minimize uncertainty.

For visual evaluation of pH in both chambers, 5 ml aliquots from both the catholyte and the anolyte were added in two small 50 ml beakers. 5 drops of universal pH indicator solution (Cat. No. 36828 Farbskala, Fluka analytical, Germany) of pH range 4 to 10 were added to the 5 ml aliquots in each beaker. Both the pH and the conductivity of a reference water sample were measured during the period of the experiments.

4.3 RESULTS AND DISCUSSION

4.3.1 Demonstration of localized excess protons on proton sensing film using two isolated water chambers

When 200V was applied to the two isolated water chambers that were placed 30 cm apart in which the anode chamber had sodium bicarbonate solution (700 mM final concentration as shown in the methods section), the proton sensing films placed at side surface of the anode chamber solution integrated within one end of the center chamber assembly showed -after 10 hours- localized proton activity. Meanwhile there was no observable proton activity for the proton sensing film suspended in the bulk liquid phase of the anode as shown in Figure 19. The proton-sensing detection employed here was in the form of Al surface corrosion when the proton concentration was above 0.1 mM (equivalent to a pH value below 4) (92, 93). This indicated that excess protons were distributed at the water surface in the anode chamber as predicted by proton electrostatics localization hypothesis and not in the bulk aqueous phase, which clearly rejects the Mitchellian proton delocalized view.

Interestingly, when 200V was applied to the two isolated water chambers that were filled with 550 ml of ultrapure de-ionized water (without the addition of sodium bicarbonate), the proton sensing films placed at side surface of the anode chamber solution had no change after 10 hours. This indicates the localized excess proton population density at the anode chamber solution side surface is not high enough to be sensed by the Al film. This could be attributed to the relatively limited production of excess protons in pure water compared to that of the bicarbonate solution in the anode chamber during the open-circuit electrolysis. In the latter, the so-created localized proton population density in the isolated bicarbonate solution was high enough to be detected by the Al film placed at the anode chamber solution side surface. We believe that adding bicarbonate salt to pure water (pH 5.87 ± 0.01) would slightly raise the water pH value (in a range from pH 8.41 to 8.31) creating more hydroxyl groups that could be oxidized

at the anode to O_2 gas and protons, and hence increasing the excess proton production which can be detected by the proton sensing films.

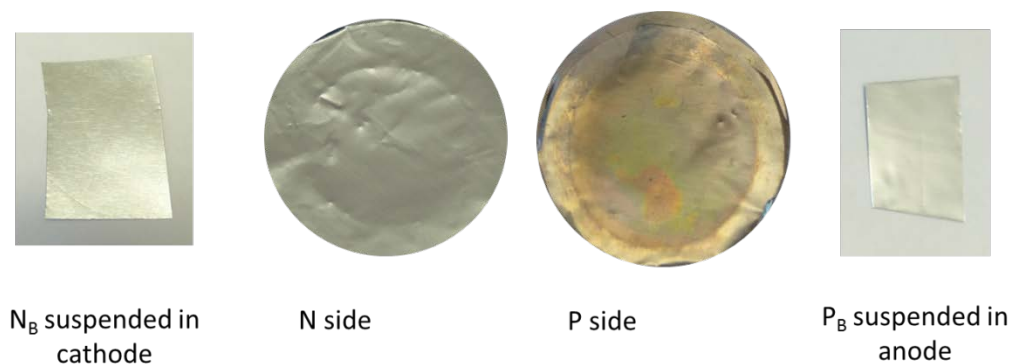N_B suspended in cathode   N side   P side   P_B suspended in anode

Figure 19. Observations of the proton-sensing Al films that were placed in the two isolated water chambers experiment after applying 200 V. N: Proton-sensing film placed at the N side surface facing the catholyte water that has excess hydroxides detected no proton activity. P: Proton-sensing film placed at the P side surface facing the anolyte chamber detected significant activity of localized protons. N_B: Proton-sensing film suspended inside the water of the cathode chamber. P_B: Proton-sensing film suspended inside the water of the anode chamber. The initial water pH at the beginning of the experiment was 5.87 ± 0.02. While at the end of the experiment, the pH of the catholyte (water) was 5.84 ± 0.01 and the pH of the anolyte containing sodium bicarbonate solution was 8.31 ± 0.01 (See Appendix C, Table S25 for more detailed information).

4.3.2 Evaluating the conductivity of water with respect to excess protons

The initial conductivity of the ultrapure deionized water was measured with an AC conductivity meter integrated within the Millipore synergy water system and was determined to be 0.055 µS cm^{-1} (resistivity 18.2 MΩ.cm at 22.5 °C). This conductivity was due to the equilibrium concentration of H_3O^+ and OH^- that results from the self-dissociation of water (107). This conductivity value was also matching the theoretical value for the pure water conductivity when

using the ionic equivalent conductivities of the self-dissociation products and the dissociation constant of water at 25 ºC (138, 139).

Although glass is considered inert and unreactive material, Hench et al (140) have showed that there is trace amounts of (Na^+, K^+, Mg^{2+}, Zn^{2+} and Ca^+) dissolve from the glass beaker into the ultrapure water. However, their concentrations are negligible and would not contribute to the overall water conductivity but their diffusion/leaching might increase when high voltage is applied to pure water in glass containers. In order to prevent this, we have carried our experiments in inert Teflon chambers instead of glass beakers.

During electrolysis process, excess protons were produced in the anode chamber where they reside at the water-membrane interface rather than the bulk water as we demonstrated before in Chapter 2. If the anode water chamber was connected to the cathode via a column of water, we expect that the protonic excess charges will transfer rapidly through the water column (bridge) and be reduced to molecular hydrogen or recombine in the cathode water chamber with the negative hydroxide charges to form water molecule and to maintain electro-neutrality. This transfer mechanism is shown in Figure 18 and was confirmed by the pH measurements that showed no difference between the anode (5.73 ± 0.048) and the cathode (5.73 ± 0.06) chambers as shown in Table 8. This protonic movement was also hypothesized by Sammer et al when they observed a mass transfer of water from the anolyte to the catholyte under the influence of very high applied potential (~30 kV) (141). It is important to mention that the pH for the anode chamber and the cathode chamber was nearly the same at the end of the experiment regardless the tube was connected or quickly removed.

Table 8. Averaged pH values measured in bulk water phase before and after the experiment.

Experiments (tube length)		pH of Cathode Water	pH of Anode Water	pH of control
50 cm	Before	*5.82 ± 0.17*	*5.82 ± 0.17*	*5.82 ± 0.17*
	After	*5.73 ± 0.06*	*5.73 ± 0.05*	*5.72 ± 0.00*
100 cm	Before	*5.93 ± 0.21*	*5.93 ± 0.21*	*5.93 ± 0.21*
	After	*5.75 ± 0.07*	*5.75 ± 0.06*	*5.85 ± 0.01*
150 cm	Before	*6.05 ± 0.23*	*6.08 ± 0.23*	*6.08 ± 0.23*
	After	*5.72 ± 0.01*	*5.65 ± 0.04*	*5.71 ± 0.01*
200 cm	Before	*6.18 ± 0.02*	*6.18 ± 0.02*	*6.18 ± 0.02*
	After	*5.64 ± 0.08*	*5.60 ± 0.07*	*5.69 ± 0.01*
275 cm	Before	*6.09 ± 0.03*	*6.09 ± 0.03*	*6.09 ± 0.03*
	After	*5.67 ± 0.07*	*5.67 ± 0.06*	*5.67 ± 0.11*
350 cm	Before	*6.21 ± 0.01*	*6.21 ± 0.01*	*6.21 ± 0.01*
	After	*5.73 ± 0.02*	*5.70 ± 0.00*	*5.72 ± 0.00*

When applying voltages below 1.23V, the electrode surface started to be polarized by attracting H^+ and OH^- ions resulting from the natural self-dissociation of pure water and forming Gouy-Chapman-stern double layer at the charged electrode-water interface as illustrated in Figure 17. To determine the conductivity of water with respect to excess protons, the first 20 sec of current versus time measurements were excluded since they represent the charging current in which the counter ions bearing opposite charges tend to accumulate on the charged electrode surface forming a stationary stern layer. For example, in the anode chamber the HCO_3^- from the atmospheric carbon dioxide and the OH^- ions form the self- dissociation of water molecules could migrate and accumulate at the surface of the anode forming the first layer (stern layer) of

the diffused double layer. Since we are not interested in the current in the first 20 seconds, we have averaged the current measured after 20 seconds when it reached steady state as shown Figure 20. The measurements averaged (from 20 sec to 120 sec) after the elapse of the first 20 sec represented the current due to proton conductance under DC voltage.
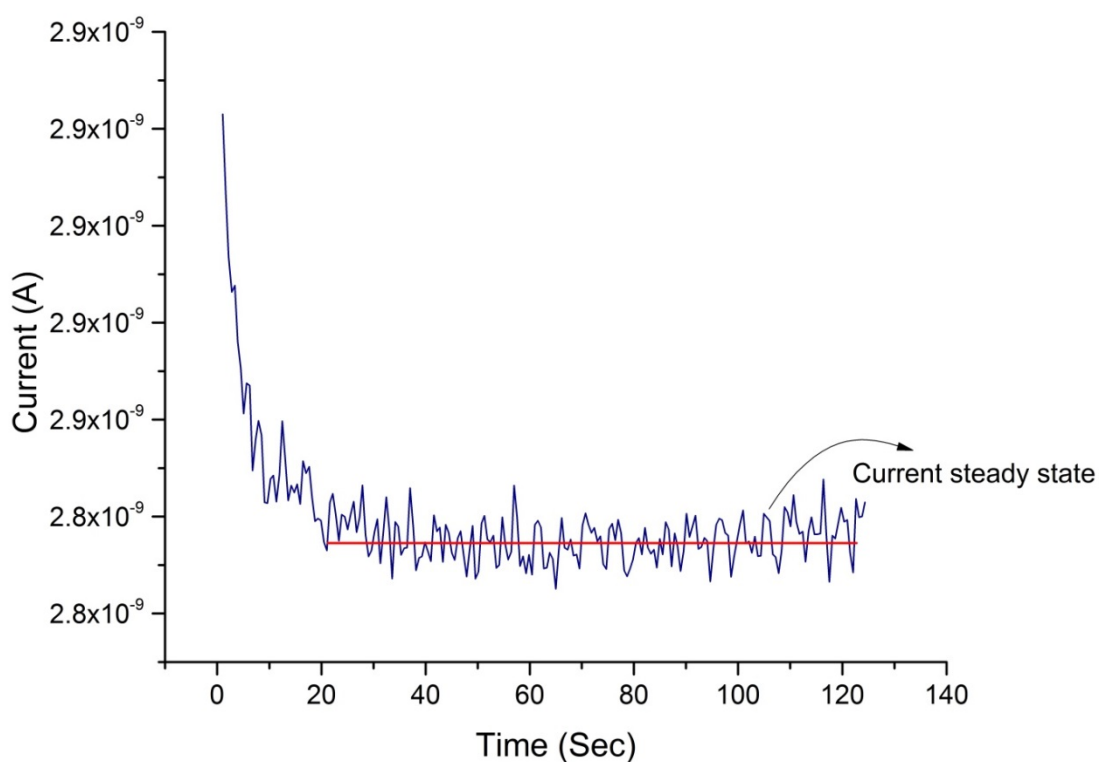

Figure 20. Example for current measurement versus time for the 350 cm tube length when 12 V was applied. After the elapse of 20 seconds, the current steady state was reached which represented the current due to proton conductance under DC applied voltage.

It is well known that water electrolysis which entails molecular hydrogen and oxygen evolution occurs thermodynamically when the applied potential difference is above 1.23V.

Accordingly, significant DC electric current started to be observed when the applied potential is above 1.23V as shown in Figure 21. Electrolytic ionization of water created excess protons and excess hydroxides which were carriers for electric charge. Excess protons are fast carriers that transfer the electric charge so quickly producing electrolytic current flow. Increasing the voltage created more mobile ions in form of excess protons in anode chamber and excess hydroxyl anions in cathode chamber which were electric charge carriers that resulted in electric current increase. The water column in the silicon tube was acting as an aqueous protonic resistor limiting the current and the movement of protons. The effect of the tube length containing the water column on the current measurement was observed in which shorter tubes made shorter bridges with low protonic resistance and hence more proton conductance (more proton flow) while longer tubes made longer bridges with high protonic resistance and hence lower proton conductance (Low proton flow) as shown in (Appendix B, Figure S6). When plotting the measured resistance versus the applied voltage, it was noticed that the resistance slightly decreased when the applied voltage was above 1.23 V, indicating that our system behaved in a non-ohmic manner. In addition, longer water columns were observed to have higher protonic resistance while shorter water columns were observed to have lower resistance as shown in (Appendix B, Figure S7).
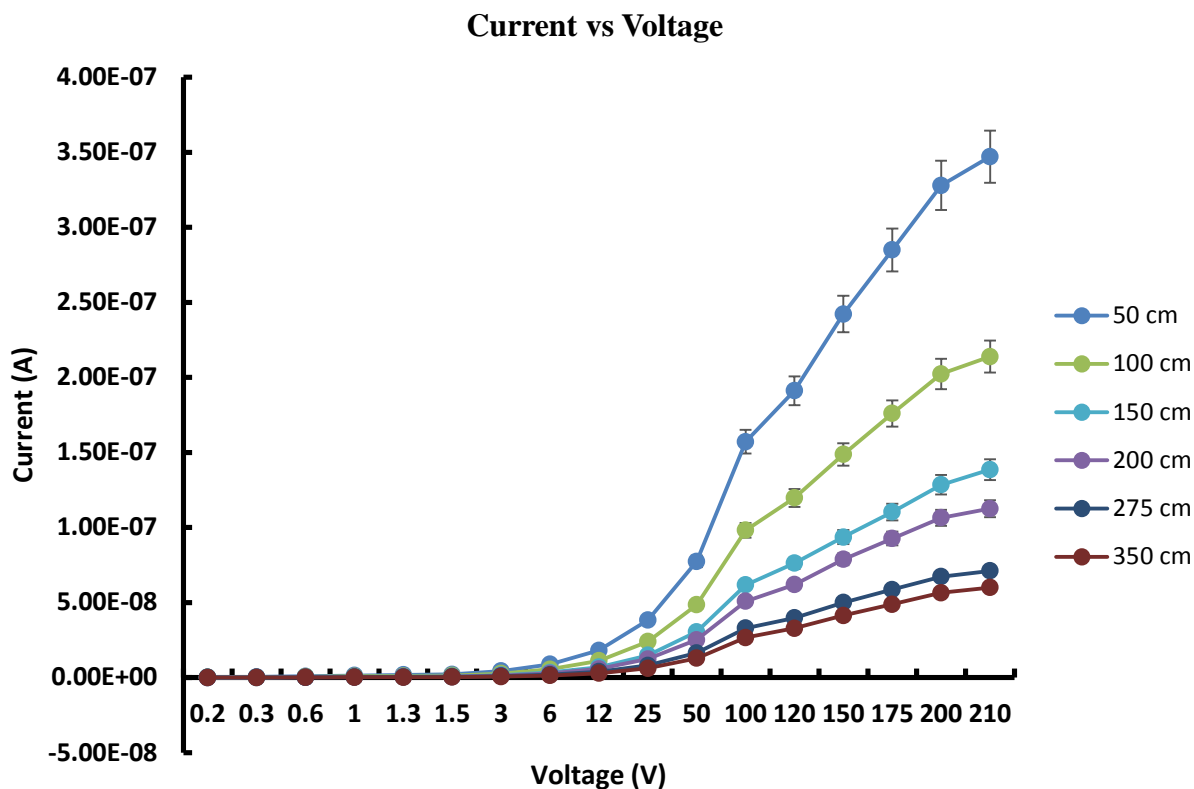
Current vs Voltage

Figure 21. Plot of current versus voltage showing the electric current was increasing gradually above 1.3V due to water electrolysis into H_2 and O_2 by increasing the voltage. Ionization of water created excess protons and excess hydroxides which were carriers for electric charge. Excess protons are fast carriers that carry the electric charge so quickly producing electrolytic current flow. Increasing the voltage created more mobile ions which were the electric charge carriers and this lead to an increase in the electric current. The effect of tube length including the water column on the detected current was well observed. Shorter tubes constituted shorter bridges of lower resistance and hence more proton conductance (more proton flow) while longer tubes constituted longer bridges of higher resistance and hence lower proton conductance (Low proton flow).
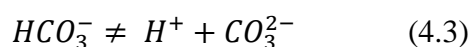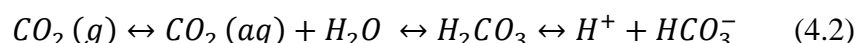
The water pH measurements were performed before the electrolysis process in a separate beaker. While after electrolysis, the pH was measured for 5 ml aliquots from both the anode and cathode chambers that were introduced into two small 50 ml beakers as reported in the method

section. It is worth mentioning that regular pH electrodes response in pure water is usually slow, drifting and unstable since pure water has very low conductivity and low ionic strength. In order to better measure the pH of pure water, a low resistance glass pH electrode (Mettler Toledo inlab pure pro) was used. This electrode showed improved stability and response especially after adding ionic strength adjustor (Thermo Scientific Orion pHISA). The ionic strength adjustor increases the ionic strength of the sample without altering its pH (shift was only 0.005-0.01 pH units which was negligible). Also 6 pH readings were recorded and the averages were taken to minimize uncertainty. As shown in Table 8, pH values for both the anode and the cathode chamber water at the end of the experiment were in the range from (5.60 ± 0.07) to (5.75 ± 0.06) which was quite similar to the control pH. The drop in the pH was due to the atmospheric carbon dioxide dissolution into the water samples. This physical phenomenon of equilibrated atmospheric carbon dioxide in the aqueous phase was described by Henry's law (142):

$$[CO_2(aq)] = K_{H(CO_2)} \, P_{CO_2} \qquad (4.1)$$

Where: $[CO_2]$ (mol/L) is the equilibrium concentration of carbon dioxide in the aqueous phase, K_H is the Henry's law constant for carbon dioxide (3.38×10^{-2} mol/L.atm at 25 °C), and P_{CO2} is the partial pressure of the gas in the bulk atmosphere (atm). Under standard atmospheric conditions, the equilibrium concentration of carbon dioxide in the aqueous phase$[CO_2 \, (aq)]$ can be easily calculated using henry's law (equation 4.1). Since on average, carbon dioxide make up 0.0355% of atmosphere, the partial pressure of carbon dioxide (P_{CO2}) in the atmosphere would be 0.000355 atm. Therefore, the concentration of the dissolved carbon dioxide in aqueous phase $[CO_2 \, (aq)]$ would be 1.2×10^{-5} mol/L. Carbon dioxide in aqueous phase could form small amount of carbonic acid that has two protons and consequently two dissociation constants.

However, the second dissociation constant of carbonic acid (equation 4.3) is so small compared to the first dissociation constant (equation 4.2) and therefore it can be neglected. Since the first acid equilibrium reaction is the predominant one, the equilibrium expression (equation 4.4) could be simplified to equation 4.5 because both the proton and the bicarbonate concentrations are equal. The theoretical [H$^+$] can now be determined from equation 4.5 when $[CO_2\,(aq)] = 1.2$ x 10^{-5} mol/L is substituted. Solving for the pH, one would get a theoretical pH of 5.64. Our reference water pH was measured to be in the range 5.6 to 5.8 as shown in Table 8 which was in agreement with the theoretical pH. The conventional electrolysis which entails pH change was not observed during our experiment which was also reported by Fuchs etal (143). This observation was also so clear upon investigation of the color of the universal pH indicator solution (pH range 4-10) when added to 5 ml aliquots from the anolyte and the catholyte. Both solutions had the same pH in the range from 5.5 to 6.0 as indicated in the pH color chart which is shown in Figure 22.

$$CO_2\,(g) \leftrightarrow CO_2\,(aq) + H_2O \ \leftrightarrow H_2CO_3 \leftrightarrow H^+ + HCO_3^- \qquad (4.2)$$

$$HCO_3^- \neq H^+ + CO_3^{2-} \qquad (4.3)$$

$$K_{A1} = \frac{[H^+][HCO_3^-]}{[CO_2(aq)]} = 4.45 \times 10^{-7} \qquad (4.4)$$

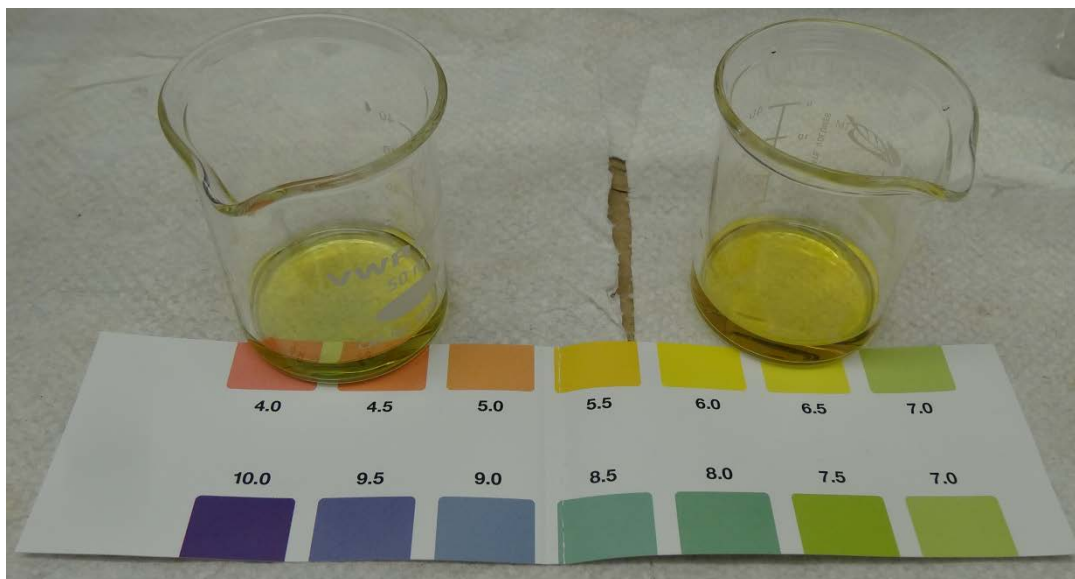$$K_{A1} = \frac{[H^+]^2}{[CO_2(aq)]} \qquad (4.5)$$

Figure 22. Aliquots from the anolyte (beaker on the right side) and the catholyte (beaker on the left side) after applying universal indicator solution (pH 4-10). Both solutions have the same pH in the range from 5.5 to 6.0 as indicated in the pH color chart.

Excess protons are fast charge carriers that transfer the electric charge so quickly producing electrolytic current flow. The mobility of the hydronium ion ($3.62 \times 10^{-3} \ cm^2 \ V^{-1} \ s^{-1}$) itself is relatively high, being five to seven times that of similarly sized cations (107, 122). H^+ and OH^- can move through water very rapidly and are very good charge carriers. However, not all ions can carry charge equally. For example, Na^+ (ionic mobility $0.53 \times 10^{-3} \ cm^2 \ V^{-1} \ s^{-1}$) and HCO_3^- (ionic mobility $0.46 \times 10^{-3} \ cm^2 \ V^{-1} \ s^{-1}$) move in solution slower than H^+ (ionic mobility $3.62 \times 10^{-3} \ cm^2 \ V^{-1} \ s^{-1}$) and therefore doesn't conduct electricity as efficient as protons. Accordingly, water with excess protons has high proton-electrical conductance than any water with any other charge. But the problem is that these excess protons couldn't be measured by conventional ways. Consequently the water electrical conductance with respect to these excess

protons is so challenging to evaluate. It is worthwhile to note that the conventional electrical resistivity of water is measured typically with non-electrolytic high frequency AC probing voltage which does not drive electrolysis of water. Because of the use of non-electrolytic high-frequency AC probing voltage that does not electrolyze water; no excess protons are generated in the water aqueous phase during conventional electric resistivity measurement. Therefore, the conventional water electrical resistivity measurement would not accurately measure the protonic conductivity of water as it would significantly underestimate the true conductivity of water with respect to excess protons. In our experiment, DC protonic conductivity was determined by plotting specific resistance (R/L) versus (1/L) as shown in (Appendix B, Figure S5). The intercept was then determined by extrapolation of the straight line for each applied voltage. Then the intercept (R/L) was plotted versus (1/V) as shown in Figure 23. The resistivity which is (R/L) multiplied by cross sectional area and the conductivity which is the reciprocal of resistivity were determined and plotted versus applied voltage. For example, the intercept (R/L) for the 200 V series of the "(R/L) versus (1/L)" plot was determined to be 11677856.08 Ω/cm. From this value the resistivity was determined by multiplying it with the cross sectional area (0.071 cm^2) and it was found to be 829127.7817 Ω-cm. Then the conductivity (the reciprocal of resistivity) was determined to be 1.206 x 10^{-6} S/cm which was 22 times higher than the conventionally pure DI water conductivity measurement. It was found that the DC conductivity of excess protons increased slightly upon increasing the applied voltage as shown in Figure 24. This also explains why our observed experimental conductivity (0.990 x 10^{-6} S/cm) measured at 3V DC is 18 times more than the conventional AC conductivity measurement (0.055x10^{-6} S/cm) as shown in Figure 24. In fact, this discrepancy may be explained by understanding that liquid water is a proton conductor, where the "hop and turns" conduction of excess protons generated by electrolysis

may contribute to a much greater conductivity. To estimate the proton conductivity at extremely high voltage (> 210V), DC proton conductivity was plotted verses (1/V) (Figure 25) and the intercept was determined from the linear equation. The intercept represents the protonic conductivity at extremely high voltage which was estimated to be 1.28×10^{-6} S/cm by extrapolation. To get a better representative intercept, it is recommended to acquire data points at extremely high voltage magnitude (kilo volts) which requires a new experimental design that ensures safety of the operator.
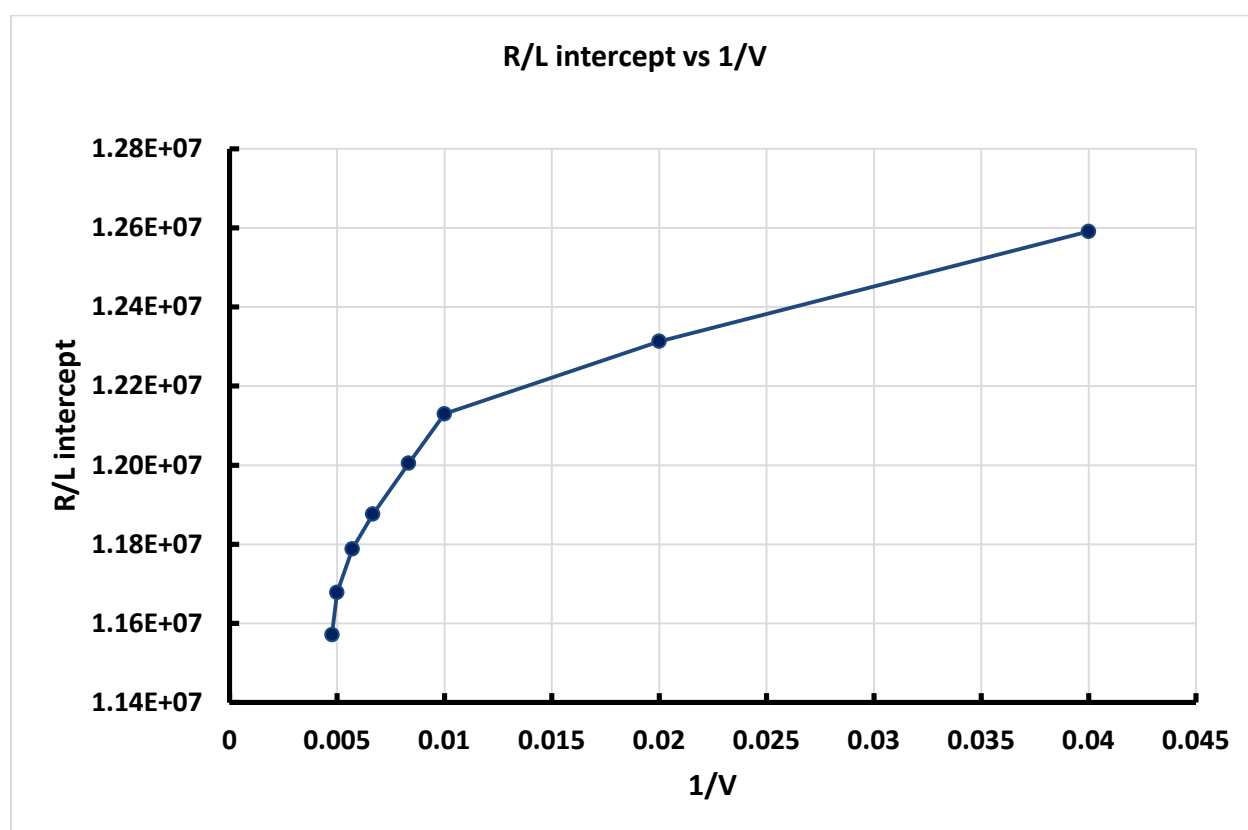

Figure 23. Shows a plot of intercept R/L versus 1/V. (average of three trials)
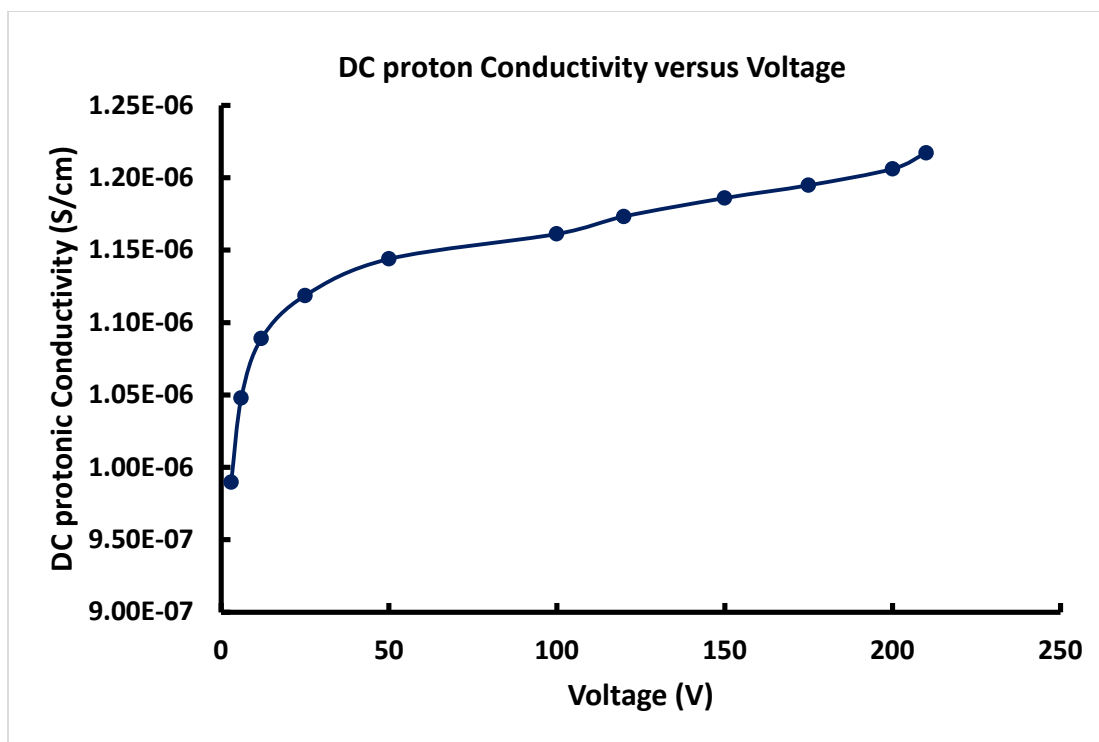
Figure 24. Plot of DC protonic conductivity (specific conductance) versus electrolytic voltage in a range from 3V to 210V. Conductivity increases by increasing voltage due to the conductivity of excess protons. (Average of three trials)
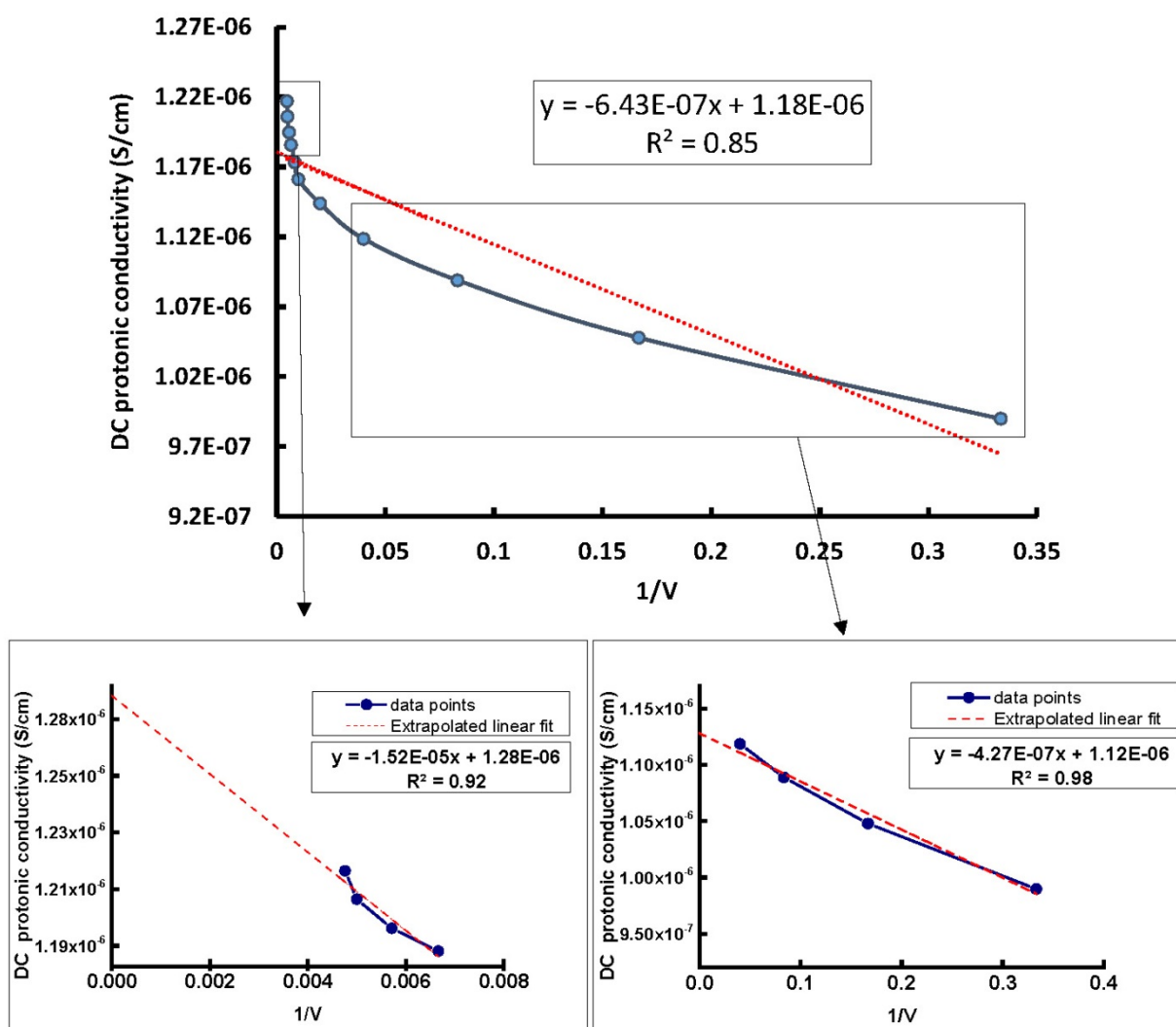
Figure 25. Plot of DC proton conductivity versus 1/V. The data points were fitted with a linear equation and the intercept was determined. The top graph shows the liner fitting with all data points. The bottom left graph shows the liner fitting with only the first 4 data points. The bottom right graph shows the linear fitting with only the last 4 data points. The intercept represents the linear extrapolation for the proton conductivity at extremely high voltage.

4.4 CONCLUSION

In this study we demonstrated experimentally that water is a proton conductor and we showed that there is a protonic charge transfer from anode water chamber to cathode water chamber via the water tube connection. Although the protonic current conduction mechanism is still unclear so far, we demonstrated that the water protonic conductivity increases with increasing the applied voltage. This indicates that the mobility of excess protons exceeds the mobility of any other ions in liquid water. This could explain why the DC experimental conductivity (1.206×10^{-6} S/cm) measured at 200V is 22 times more than the conventionally measured water conductivity (0.055×10^{-6} S/cm). Our results and findings provide further evidences that excess protons in water is behaving like electrons in metallic conductor with a difference in the conduction mechanism. That is to say that ultrapure water is a good proton conductor although it is an insulator with low electric conductivity. The experimental result demonstrated that ultrapure water with excess protons can conduct electric/protonic charges so rapidly.

Our quantitative estimations for conductivity of water with respect to excess protons are still preliminary, because of some technical limitations in the present experiment. One of these limitations is the effect of the atmospheric carbon dioxide which contributes significantly to the overall water conductivity. Another limitation is the DC applied voltage which could lead to some polarization effects. Using high frequency AC applied voltage would eliminate the polarization effects. However, high frequency AC applied voltage would not create excess protons. Overall, this study demonstrated that water is a proton conductor with respect to excess protons. This supports Lee's assumption in proton-electrostatics localization hypothesis that liquid water can be treated as a proton conductor for proton coupling energy transduction in living organisms.

CHAPTER 5

CONCLUSIONS AND FUTURE WORK

5.1 CONCLUSIONS

This study aims to seek fundamental understanding of the complex processes that convert and store energy in living systems. The Lee proton-electrostatics localization hypothesis with its associated new pmf equation (1.6) would significantly modify Mitchell's classic chemiosmotic theory in many textbooks. This dissertation attempts to verify the proton-electrostatics localization hypothesis which could help understanding the importance of water not only as a solvent and substrate but also as a proton conductor for proton coupling energy transduction. The knowledge gained from this work will certainly increase our understanding of the processes and mechanisms of biological energy transduction and storage, which could improve biochemical pathways for biofuel production, and next generation energy conversion/storage devices.

The experimental results reported in Chapter 2 clearly demonstrated that excess protons were localized at the water-membrane interface in the anode water-membrane-water cathode system. The most remarkable evidence for the localized excess protons came from the observation that the proton-sensing film placed at the P_I site of Teflon membrane facing the anode liquid showed proton-associated corrosion while the proton-sensing film placed in the bulk liquid phase (P_B) of the anode chamber showed no proton-associated corrosion activity during the entire experiment. This is a significant observation since it indicates that excess protons are localized primarily along the water-membrane interface at the P_I site, but not in the bulk liquid phase (P_B). The density of localized excess protons created in this experiment was estimated to be about 1.19 mM H^+ (pH value of 2.92) at the water-membrane interface (P_I site), which explains why it can be sensed by the proton-sensing Al membrane. Furthermore, the bulk-

phase pH measurements in both anodic and cathodic water chambers also confirmed that excess protons do not stay in the bulk aqueous phase, which clearly rejects the Mitchellian proton delocalized view. These observations clearly match with the predictions from the proton-electrostatics localization hypothesis that excess protons do not stay in the water bulk phase; they localize at the water-membrane interface in a manner similar to the behavior of excess electrons in a conductor.

The next step was testing the effect of other non- proton cations on the stability of the localized excess protons at a water–membrane interface and determining their exchange equilibrium constant. The experimental results reported in Chapter 3 showed that there is an inverse proportionality between the concentration of the salt solution and the corrosion activity of the proton sensing film placed at P′ site. By increasing the salt concentration inside the small Teflon center chamber, the proton-sensing corrosion activity of the aluminum membrane placed at P′ site would decrease till showing no proton activity when the salt concentrations are above 200 mM for both sodium and potassium salt solutions. This was attributed to the delocalization of the localized protons at the water–membrane interface through cation exchange by the added cations of the salt solution.

According to the proton electrostatic localization hypothesis, the equilibrium constant for protons to electrostatically occupy the cation sites at the water-membrane interface (in any possible competition with any other cations) is likely to be extremely larger than one. Conversely, the equilibrium constant K_{Pi} for non-proton cations such as Na^+ to delocalize the localized protons from the membrane-water interface is expected to be extremely smaller than one. Through our experiments mentioned in Chapter 3, we have now determined experimentally for the first time that the equilibrium constant for non-proton monovalent cations to exchange

with the electrostatically localized protons is indeed much less than one (likely on the order of 10^{-8}). The equilibrium constant K_{PNa^+} for sodium (Na^+) cations to exchange with the electrostatically localized protons was determined to be (5.07 ± 0.46) x 10^{-8}. Similarly, the equilibrium constant K_{PK^+} for potassium (K^+) cations to exchange with the electrostatically localized protons was determined to be (6.93 ± 0.91) x 10^{-8}. These results mean that the localized protons at the water-membrane interface are so stable that it requires ten million more sodium (or potassium) cations than protons in the bulk liquid phase to even partially delocalize the localized protons at the water-membrane interface. This provides a logical experimental support of the proton electrostatic localization hypothesis. It may also have fundamental implications in understanding the salinity tolerance in biological systems in relation to localized proton coupling bioenergetics.

The final goal in this dissertation was to test the first assumption of the proton electrostatic hypothesis that "liquid water is a proton conductor". In Chapter 4 we demonstrated experimentally that water is a proton conductor and we showed that there is a rapid protonic charge transfer from anode water chamber to cathode water chamber. We also demonstrated that the protonic conductivity increases with increasing the applied voltage and that the mobility of excess protons exceeds the mobility of any other ions in liquid water. This could explain why the experimental conductivity (1.206 x 10^{-6} S/cm) measured at 200V is 22 times more than the conventional conductivity measurement (0.055x10^{-6} S/cm). Our results and findings provide further evidences that excess protons in water is behaving like electrons in metallic conductor with differences in the conduction mechanism. That is to say that ultrapure water with excess protons can no longer be considered just as an insulator of low electric conductivity. The experimental result demonstrated that ultrapure water with excess protons can conduct

electric/protonic charges so rapidly. Our quantitative estimations for conductivity of water with respect to excess protons are still preliminary, because of some technical limitations in the present experiment. One of these limitations is the effect of the atmospheric carbon dioxide which may contribute significantly to the overall water conductivity. Another limitation is the DC applied voltage which could lead to some polarization effects. Using high frequency AC applied voltage would eliminate the polarization effects. However, high frequency AC applied voltage would not create excess protons.

In conclusion, these findings have significance not only in the science of bioenergetics but also in the fundamental understanding for the importance of water to life. The experimental findings presented in this research support Lee's assumption in proton-electrostatics localization hypothesis that water can be treated as a proton conductor for proton coupling energy transduction in living organisms.

5.2 FUTURE WORK

There are multiple research directions that would be logical extensions to this research. The most intriguing expansion would be to continue the work that focuses on detection of localized excess protons in living cells on the phospholipids membrane during the photosynthetic or oxidative phosphorylation process using ^{31}P-NMR. For example, chloroplasts can be prepared by gentle homogenization of fresh leaves (e.g., spinach, peas, or lettuce) using cold isolation buffer (isotonic sucrose or 0.33M sorbitol, 2 mM Ascorbic acid, 5 mM $MgCl_2$, and 10 mM $Na_4P_2O_7$. $10H_2O$) adjusted to pH 6.5. After removal of cell debris and broken cells via filtration, the chloroplasts can be precipitated by low-speed centrifugation. The thylakoids can be then

extracted from the chloroplasts and further purified using washing buffer (0.05 M Sorbitol, 2 mM EDTA, 1 mM $MgCl_2$, 50 mM HEPES) of low sorbitol concentration that can cause chloroplast rupture by osmotic shock. Multiple re-suspensions/centrifugations in the washing buffer would be necessary to precipitate out starch form the thylakoids. The percentage of thylakoid intactness can be then determined from the ratio of ferricyanide reduction before and after osmotic shock (144). It is important to ensure careful and rapid preparation of thylakoids on cold ice environment to yield high proportion of intact thylakoids capable of reducing $NADP^+$ and driving the photosynthetic photophosphorylation (1, 73). Chlorophyll concentration can be determined spectrophotometrically and biological activity can be determined using Clark oxygen electrode to measure photosynthetic oxygen evolution in thylakoids (145, 146).

Once the thylakoids are isolated and their photosynthetic activities are characterized, nuclear magnetic resonance especially ^{31}P-NMR can be used to detect electrostatically localized excess protons on phospholipid membrane surface. DTT (electron donor to PS II), methyl viologen (electron acceptor from PS I), and reaction medium (50 mM Tricine- KOH, 10 mM sorbitol, and 3 mM $MgCl_2.6H_2O$) should be added to the thylakoid structure in order to induce the electron transport chain which generates proton gradient across the membrane.

It is known that ^{31}P-NMR is an insensitive technique. That's means that the acquisition time and the number of scans have to be increased significantly to increase signal to noise ratio. Accordingly, the following modifications can be done in order to achieve high signal to noise ratio and to shorten the experimental run to less than an hour instead of 12 hours:

1) Increasing the sample volume by using 15 mm outer diameter NMR tubes instead of the regular 5mm.

2) Running sample containing highly concentrated thylakoid suspension (~ 2 mg chlorophyll/ml) (147).

3) Running the sample at lower temperature (<7 °C) to enhance the signal strength. Chillers will be needed to cool down the sample during acquisition. At low temperature the spin of molecules and their nuclei decreases and when put in magnetic field the only thing affects the spin would be the magnetic strength not the temperature (148).

Actually, ^{31}P-NMR technique can be used to get information about bulk properties, but in such a complex thylakoid mixture, it does not reveal specific molecular properties. Therefore, the thylakoid sample should be run in presence and in absence of light. In dark condition, it is expected to get a signal close to 0.5 ppm due to membranous phosphorus (phosphate group of the lipid bilayer membrane) and another signal at higher chemical shift due to the inorganic phosphate (P_i). However, in light conditions in presence of electron donor (DTT) and electron acceptor compounds (Methyl Violgen), the phosphorus of the lipid bilayer membranous phosphate signal is expected to shift differently (to the right). This signal shift is expected due to the proton gradient generation across the membrane and consequently the presence of excess proton environment adjacent to phospholipid membrane. These excess protons are expected to reduce the de-shielding effect for the phosphorus nucleus. Consequently, the electron density around the ^{31}P nucleus would increase and shield it from the applied field, making the effective field experienced by the nucleus smaller. In order to proof that the membranous phosphorus shift is due the excess protons environment, another sample can be run in presence of ionophore such as valinomycine and KCl to eliminate the membrane potential. The valinomycine is expected to allow the migration of certain ions including Cl^- and K^+ across the thylakoid membrane, which would neutralize the electrostatic protons and thus cause proton delocalization as well.

To investigate the lateral proton diffusion (149) at a water-membrane interface, scanning electrochemical microscopy (SECM) can be used to determine the rate of proton transfer along phospholipid and mixed phospholipid/protein monolayers. The SECM is a powerful technique that can help resolving the longstanding controversy regarding the movement of protons between source and sink sites in biological membranes (150-152).

Another aspect of research interest would be the demonstration of the proton electrostatic effect by injecting protons using a proton beam into a biologically-relevant small water body. It is possible to determine charges on solid surfaces with definite domains by using scanning electric charge or potential measurement techniques like Kelvin force microscopy (153, 154). However, it is very challenging to apply these techniques to determine excess charges on liquid surfaces. Therefore, additional ways can be employed to detect localized protons within single and multi-water bodies such as the use of radiochromic film dosimetry (155) that has been used in measuring protons in the field of nuclear physics or using a Faraday Cup type charge collection detector that is specific to our apparatus (156). To perform this detection, it requires injecting considerable amount of excess protons into a small volume of water and subsequently monitoring their distribution using these techniques. This can be done by using a proton beam that can be generated by a proton accelerator machine as a source of excess protons for this experiment. The benefit of using a proton beam as a source of protons is that the proton dosage amount can be controlled by setting specific beam energy. A lower-energy proton beam at an energy level ~0.1-10 MeV is preferred to avoid undesirable nuclear physics-related secondary effects such as the generation of neutrons or x-rays when the high-energy proton beam interacts with the target water body. According to the proton electrostatic effect, the excess protons after injection should be distributed along the outer surface of the water body. Therefore, by

monitoring the distribution of the excess protons after their injection into the water body, we should be able to test the proton-electrostatics localization bioenergetics hypothesis and quantitatively determine the amount of excess protons on the surface in relation to the amount of excess protons in the bulk aqueous phase without worrying about any side reactions that could happen during the generation of excess protons using electrolysis process. In addition, it may also become possible to measure how long it takes for the protons to move to the surface by performing a pulsed beam cyclotron measurement.

To further analyze proton electrostatic localization and delocalization in a biologically-relevant water body, molecular dynamics (MD) computer simulations can be performed. The computer simulation can then be extended to a number of bioenergetics systems including thylakoids, mitochondria and bacteria. Continuum electrostatic methods can be used for studying membrane proteins theoretically in membrane environments. The electric field and potential distributions which force movement of charges (e.g. protons) can be calculated based on the Poisson-Boltzmann-Nernst-Planck model (157). The Poisson–Boltzmann (PB) equation (158) describes electrostatic interactions between molecules, and can be applied to ionic solutions (including the Gouy–Chapman double-layer theory (96)) and biomolecular structures such as biological membranes. To use this technique it should be assumed that: (a) the ionic charge distributions are smeared out and can be represented as smoothly varying continuum functions, (b) and the charge-charge correlations are negligible. Thus the discrete nature of the ions is not taken into account and no other molecular interaction between the ions and solvent molecules (water) is considered. The Nernst–Planck (NP) equation is used to describe the electro-diffusion of ions in terms of ionic concentrations. A coupled Poisson-Boltzmann-Nernst-Planck approach can be used for accuracy while reducing the number of mathematical equations. For example,

only the ions of interest in the transport process (e.g., protons) would be described by the Nernst-Planck (NP) equations. The rest would only be treated through the Poisson-Boltzmann model. Besides, it is well established that the NP approach is equivalent to the PB scheme for zero ionic fluxes (159).

Finally, the localized excess protons that have been demonstrated for the first time through this research may have practical implications as well. For example, the utilization of localized excess protons, that can be created in pure water, may lead to clean "green chemistry" technologies for industrial applications such as metal acid washing and/or protonation of certain micro/nanometer materials without requiring the usage of conventional acid chemicals such as nitric and sulfuric acids.

REFERENCES

1. Nicholls DG, Ferguson S (2013) *Bioenergetics* (Academic Press).

2. Skulachev V, Bogachev AV, Kasparinsky FO (2012) Principles of Bioenergetics. (Springer Berlin Heidelberg, Berlin, Heidelberg).

3. Garrett R, Grisham C (2013) *Biochemistry* (Brooks/Cole) 5 Ed.

4. Cramer WA, Knaff DB (2012) *Energy transduction in biological membranes: a textbook of bioenergetics* (Springer Science & Business Media).

5. Nelson DL, Lehninger AL, Cox MM (2013) *Lehninger principles of biochemistry* (Macmillan) 6 Ed.

6. Blankenship RE (2013) *Molecular mechanisms of photosynthesis* (John Wiley & Sons).

7. Arnon DI, Allen M, Whatley F (1956) Photosynthesis by isolated chloroplasts IV. General concept and comparison of three photochemical reactions. *Biochimica et biophysica acta* 20:449-461.

8. Allen JF (2002) Photosynthesis of ATP—Electrons, Proton Pumps, Rotors, and Poise. *Cell* 110(3):273-276.

9. Elston T, Wang H, Oster G (1998) Energy transduction in ATP synthase. *Nature* 391(6666):510-513.

10. Cross RL, Duncan TM (1996) Subunit rotation in F0F1-ATP synthases as a means of coupling proton transport through F0 to the binding changes in F1. *Journal of Bioenergetics and Biomembranes* 28(5):403-408.

11. Mitchell P (2011) Chemiosmotic coupling in oxidative and photosynthetic phosphorylation. *Biochimica et Biophysica Acta (BBA)-Bioenergetics* 1807(12):1507-1538.

12. Mitchell P (1966) Chemiosmotic coupling in oxidative and photosynthetic phosphorylation. *Biological Reviews* 41(3):445-501.

13. Ferguson SJ (1995) Chemiosmotic Coupling: Protons fast and slow. *Current Biology* 5(1):25-27.

14. Raven PH, Evert RF, Eichhorn SE (2005) *Biology of plants* (Macmillan).

15. Lee J (2012) Proton-electrostatics hypothesis for localized proton coupling bioenergetics. *Bioenergetics* 1(104):2.

16. Mitchell P (1961) Coupling of phosphorylation to electron and hydrogen transfer by a chemi-osmotic type of mechanism. *Nature* 191(4784):144-148.

17. Voet D, Voet JGP, Charlotte W, Judith GV, Charlotte WP (2013) *Fundamentals of biochemistry: life at the molecular level* (John Wiley & Sons).

18. Berg JM, Tymoczko JL, Stryer L (2012) *Biochemistry* (W.H. Freeman, Basingstoke).

19. Mathews CK (2013) *Biochemistry* (Pearson, Toronto).

20. Dilley RA (2004) On why thylakoids energize ATP formation using either delocalized or localized proton gradients–a Ca^{2+} mediated role in thylakoid stress responses. *Photosynth Res* 80(1-3):245-263.

21. Brändén M, Sandén T, Brzezinski P, Widengren J (2006) Localized proton microcircuits at the biological membrane–water interface. *Proceedings of the National Academy of Sciences* 103(52):19766-19770.

22.   Lee J (2015) Proton-electrostatic localization: explaining the bioenergetic conundrum in alkalophilic bacteria. *Bioenergetics* 4(121).

23.   Olsson K, Keis S, Morgan HW, Dimroth P, Cook GM (2003) Bioenergetic properties of the thermoalkaliphilic Bacillus sp. strain TA2. A1. *J Bacteriol* 185(2):461-465.

24.   Krulwich TA, Guffanti AA (1989) Alkalophilic bacteria. *Annual Reviews in Microbiology* 43(1):435-463.

25.   Krulwich TA (1986) Bioenergetics of alkalophilic bacteria. *The Journal of membrane biology* 89(2):113-125.

26.   Sturr MG, Guffanti AA, Krulwich TA (1994) Growth and bioenergetics of alkaliphilic Bacillus firmus OF4 in continuous culture at high pH. *J Bacteriol* 176(11):3111-3116.

27.   Padan E, Bibi E, Ito M, Krulwich TA (2005) Alkaline pH homeostasis in bacteria: new insights. *Biochimica et biophysica acta (BBA)-biomembranes* 1717(2):67-88.

28.   Mulkidjanian A, Cherepanov D, Heberle J, Junge W (2005) Proton transfer dynamics at membrane/water interface and mechanism of biological energy conversion. *Biochemistry (Moscow)* 70(2):251-256.

29.   Krulwich TA, et al. (2011) Adaptive mechanisms of extreme alkaliphiles. *Extremophiles handbook*:119-139.

30.   Krulwich TA, Gilmour R, Hicks DB, Guffanti AA, Ito M (1998) Energetics of alkaliphilic Bacillus species: physiology and molecules. *Advances in microbial physiology* 40:401-438.

31.   Krulwich TA (1995) Alkaliphiles:'basic'molecular problems of pH tolerance and bioenergetics. *Mol Microbiol* 15(3):403-410.

32. Guffanti AA, Krulwich TA (1988) ATP synthesis is driven by an imposed ΔpH or $\Delta\tilde{\mu}H+$ but not by an imposed ΔpNa^+ or $\Delta\tilde{\mu}Na^+$ in alkalophilic Bacillus firmus OF4 at high pH. *J Biol Chem* 263(29):14748-14752.

33. Guffanti AA, Hicks DB (1991) Molar growth yields and bioenergetic parameters of extremely alkaliphilic Bacillus species in batch cultures, and growth in a chemostat at pH 10.5. *J Gen Microbiol* 137(10):2375-2379.

34. Guffanti A, Krulwich T (1984) Bioenergetic problems of alkalophilic bacteria. *Biochem Soc T* 12(3):411.

35. Michel H, Oesterhelt D (1980) Electrochemical proton gradient across the cell membrane of Halobacterium halobium: comparison of the light-induced increase with the increase of intracellular adenosine triphosphate under steady-state illumination. *Biochemistry* 19(20):4615-4619.

36. Michel H, Oesterhelt D (1980) Electrochemical proton gradient across the cell membrane of Halobacterium halobium: effect of N, N'-dicyclohexylcarbodiimide, relation to intracellular adenosine triphosphate, adenosine diphosphate, and phosphate concentration, and influence of the potassium gradient. *Biochemistry* 19(20):4607-4614.

37. Heberle J, Riesle J, Thiedemann G, Oesterhelt D, Dencher NA (1994) Proton migration along the membrane surface and retarded surface to bulk transfer. *Nature* 370(6488):379-382.

38. Vinkler C, Avron M, Boyer PD (1978) Initial formation of ATP in photophosphorylation does not require a proton gradient. *FEBS letters* 96(1):129-134.

39. Williams RJP (1975) Proton-Driven Phosphorylation Reactions in Mitochondrial and Chloroplast Membranes. *FEBS letters* 53(2):123-125.

40. Williams RJP (1961) Possible functions of chains of catalysts. *Journal of Theoretical Biology* 1(1):1-17.

41. Williams R (1978) The multifarious couplings of energy transduction. *Biochimica et Biophysica Acta (BBA)-Reviews on Bioenergetics* 505(1):1-44.

42. Kell DB (1986) [40] Localized protonic coupling: Overview and critical evaluation of techniques. *Methods in Enzymology*, (Academic Press), Vol Volume 127, pp 538-557.

43. Kell DB (1979) On the functional proton current pathway of electron transport phosphorylation: an electrodic view. *Biochimica et Biophysica Acta (BBA)-Reviews on Bioenergetics* 549(1):55-99.

44. Dilley RA, Theg SM, Beard WA (1987) Membrane-proton interactions in chloroplast bioenergetics: Localized proton domains. *Annual review of plant physiology* 38(1):347-389.

45. Cherepanov DA, Feniouk BA, Junge W, Mulkidjanian AY (2003) Low Dielectric Permittivity of Water at the Membrane Interface: Effect on the Energy Coupling Mechanism in Biological Membranes. *Biophysical journal* 85(2):1307-1316.

46. Cherepanov DA, Junge W, Mulkidjanian AY (2004) Proton Transfer Dynamics at the Membrane/Water Interface: Dependence on the Fixed and Mobile pH Buffers, on the Size and Form of Membrane Particles, and on the Interfacial Potential Barrier. *Biophysical journal* 86(2):665-680.

47. Junge W, Haumann M, Ahlbrink R, Mulkidjanian A, Clausen J (2002) Electrostatics and proton transfer in photosynthetic water oxidation. *Philosophical Transactions of the Royal Society of London B: Biological Sciences* 357(1426):1407-1418.

48. Mulkidjanian AY (2006) Proton in the well and through the desolvation barrier. *Biochimica et Biophysica Acta (BBA) - Bioenergetics* 1757(5–6):415-427.

49. Mulkidjanian AY, Heberle J, Cherepanov DA (2006) Protons @ interfaces: implications for biological energy conversion. *Biochimica et biophysica acta* 1757(8):913-930.

50. Davenport JW, McCarty RE (1980) The onset of photophosphorylation correlates with the rise in transmembrane electrochemical proton gradients. *Biochimica et Biophysica Acta (BBA)-Bioenergetics* 589(2):353-357.

51. Sandén T, Salomonsson L, Brzezinski P, Widengren J (2010) Surface-coupled proton exchange of a membrane-bound proton acceptor. *Proceedings of the National Academy of Sciences* 107(9):4129-4134.

52. McLaughlin S (1989) The Electrostatic Properties of Membranes. *Annual Review of Biophysics and Biophysical Chemistry* 18(1):113-136.

53. Lee JW (2013) Membrane Surface Charges Attracted Protons are not Relevant to Proton Motive Force. *Bioenergetics: Open Access* 2013.

54. Petersen MK, Iyengar SS, Day TJ, Voth GA (2004) The hydrated proton at the water liquid/vapor interface. *The Journal of Physical Chemistry B* 108(39):14804-14806.

55. Mucha M, et al. (2005) Unified molecular picture of the surfaces of aqueous acid, base, and salt solutions. *The Journal of Physical Chemistry B* 109(16):7617-7623.

56. Buch V, Milet A, Vacha R, Jungwirth P, Devlin JP (2007) Water surface is acidic. *Proceedings of the National Academy of Sciences of the United States of America* 104(18):7342-7347.

57.   Vácha R, Buch V, Milet A, Devlin JP, Jungwirth P (2007) Autoionization at the surface of neat water: is the top layer pH neutral, basic, or acidic? *Physical Chemistry Chemical Physics* 9(34):4736-4747.

58.   Pollack GH (2013) *The fourth phase of water: beyond solid, liquid, and vapor* (Seattle).

59.   Zheng J-m, Chin W-C, Khijniak E, Pollack GH (2006) Surfaces and interfacial water: evidence that hydrophilic surfaces have long-range impact. *Advances in colloid and interface science* 127(1):19-27.

60.   Green K, Otori T (1970) Direct measurements of membrane unstirred layers. *The Journal of physiology* 207(1):93.

61.   Chai B, Mahtani A, Pollack G (2012) Unexpected presence of solute-free zones at metal-water interfaces. *Contemporary materials* 3(1):1.

62.   Ling GN (1992) *A Revolution in the Physiology of the Living Cell* (Krieger Publ. Co, Melbourne, FL).

63.   Lippincott ER, Stromberg RR, Grant WH, Cessac GL (1969) Polywater. *Science* 164(3887):1482-1487.

64.   Henderson MA (2002) The interaction of water with solid surfaces: fundamental aspects revisited. *Surface Science Reports* 46(1):1-308.

65.   McGeoch JE, McGeoch MW (2008) Entrapment of water by subunit c of ATP synthase. *Journal of The Royal Society Interface* 5(20):311-318.

66.   Kimmel GA, et al. (2009) No confinement needed: Observation of a metastable hydrophobic wetting two-layer ice on graphene. *Journal of the American Chemical Society* 131(35):12838-12844.

67.   Ji N, Ostroverkhov V, Tian C, Shen Y (2008) Characterization of vibrational resonances of water-vapor interfaces by phase-sensitive sum-frequency spectroscopy. *Physical review letters* 100(9):096102.

68.   Chai B, Yoo H, Pollack GH (2009) Effect of radiant energy on near-surface water. *The Journal of Physical Chemistry B* 113(42):13953-13958.

69.   Zheng J-m, Pollack GH (2003) Long-range forces extending from polymer-gel surfaces. *Physical Review E* 68(3):031408.

70.   Chai B-h, Zheng J-m, Zhao Q, Pollack GH (2008) Spectroscopic studies of solutes in aqueous solution. *The Journal of Physical Chemistry A* 112(11):2242-2247.

71.   von Grotthuss T (1906) Die Zersetzung des Wassers und der in ihm gelösten Körper durch galvanische Elektrizität. *Abhandlungen über Elektrizität und Licht von Theodor von Grotthuss, Vorlag von Wilhelm Engelmann, Leipzig*:3-12.

72.   Agmon N (1995) The Grotthuss mechanism. *Chemical Physics Letters* 244(5–6):456-462.

73.   Chiang GG, Dilley RA (1989) Intact Chloroplasts Show Ca-2+-Gated Switching between Localized and Delocalized Proton Gradient Energy Coupling (Atp Formation). *Plant physiology* 90(4):1513-1523.

74.   Nicholls DG (2008) Forty years of Mitchell's proton circuit: From little grey books to little grey cells. *Biochimica et Biophysica Acta (BBA)-Bioenergetics* 1777(7):550-556.

75.   Kornyshev A, Kuznetsov A, Spohr E, Ulstrup J (2003) Kinetics of proton transport in water. *The Journal of Physical Chemistry B* 107(15):3351-3366.

76.   Marx D, Tuckerman ME, Hutter J, Parrinello M (1999) The nature of the hydrated excess proton in water. *Nature* 397(6720):601-604.

77.   Bell RP (2013) *The proton in chemistry* (Springer Science & Business Media).

78.   Mohammed OF, Pines D, Dreyer J, Pines E, Nibbering ET (2005) Sequential proton transfer through water bridges in acid-base reactions. *Science* 310(5745):83-86.

79.   Zundel G (2007) *Hydrogen bonds with large proton polarizability and proton transfer processes in electrochemistry and biology* (John Wiley & Sons, Inc.).

80.   Kirchner B (2007) Eigen or Zundel ion: News from calculated and experimental photoelectron spectroscopy. *ChemPhysChem* 8(1):41-43.

81.   Hynes JT (1999) Physical chemistry: The protean proton in water. *Nature* 397(6720):565-567.

82.   Mitchell P (1976) Possible molecular mechanisms of the protonmotive function of cytochrome systems. *J Theor Biol* 62(2):327-367.

83.   Mitchell P (1978) David Keilin's respiratory chain concept and its chemiosmotic consequences. *Nobel prize lecture* 1:295-330.

84.   Nicholls DG, Ferguson S (1992) *Bioenergetics 2* (New York: Academic Press).

85.   Junge W (2013) Half a century of molecular bioenergetics. *Biochemical Society Transactions* 41:1207-1218.

86.   Ferguson SJ (1985) Fully delocalised chemiosmotic or localised proton flow pathways in energy coupling?: A scrutiny of experimental evidence. *Biochimica et Biophysica Acta (BBA)-Reviews on Bioenergetics* 811(1):47-95.

87.   Williams R (2011) Chemical advances in evolution by and changes in use of space during time. *J Theor Biol* 268(1):146-159.

88.   Mulkidjanian AY, Heberle J, Cherepanov DA (2006) Protons@ interfaces: implications for biological energy conversion. *Biochimica et Biophysica Acta (BBA)-Bioenergetics* 1757(8):913-930.

89.   Pomès R, Roux B (2002) Molecular mechanism of H+ conduction in the single-file water chain of the gramicidin channel. *Biophysical journal* 82(5):2304-2316.

90.   Marx D (2006) Proton transfer 200 years after von Grotthuss: Insights from ab initio simulations. *Chemphyschem* 7(9):1848-1870.

91.   Nicholls DG, Ferguson SJ (2013) 4 - The Chemiosmotic Proton Circuit in Isolated Organelles: Theory and Practice. *Bioenergetics (Fourth Edition)*, (Academic Press, Boston), pp 53-87.

92.   Pourbaix M (1974) Applications of electrochemistry in corrosion science and in practice. *Corrosion Science* 14(1):25-82.

93.   Pourbaix M (1974) Atlas of electrochemical equilibria in aqueous solutions.

94.   Dilley RA (2004) On why thylakoids energize ATP formation using either delocalized or localized proton gradients - a ca(2+) mediated role in thylakoid stress responses. *Photosynth Res* 80(1-3):245-263.

95.   Von Helmholtz H (1879) Studies of electric boundary layers. *Wied. Ann* 7:337-382.

96.   Gouy G (1910) Sur la constitution de la charge electrique a la surface d'un electrolyte. *J. phys* 9(4):457-468.

97.   Torrie GM, Valleau JP (1982) Electrical double layers. 4. Limitations of the Gouy-Chapman theory. *The Journal of Physical Chemistry* 86(16):3251-3257.

98.   Bolt G (1955) Analysis of the validity of the Gouy-Chapman theory of the electric double layer. *Journal of Colloid Science* 10(2):206-218.

99.   McLaughlin S (1977) Electrostatic potentials at membrane-solution interfaces. *Current topics in membranes and transport* 9:71-144.

100.   Barber J (1980) Membrane surface charges and potentials in relation to photosynthesis. *Biochimica et Biophysica Acta (BBA)-Reviews on Bioenergetics* 594(4):253-308.

101.   Cevc G (1990) Membrane electrostatics. *Biochimica et Biophysica Acta (BBA)-Reviews on Biomembranes* 1031(3):311-382.

102.   Hiemenz PC, Rajagopalan R (1997) *Principles of Colloid and Surface Chemistry, revised and expanded* (CRC press).

103.   Israelachvili JN (2011) *Intermolecular and surface forces: revised third edition* (Academic press).

104.   Grahame DC (1947) The electrical double layer and the theory of electrocapillarity. *Chemical reviews* 41(3):441-501.

105.   Lee JW (2015) Proton-Electrostatic Localization: Explaining the Bioenergetic Conundrum in Alkalophilic Bacteria. *Bioenergetics: Open Access* 2015.

106.   Saeed H, Lee J (2015) Experimental Demonstration of Localized Excess Protons at a Water-Membrane Interface. *Bioenergetics* 4(127):2.

107.   Eigen M, De Maeyer L (1958) Self-dissociation and protonic charge transport in water and ice. *Proceedings of the Royal Society of London. Series A, Mathematical and Physical Sciences*:505-533.

108.   Vargel C (2004) *Corrosion of aluminium* (Elsevier).

109.   Bell WA (1962) Effect of calcium carbonate on corrosion of aluminium in waters containing chloride and copper. *Journal of Applied Chemistry* 12(2):53-55.

110. D.P. Verdonik RLD, F.W. Williams (1999) U.S. Navy Halon 1211 Replacement Program: Assessment of Aircraft Collateral Damage from Dry Chemical Fire Extinguishing Agents. (Naval Research Laboratory, Washington, DC).

111. Scamans GM, Birbilis N, Buchheit RG (2010) 3.08 - Corrosion of Aluminum and its Alloys. *Shreir's Corrosion*, ed Editor-in-Chief: Tony JAR (Elsevier, Oxford), pp 1974-2010.

112. Heine M, Keir D, Pryor M (1965) The specific effects of chloride and sulfate ions on oxide covered aluminum. *Journal of The Electrochemical Society* 112(1):24-32.

113. Britton SC, Evans UR (1930) CCXXXIII.—The passivity of metals. Part VI. A comparison between the penetrating powers of anions. *Journal of the Chemical Society (Resumed)*:1773-1784.

114. Dacres CM (1977) *An Investigation of the Influence of Various Environmental Factors Upon the Aqueous Corrosion of Aluminum Alloys* (American University).

115. Afzal S, et al. (2007) Study of Aluminum Corrosion in Chloride and Nitrate Media and its Inhibition by Nitrite. *Journal of Nepal Chemical Society* 22:26-33.

116. Barron J, Ashton C, Geary L (2006) The effects of temperature on pH measurement. *57th Annual Meeting of the International Society of Electrochemistry, Edinburgh, Technical Services Department, Reagecon Diagnostics Ltd, Ireland*.

117. Galster H (1991) *pH measurement: fundamentals, methods, applications, instrumentation* (VCH).

118. Galster H (2000) pH Measurement and Control. *Ullmann's Encyclopedia of Industrial Chemistry*, (Wiley-VCH Verlag GmbH & Co. KGaA).

119. Giguère PA, Turrell S (1976) H3O+ ions in aqueous acid solutions. The infrared spectra revisited. *Canadian Journal of Chemistry* 54(21):3477-3482.

120. Knight C, Voth GA (2012) The Curious Case of the Hydrated Proton. *Accounts of Chemical Research* 45(1):101-109.

121. Ben-Naim A (1933) Statistical Thermodynamics for Chemists and Biochemists Plenum, New York, 1992.[-11] JD Bernal and RH Fowler. *J. Chem. Phys* 1:515.

122. Lobaugh J, Voth GA (1996) The quantum dynamics of an excess proton in water. *The Journal of chemical physics* 104(5):2056-2069.

123. Cukierman S (2006) Et tu, Grotthuss! and other unfinished stories. *Biochimica et Biophysica Acta (BBA)-Bioenergetics* 1757(8):876-885.

124. Conway B, Bockris JM, Linton H (1956) Proton conductance and the existence of the H3O· ion. *The Journal of Chemical Physics* 24(4):834-850.

125. Schuster P, Zundel G, Sandorfy C (1976) Hydrogen bond; recent developments in theory and experiments. *Hydrogen bond; recent developments in theory and experiments*, (North-Holland Publishing Company).

126. Eigen M (1964) Proton Transfer, Acid-Base Catalysis, and Enzymatic Hydrolysis. Part I: ELEMENTARY PROCESSES. *Angewandte Chemie International Edition in English* 3(1):1-19.

127. Eigen M, De Maeyer L (1959) The Structure of Electrolytic Solutions. *by WJ Hamer, Wiley, New York, NY*:70.

128. Luz Z, Meiboom S (1964) The activation energies of proton transfer reactions in water. *Journal of the American Chemical Society* 86(22):4768-4769.

129. Fuchs EC, Gatterer K, Holler G, Woisetschläger J (2008) Dynamics of the floating water bridge. *Journal of Physics D: Applied Physics* 41(18):185502.

130. Fuchs EC, et al. (2007) The floating water bridge. *Journal of Physics D: Applied Physics* 40(19):6112.

131. Armstrong W (1893) Electrical phenomena The newcastle literary and philosophical society. *The Electrical Engineer* 10:153.

132. Piatkowski L, Wexler AD, Fuchs EC, Schoenmaker H, Bakker HJ (2012) Ultrafast vibrational energy relaxation of the water bridge. *Physical Chemistry Chemical Physics* 14(18):6160-6164.

133. Fuchs EC, et al. (2012) Investigation of the mid-infrared emission of a floating water bridge. *Journal of Physics D: Applied Physics* 45(47):475401.

134. Woisetschläger J, Gatterer K, Fuchs EC (2010) Experiments in a floating water bridge. *Experiments in fluids* 48(1):121-131.

135. Fuchs EC, Agostinho LL, Eisenhut M, Woisetschläger J (2010) Mass and charge transfer within a floating water bridge. *Laser Applications in Life Sciences 2010*, (International Society for Optics and Photonics), pp 73761E-73761E-73715.

136. Agmon N (1999) Proton solvation and proton mobility. *Israel Journal of Chemistry* 39(3-4):493-502.

137. Kendall J (1916) The specific conductivity of pure water in equilibrium with atmospheric carbon dioxide. *Journal of the American Chemical Society* 38(8):1480-1497.

138. Wu YC, Berezansky P (1995) Low electrolytic conductivity standards. *Journal of research of the National Institute of Standards and Technology* 100(5):521-528.

139. Hamer WJ, King C (1959) The structure of electrolytic solutions. *Journal of The Electrochemical Society* 106(9):254C-255C.

140. Hench LL, Clark DE (1978) Physical chemistry of glass surfaces. *Journal of Non-Crystalline Solids* 28(1):83-105.

141. Sammer M, et al. (2015) Proton production, neutralisation and reduction in a floating water bridge. *Journal of Physics D: Applied Physics* 48(41):415501.

142. Duffy SJ (2011) *Environmental chemistry: a global perspective* (Oxford university press).

143. Fuchs EC, Sammer M, Wexler AD, Kunkte P, Woisetschläger J (2016) A floating water bridge produces water with excess charge. *Journal of Physics D: Applied Physics* 49(12):125502.

144. Kreimer G, Melkonian M, Holtum JA, Latzko E (1988) Stromal free calcium concentration and light-mediated activation of chloroplast fructose-1, 6-bisphosphatase. *Plant physiology* 86(2):423-428.

145. Lee JW, Collins RT, Greenbaum E (1998) Molecular ionic probes: a new class of Hill reagents and their potential for nanofabrication and biometallocatalysis. *The Journal of Physical Chemistry B* 102(11):2095-2100.

146. Delieu T, Walker D (1972) An improved cathode for the measurement of photosynthetic oxygen evolution by isolated chloroplasts. *New Phytologist* 71(2):201-225.

147. Bligny R, Gardestrom P, Roby C, Douce R (1990) 31P NMR studies of spinach leaves and their chloroplasts. *Journal of Biological Chemistry* 265(3):1319-1326.

148. Krumova SB, et al. (2008) Phase behavior of phosphatidylglycerol in spinach thylakoid membranes as revealed by 31 P-NMR. *Biochimica et Biophysica Acta (BBA)-Biomembranes* 1778(4):997-1003.

149. Wolf MG, Grubmüller H, Groenhof G (2014) Anomalous surface diffusion of protons on lipid membranes. *Biophysical journal* 107(1):76-87.

150. Slevin CJ, Unwin PR (2000) Lateral proton diffusion rates along stearic acid monolayers. *Journal of the American Chemical Society* 122(11):2597-2602.

151. Bard AJ, Mirkin MV (2012) *Scanning electrochemical microscopy* (CRC Press).

152. Gutman M, Nachliel E (1995) The dynamics of proton exchange between bulk and surface groups. *Biochimica et Biophysica Acta (BBA)-Bioenergetics* 1231(2):123-138.

153. Santos LP, Ducati TRD, Balestrin LBS, Galembeck F (2011) Water with Excess Electric Charge. *The Journal of Physical Chemistry C* 115(22):11226-11232.

154. Gouveia RF, Costa CA, Galembeck F (2005) Electrostatic patterning of a silica surface: a new model for charge build-up on a dielectric solid. *The Journal of Physical Chemistry B* 109(10):4631-4637.

155. Piermattei A, et al. (2000) Radiochromic film dosimetry of a low energy proton beam. *Medical physics* 27(7):1655-1660.

156. Grusell E, Isacsson U, Montelius A, Medin J (1995) Faraday cup dosimetry in a proton therapy beam without collimation. *Physics in Medicine and Biology* 40(11):1831.

157. Zheng Q, Wei G-W (2011) Poisson–Boltzmann–Nernst–Planck model. *The Journal of chemical physics* 134(19):194101.

158.   Fogolari F, Brigo A, Molinari H (2002) The Poisson–Boltzmann equation for biomolecular electrostatics: a tool for structural biology. *Journal of Molecular Recognition* 15(6):377-392.

159.   Roux B, Allen T, Berneche S, Im W (2004) Theoretical and computational models of biological ion channels. *Quarterly reviews of biophysics* 37(01):15-103.

160.   Sukiman N, et al. (2012) *Durability and corrosion of aluminium and its alloys: overview, property space, techniques and developments* (INTECH Open Access Publisher).

161.   Talbot DT, James (1998) *Corrosion Science and Technology* (CRS Press, Boca Raton, Florida).

162.   Pourbaix M (1990) Thermodynamics and corrosion. *Corrosion Science* 30(10):963-988.

APPENDIX A

ABBREVIATIONS AND ACRONYMS

ATP	Adenosine 5'-triphosphate
ADP	Adenosine diphosphate
PS I	Photosystem I
PS II	Photosystem II
PQ	Plastoquinone
$\boldsymbol{b_6f}$	Cytochrome b_6f complex
PC	Plastocyanin
$\mathbf{e^-}$	Electron
Fd	Ferredoxin
$\mathbf{NADP^+}$	Nicotinamide adenine dinucleotide phosphate
$\boldsymbol{Pi}$	Inorganic phosphate
pmf (Δp)	Proton motive force
$\Delta\boldsymbol{\mu}_{H^+}$	Proton electrochemical gradient
$\Delta\boldsymbol{\psi}$	The trans-membrane potential generated due to the difference in electrical potential across the biological membrane
R	Gas constant

ΔpH	The difference of protons concentration between the two bulk aqueous phases separated by the membrane
F	Faraday constant
ε	Dielectric permittivity
EZ	Exclusion zone
pH_{nB}	Stroma (or cytoplasmic) bulk phase pH
pH_{pB}	Lumen (or periplasmic) bulk phase pH
$[\text{H}^+]^L_{\text{eff}}$	Effective concentration of the localized protons at the membrane-water interface at equilibrium with non-proton cations
$[H_L^+]^0$	Effective localized proton concentration at the membrane-water interface without cation exchange.
C/S	Membrane capacitance per unit surface area
κ	Dielectric constant of the membrane
d	Thickness of the membrane
l	Thickness of the localized proton layer
K_{pi}	Equilibrium constant for non-proton cations to exchange with the localized protons at the water-membrane interface.
$[M_{pB}^{i+}]$	Concentration of the non-proton cations in the bulk phase of the liquid culture medium.

$[H^+_{pB}]$	Concentration of protons in the bulk phase of the liquid culture medium
ΔG	Gibbs energy change
Al-Tf-Al	Aluminum-Teflon-Aluminum compact films
Tf-Al-Tf	Teflon-Aluminum-Teflon compact films
DI water	De-ionized water
P_I	Proton sensitive membrane interface site facing the anode (P) water chamber.
N_I	Proton sensitive membrane interface site facing the cathode (N) water chamber.
P_S	Proton-sensitive film applied on the anode water surface
N_S	Proton-sensitive film applied on the cathode water surface
P_B	Proton-sensitive film applied in the middle of the anode chamber water bulk phase
N_B	Proton-sensitive film applied in the middle of the cathode chamber water bulk phase
C_B	Proton-sensitive film placed into the bulk liquid phase of the Teflon center chamber
P'	Proton-sensing film placed at cathode site facing the solution within the Teflon center chamber

N′	Proton-sensing film placed at anode site facing the solution within the Teflon center chamber
$\mathbf{r_D}$	The Debye length
$\mathbf{[Na_L^+]}$	Localized sodium ions concentration on the water-membrane interface
$\mathbf{[Na^+]}$	Free sodium ions concentration in the bulk liquid phase.
EHD	Electrohydrodynamic
DC	Direct Current
AC	Alternating Current
^{31}P-NMR	Phosphorus Nuclear magnetic resonance
$\mathbf{NO_3^-}$	Nitrate ion
$\mathbf{Cl^-}$	Chloride ion
$\mathbf{K^+}$	Potassium ion
$\mathbf{Na^+}$	Sodium ion
$\mathbf{HCO_3^-}$	Bicarbonate ion
$\mathbf{(CO_3)^{2-}}$	Carbonate ion
$\mathbf{OH^-}$	Hydroxide ion
$\mathbf{(SO_4)^{-2}}$	Sulfate ion
$\mathbf{CH_3COO^-}$	Acetate ion

H_3O^+	Protons
K_a	Acid dissociation constant
K_H	Henry's laws constant
K_{PNa^+}	Equilibrium constant for Na^+ exchange with localized protons
K_{PK^+}	Equilibrium constant for K^+ exchange with localized protons
P_{CO2}	Partial pressure of carbon dioxide
H_2	Hydrogen gas
O_2	Oxygen gas
MS-EVB	Multistate Empirical Valence Bond
SECM	Scanning electrochemical microscopy
SCE	Standard Calomel Electrode

APPENDIX B

SUPPLEMENTARY FIGURES
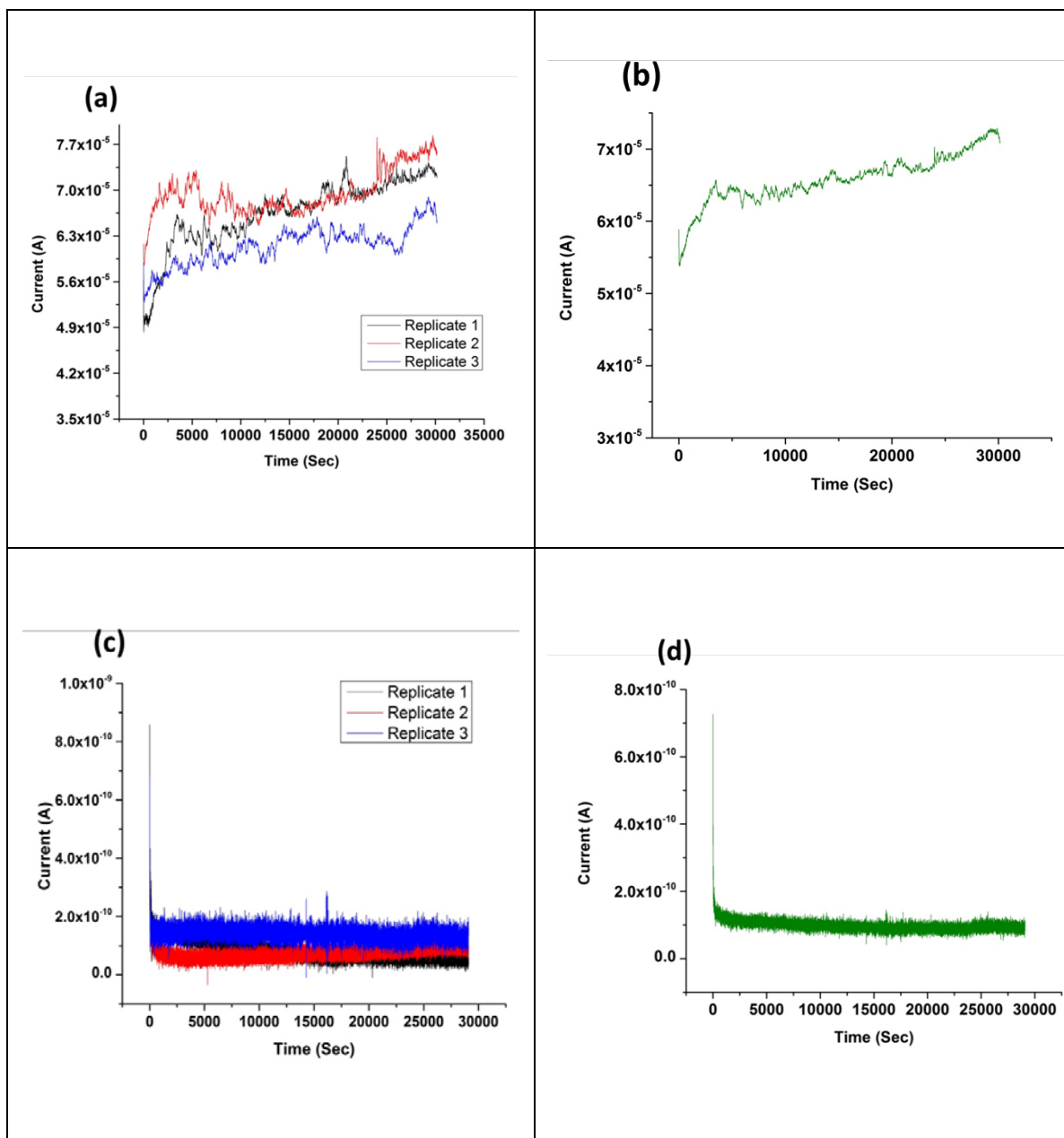
Figure S1. The electric current of pure water electrolysis measured as a function of time with 200 V during 10 hours experimental run: a) All replicates for Al-Tf-Al setup experiments, b) Average Al-Tf-Al setup experiments, c) All replicates for Tf-Al-Tf setup experiments, and d) Average Al-Tf-Al setup experiments.
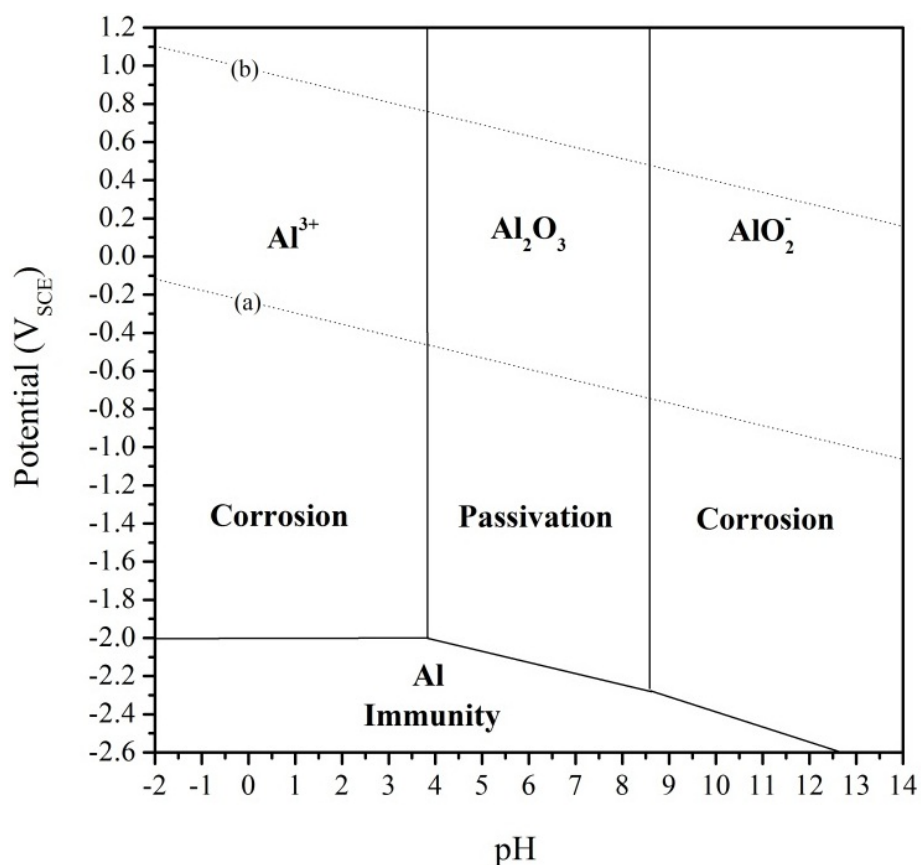
Figure S2. Potential-pH diagram for pure Al at 25˚C in aqueous solution (adapted from Pourbaix 1974). The lines (a) and (b) correspond to water stability and its decomposed product (160). (Copied with permissions, Appendix E)

Corrosion of aluminum in aqueous environment is governed mainly by two important factors: the pH of the solution (the surrounding environment) and the applied voltage (92, 111, 161, 162). The thermodynamic principles which control the corrosion of aluminum could be better understood by Pourbaix (Potential-pH) diagram which is a graphical representation of solid phases and soluble ions of the aluminum metal that are produced electrochemically (Figure S2).

Figure S2 shows that there are three possible states of the Al in aqueous solution:

1) Corrosion region in which Al metal is vulnerable to corrosion and becomes stable in its ionic (soluble) product when the pH of the surrounding environment is below 4 or above 8.5 and the potential is above -2.0 V versus SCE (Standard Calomel Electrode). In acidic environment (< pH 4), aluminum is oxidized forming Al^{3+} soluble ions while in alkaline environment (> pH 8.5) aluminum forms AlO^{2-} which is soluble in aqueous phase.

2) Passive region in which the Al metal tends to be protected by a coating of aluminum oxide which is a passive layer that acts as a barrier between Al metal and the surrounding environment thus preventing any contact between the metal and the environment. This passive layer is stable when the pH of the surrounding is in between 4 and 8.5.

3) Immunity region in which the Al metal is considered to be immune from corrosion attack. This region is achieved when the potential of the metal is kept below -2.0 V versus SCE.

a) Observation of Al sensing films placed at one end (picture on right), in the middle (middle picture) and at the other end (picture on left) of the small Teflon chamber contained 10 mM sodium bicarbonate.

b) Observation of Al sensing films placed in a small beaker contained 10 mM bicarbonate solution that was kept exposed to air for 10 hours at room temperature (26 ℃).

c) Observation of Al sensing films placed in a small beaker contained 10 mM bicarbonate solution that was kept for 10 hours at 16 ℃. Slight corrosive effect was observed on the aluminum pieces compared to that at room temperature.

Figure S3. Evaluation of the effect of exposure of bicarbonate solution to the atmospheric air by introducing 10 mM of sodium bicarbonate that was freshly prepared (had initial pH (8.40 ± 0.00)) in the following and left for 10 hours: a) Inside the Teflon center chamber that was sealed at both ends with Al along with a small piece of Al that was suspended inside, b) In a small glass beaker where pieces of Al were placed on the surface (picture on the right) and suspended in the bulk (picture on the left) of the solution that was kept for 10 hours at room temperature (26 ℃), and c) In a small glass beaker where pieces of Al were placed on the surface (picture on the right) and suspended in the bulk (picture on the left) of the solution that was kept for 10 hours at 16 ℃.
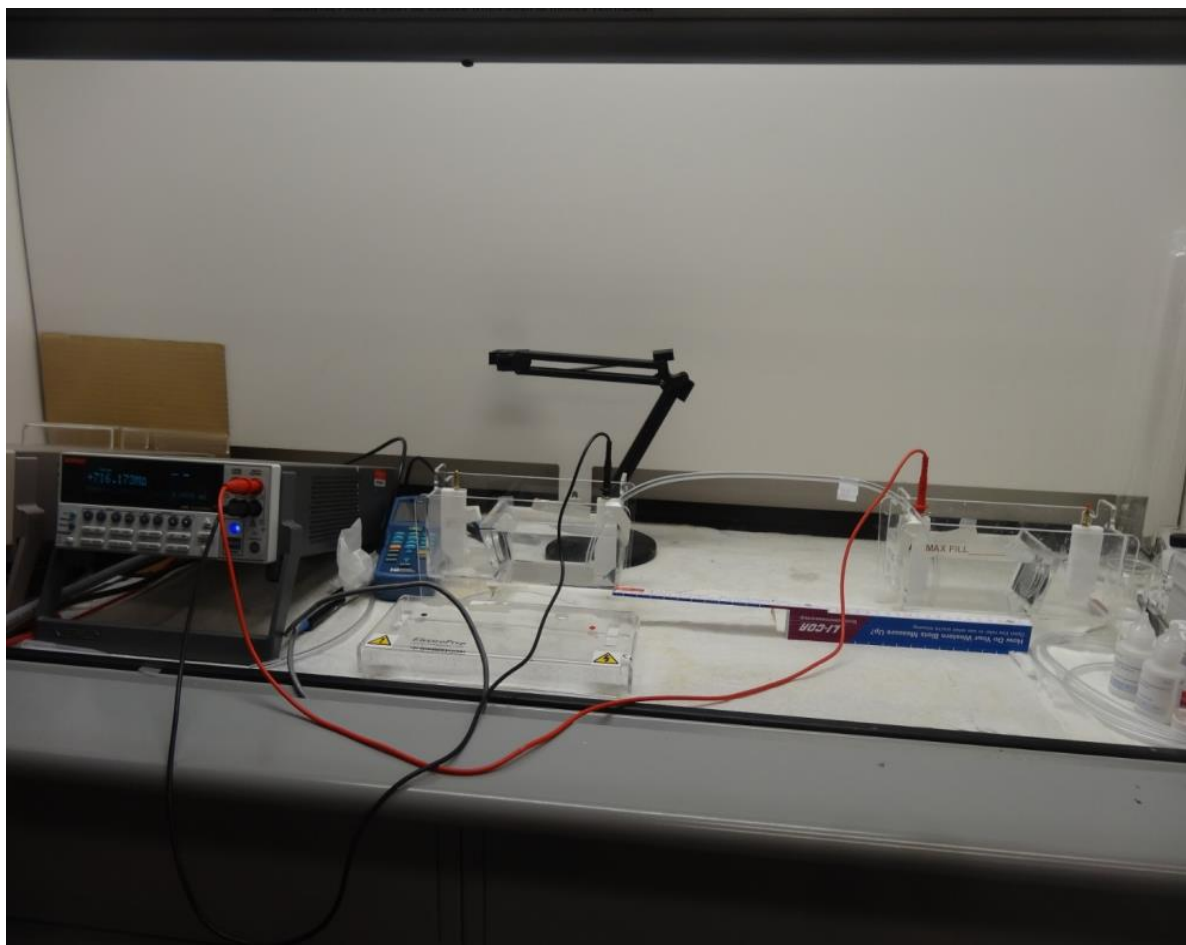
Figure S4. Shows the experimental set up when the two Teflon chambers were placed 30 cm apart, filled with 600 ml ultrapure water and connected with a continuous column of water with in a silicon tube bridge of 0.3 cm diameter. To ensure safety, all experiments were performed inside a fume hood that has a built-in air-fan driven ventilation system to disperse the small amount of potentially explosive H_2 and O_2 gases generated from the water electrolysis process.
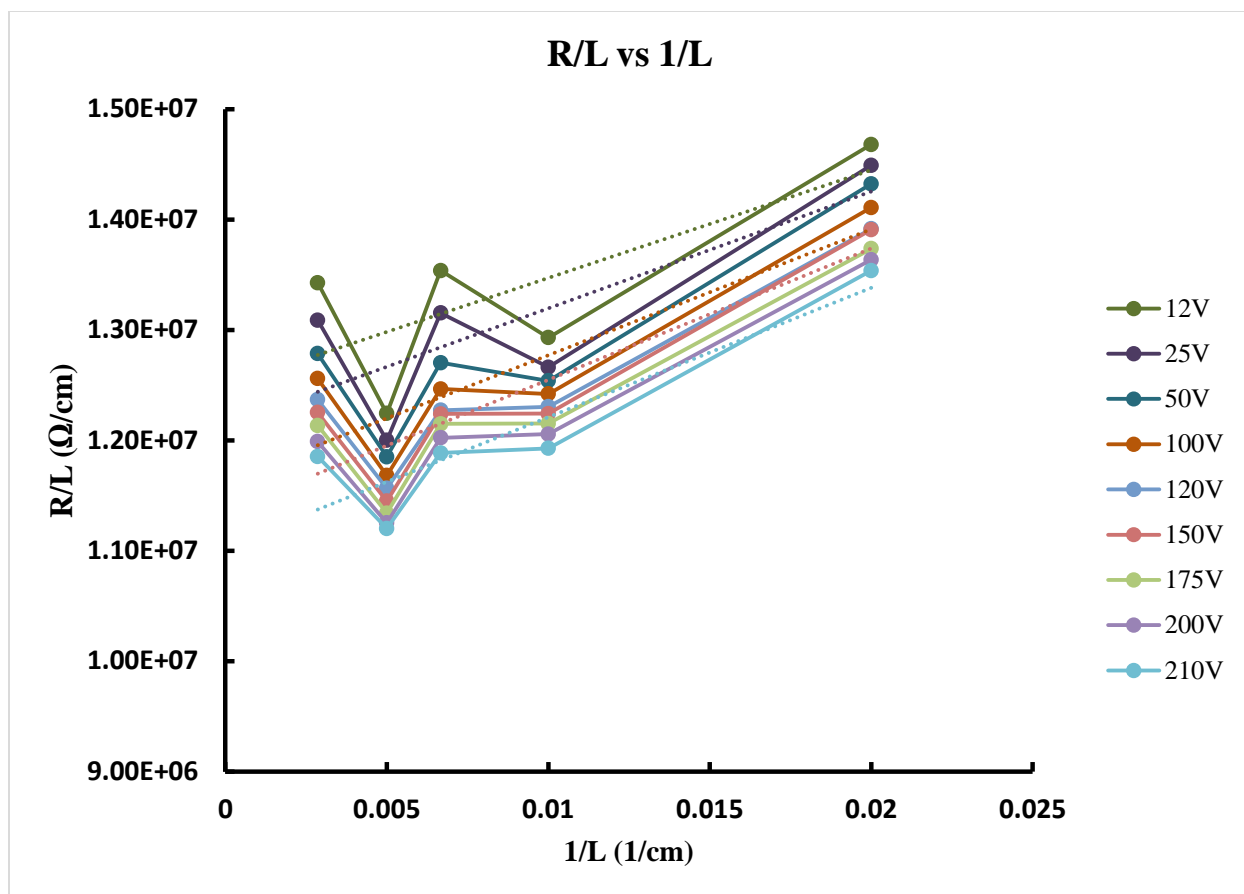
Figure S5. Plot of specific resistance (R/L) versus (1/L). The intercept was then determined by extrapolation of the straight line for each applied voltage.
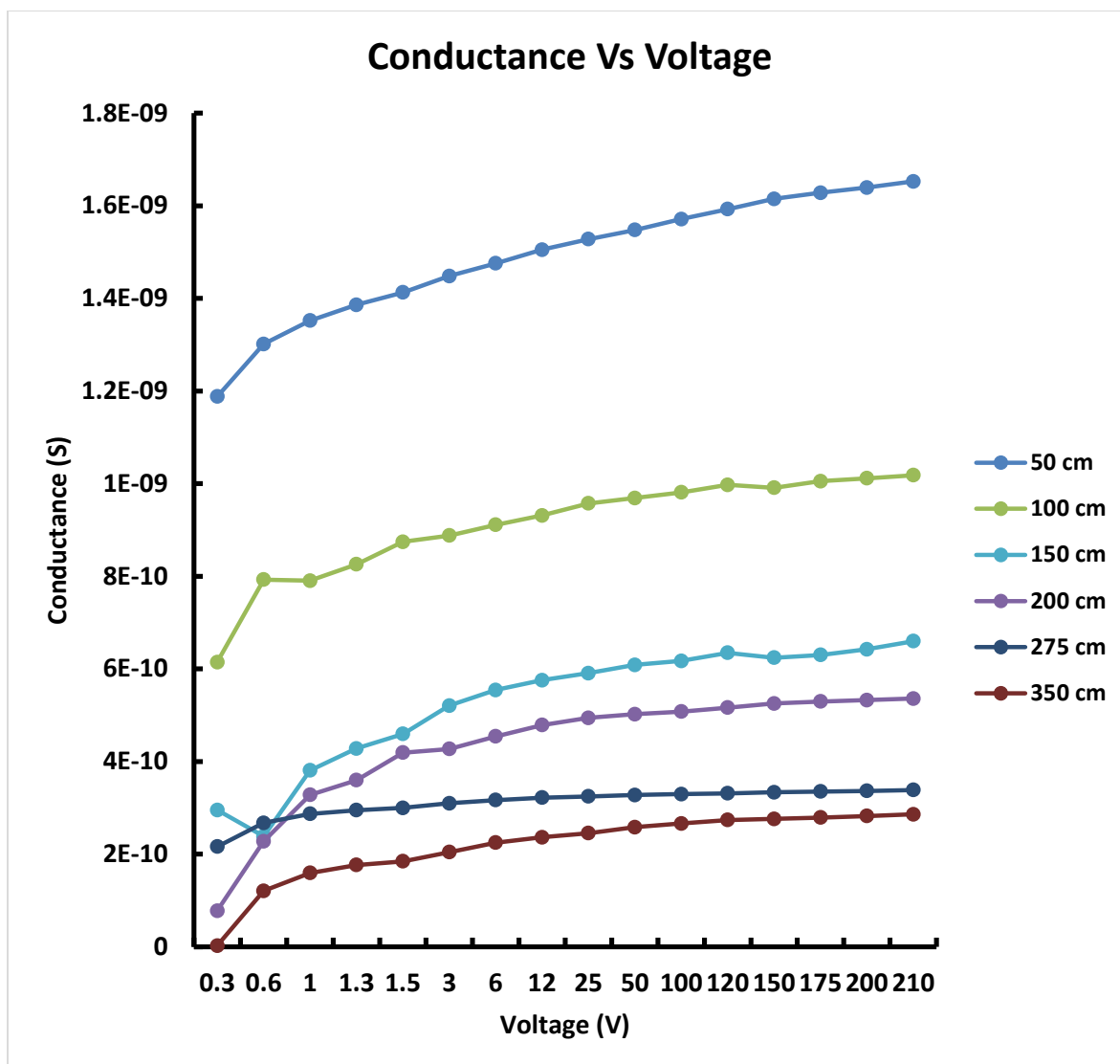
Figure S6. Plot of conductance versus voltage shows that longer tube has lower conductance while shorter tubes have higher conductance. It was noticed that the proton conductance tends to increase with increasing the applied voltage indicating that our system behaved in a non-ohmic manner.
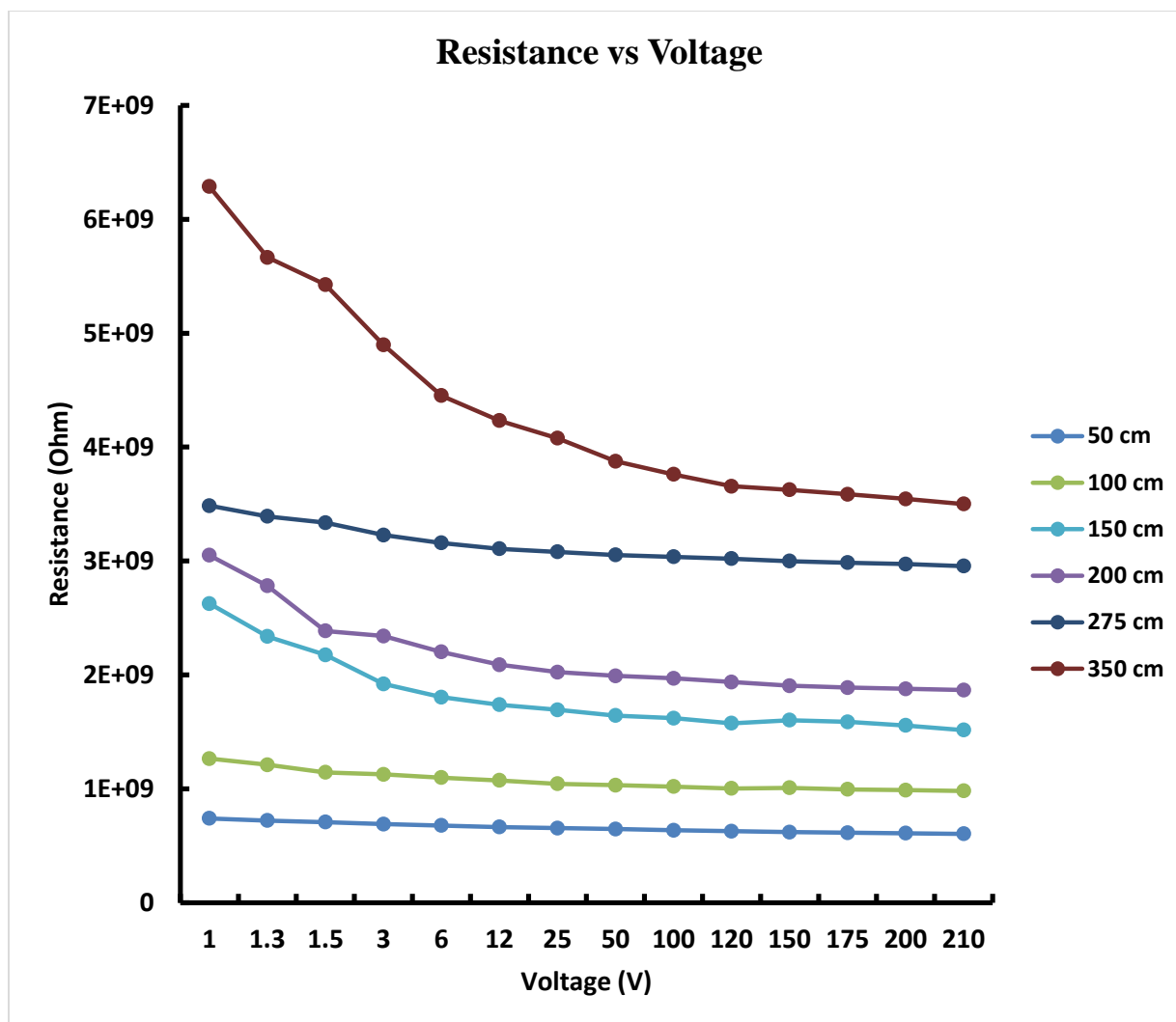
Figure S7. Plot of measured resistance versus applied voltage shows that longer water column has higher resistance while shorter water column has lower resistance. It was noticed that the resistance slightly decrease with increasing the applied voltage indicating that our system behaved in a non-ohmic manner.
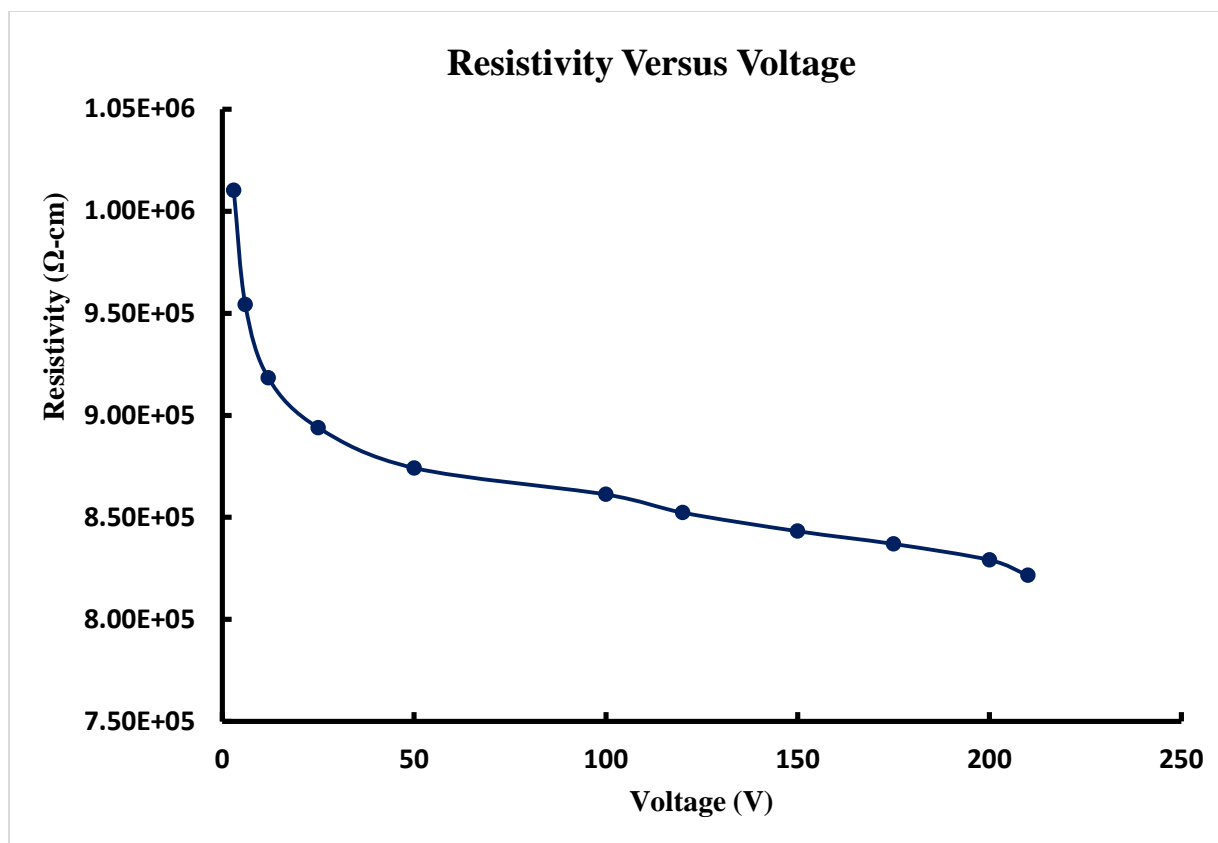
Figure S8. Resistivity of pure water (specific resistance) decreases as applied voltage increase. (Average of three trials)

APPENDIX C

SUPPLEMENTARY TABLES

Table S1. Raw data of initial pH measured with samples of deionized water source for experiments with "cathode water -**Tf-Al-Tf** -water anode". For deionized water used in each replication experiment, 12 readings of pH were recorded.

Tf-Al-Tf (Replicate # 1)	Initial pH	
	6.80	6.99
	6.49	6.96
	6.48	6.82
	6.46	6.62
	6.42	6.61
	6.43	6.50
Average of 12 replicates	*6.63 ± 0.20*	
Tf-Al-Tf (Replicate # 2)	Initial pH	
	6.89	6.96
	6.85	7.02
	6.81	7.01
	6.80	6.80
	6.49	6.45
	6.52	6.56
Average of 12 replicates	*6.76 ± 0.21*	
Tf-Al-Tf (Replicate # 3)	Initial pH	
	6.95	6.85
	6.90	6.75
	6.80	6.70
	6.45	6.74
	6.55	6.77
	6.58	6.60
Average of 12 replicates	*6.72 ± 0.15*	

Table S2. Raw data of bulk-phase pH measured in the cathode and anode water chambers at the end of the 10-hour experiments with the "cathode water-**Tf-Al-Tf** -water anode" system.

Tf-Al-Tf	Experiment (200V)		Control (0V)	
	pH of cathode	pH of anode	pH of cathode	pH of anode
Replicate 1	5.88	5.75	5.78	5.80
	5.81	5.72	5.79	5.75
	5.82	5.75	5.72	5.72
	5.81	5.77	5.81	5.73
	5.79	5.72	5.80	5.71
	5.75	5.73	5.75	5.76
Average final pH	*5.81 ± 0.04*	*5.74 ± 0.02*	*5.77 ± 0.03*	*5.75 ± 0.03*
Tf-Al-Tf	Experiment (200V)		Control (0V)	
	pH of cathode	pH of anode	pH of cathode	pH of anode
Replicate 2	5.79	5.71	5.78	5.81
	5.78	5.78	5.72	5.82
	5.81	5.76	5.70	5.81
	5.79	5.78	5.81	5.81
	5.75	5.72	5.82	5.80
	5.72	5.73	5.80	5.79
Average final pH	*5.77 ± 0.03*	*5.75 ± 0.03*	*5.77 ± 0.05*	*5.81 ± 0.01*
Tf-Al-Tf	Experiment (200V)		Control (0V)	
	pH of cathode	pH of anode	pH of cathode	pH of anode
Replicate 3	5.98	5.77	5.79	5.80
	5.88	5.78	5.75	5.82
	5.87	5.88	5.77	5.81
	5.79	5.80	5.72	5.85
	5.80	5.77	5.71	5.79
	5.75	5.75	5.73	5.78
Average final pH	*5.84 ± 0.08*	*5.79 ± 0.05*	*5.74 ± 0.03*	*5.80 ± 0.02*

Table S3. Raw data of initial pH measured with samples of deionized water source for experiments with "cathode water-**Al-Tf-Al**-water anode". For deionized water used in each replication experiment, 12 readings of pH were recorded.

Al-Tf-Al (Replicate # 1)	Initial pH	
	6.95	6.89
	6.90	6.90
	6.92	6.88
	6.91	6.87
	6.92	6.89
	6.93	6.96
Average of 12 replicates	*6.91±0.02*	
Al-Tf-Al (Replicate # 2)	Initial pH	
	6.96	6.85
	6.95	6.81
	6.93	6.82
	6.90	6.80
	6.89	6.75
	6.80	6.70
Average of 12 replicates	*6.85±0.08*	
Al-Tf-Al (Replicate # 3)	Initial pH	
	6.90	6.89
	6.89	6.88
	6.88	6.87
	6.91	6.87
	6.95	6.86
	6.92	6.85
Average of 12 replicates	*6.89 ±0.03*	

Table S4. Raw data of bulk-phase pH measured in the cathode and anode water chambers at the end of the 10-hour experiments with the "cathode water-**Al-Tf-Al**-water anode" system.

Al-Tf-Al	Experiment (200V)		Control (0V)	
	pH of cathode	pH of anode	pH of cathode	pH of anode
Replicate 1	5.91	5.71	5.75	5.76
	5.90	5.72	5.73	5.79
	5.92	5.79	5.72	5.78
	5.91	5.78	5.71	5.76
	5.89	5.8	5.74	5.72
	5.91	5.75	5.77	5.78
Average final pH	*5.91 ± 0.01*	*5.76 ± 0.04*	*5.73 ± 0.02*	*5.76 ± 0.02*

Al-Tf-Al	Experiment (200V)		Control (0V)	
	pH of cathode	pH of anode	pH of cathode	pH of anode
Replicate 2	5.85	5.87	5.63	5.77
	5.85	5.81	5.64	5.76
	5.82	5.85	5.58	5.73
	5.65	5.82	5.61	5.81
	5.79	5.89	5.60	5.82
	5.91	5.88	5.68	5.87
Average final pH	*5.81 ± 0.09*	*5.85 ± 0.03*	*5.62 ± 0.03*	*5.79 ± 0.05*

Al-Tf-Al	Experiment (200V)		Control (0V)	
	pH of cathode	pH of anode	pH of cathode	pH of anode
Replicate 3	5.55	5.69	5.74	5.78
	5.66	5.67	5.73	5.89
	5.61	5.71	5.66	5.78
	5.67	5.65	5.55	5.75
	5.69	5.66	5.74	5.73
	5.65	5.64	5.77	5.76
Average final pH	*5.64 ± 0.05*	*5.67 ± 0.03*	*5.69 ± 0.08*	*5.78 ± 0.06*

Table S5. Averaged pH values measured in bulk water phase before and after 10 hours experiment with the "cathode water **Tf-Al-Tf** water anode" system (summary of Tables S1 and S2).

Replicate number **Tf-Al-Tf**		200 V applied 10 hours		Control (0 V) left for 10 hours	
		pH of Cathode water	pH of Anode water	pH of Cathode water	pH of Anode water
Rep # 1	Initial	6.63 ± 0.20		6.63 ± 0.20	
	Final	5.81± 0.04	5.74± 0.02	5.77± 0.03	5.74± 0.03
Rep # 2	Initial	6.76 ± 0.21		6.76 ± 0.21	
	Final	5.77± 0.03	5.75± 0.03	5.77± 0.05	5.81± 0.01
Rep# 3	Initial	6.72 ± 0.15		6.72 ± 0.15	
	Final	5.84± 0.08	5.79± 0.05	5.74± 0.03	5.80± 0.02

Table S6. Averaged pH values measured in bulk water phase before and after the 10-hour experiments using "cathode water **Al-Tf-Al** water anode" system with *in situ* sensing of localized excess protons (summary of Tables S3 and S4).

Replicate number **Al-Tf-Al**		200 V applied 10 hours		Control (0 V) left for 10 hours	
		pH of Cathode water	pH of Anode water	pH of Cathode water	pH of Anode water
Rep # 1	Initial	6.91± 0.02		6.91± 0.02	
	Final	5.91± 0.01	5.76± 0.04	5.73± 0.02	5.76± 0.02
Rep # 2	Initial	6.85± 0.08		6.85± 0.08	
	Final	5.81± 0.09	5.85± 0.03	5.62± 0.03	5.79± 0.05
Rep# 3	Initial	6.89 ± 0.03		6.89 ± 0.03	
	Final	5.64± 0.05	5.67± 0.03	5.69± 0.08	5.78± 0.06

Table S7. Shows three replicates (12 readings each) of raw data initial pH measurements for experiments with arrangement "cathode water-Al-Tf-Al-**DI water**- Al-Tf-Al- water anode".

Al-Tf-Al	Initial pH	
(Replicate # 1)	6.66	6.67
	6.27	6.30
	6.08	6.12
	6.06	6.11
	6.06	6.05
	6.10	6.06
Average of 12 replicates	*6.21 ± 0.24*	
Al-Tf-Al	Initial pH	
(Replicate # 2)	6.65	6.11
	6.60	6.08
	5.96	6.10
	5.88	5.90
	5.92	5.75
	5.95	5.76
Average of 12 replicates	*6.055 ± 0.29*	
Al-Tf-Al	Initial pH	
(Replicate # 3)	6.75	6.27
	6.54	6.28
	6.20	6.11
	6.15	6.04
	6.17	6.06
	5.93	6.13
Average of 12 replicates	*6.22 ± 0.22*	

—

Table S8. Shows three replicates of raw data final pH measurements for experiments with arrangement "cathode water-Al-Tf-Al-**DI water**- Al-Tf-Al- water anode "after 10 hours electrolysis.

Al-Tf-Al	Experiment (200v)			Control (0V)		
	pH of cathode	**Sample chamber pH**	**pH of anode**	**pH of cathode**	**Sample chamber pH**	**pH of anode**
Replicate 1	6.07	6.99	5.76	6.01	5.93	5.75
	5.97	7.23	5.74	5.70	5.83	5.78
	5.93	7.32	5.75	5.66	5.83	5.72
	5.77	7.34	5.99	5.63	5.94	5.61
	5.76	7.27	5.85	5.84	5.95	5.59
	5.80	7.54	5.82	5.83	5.97	5.77
Average final pH	*5.88 ±0.13*	*7.28± 0.18*	*5.82±0.09*	*5.78±0.14*	*5.91±0.06*	*5.70±0.08*

Al-Tf-Al	Experiment (200v)			Control (0V)		
	pH of cathode	**Sample chamber pH**	**pH of anode**	**pH of cathode**	**Sample chamber pH**	**pH of anode**
Replicate 2	5.95	7.09	5.80	5.74	6.22	5.91
	5.95	7.14	5.83	5.81	6.12	5.85
	6.12	7.12	5.81	5.72	6.11	6.56
	5.95	6.97	5.82	5.76	6.09	5.68
	5.94	6.96	5.80	5.69	6.09	5.69
	6.14	6.96	5.79	5.79	6.05	5.70
Average final pH	*6.01±0.09*	*7.04±0.08*	*5.80 ±0.01*	*5.75±0.04*	*6.11±0.05*	*5.89±0.34*

Al-Tf-Al	Experiment (200v)			Control (0V)		
	pH of cathode	**Sample chamber pH**	**pH of anode**	**pH of cathode**	**Sample chamber pH**	**pH of anode**
Replicate 3	5.85	7.09	5.81	5.71	6.15	5.78
	5.88	7.10	5.82	5.65	6.16	5.85
	5.88	7.28	5.87	5.71	6.14	5.57
	5.72	7.38	5.64	5.72	6.17	5.64
	6.03	7.36	5.81	5.75	6.19	5.67
	5.79	7.40	5.82	5.74	6.23	5.79
Average final pH	*5.85±0.10*	*7.27±0.14*	*5.79±0.08*	*5.71±0.03*	*6.17±0.03*	*5.72±0.10*

Table S9. Observation of proton-sensing films after 10 hours electrolysis (200 V) for the "cathode water Al-Tf-Al- **Sodium bicarbonate** - Al-Tf-Al water anode" experiment. Images show proton-sensing films that were placed at P, P′ sites and middle piece (First replication).
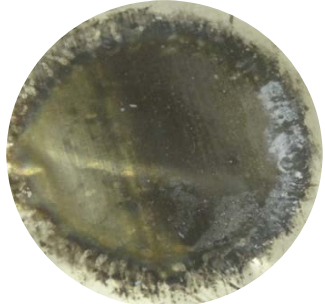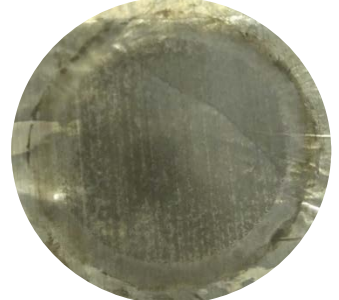
Conc of sodium bicarbonate (replicate 1)	Proton-sensing film placed at cathode (P′) site in contact with sodium salt solution.	Proton-sensing film placed at anode (P) site in contact with pure deionized water.	Middle piece placed inside the center Teflon chamber
0 mM			
10 mM			
25 mM			
50 mM			

Table S9. Continued
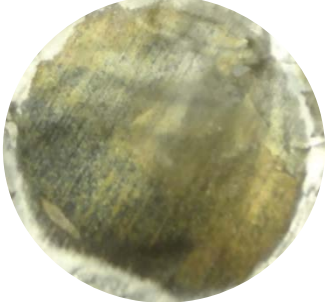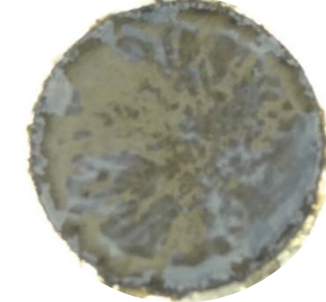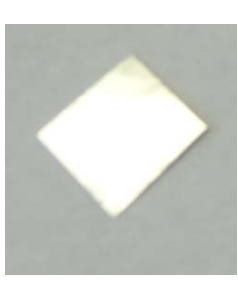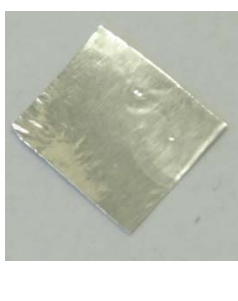
Conc of sodium bicarbonate (replicate 1)	Proton-sensing film placed at cathode (P′) site in contact with sodium salt solution.	Proton-sensing film placed at anode (P) site in contact with pure deionized water.	Middle piece placed inside the center Teflon chamber
75 mM			
100 mM			
200 mM			
500 mM			

Table S10. Observation of proton-sensing films after 10 hours electrolysis (200 V) for the "cathode water Al-Tf-Al- **Sodium bicarbonate** - Al-Tf-Al water anode" experiment. Images show proton-sensing films that were placed at P, P′ sites and middle piece (Second replication).
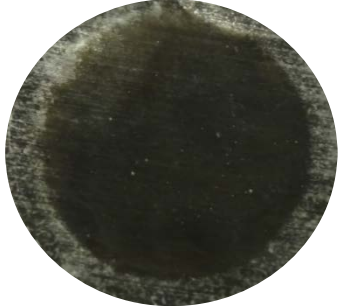
Conc of sodium bicarbonate (replicate 2)	Proton-sensing film placed at cathode (P′) site in contact with sodium salt solution.	Proton-sensing film placed at anode (P) site in contact with pure deionized water.	Middle piece placed inside the center Teflon chamber
0 mM			
10 mM			
25 mM			
50 mM			

Table S10. Continued.

Conc of sodium bicarbonate (replicate 2)	Proton-sensing film placed at cathode (P′) site in contact with sodium salt solution.	Proton-sensing film placed at anode (P) site in contact with pure deionized water.	Middle piece placed inside the center Teflon chamber
75 mM			
100 mM			
200 mM			
500 mM			

Table S11. Observation of proton-sensing films after 10 hours electrolysis (200V) for the "cathode water Al-Tf-Al- **Potassium bicarbonate** - Al-Tf-Al water anode" experiment. Images show proton-sensing films that were placed at P, P′ sites and middle piece (First replication).
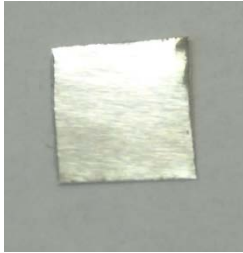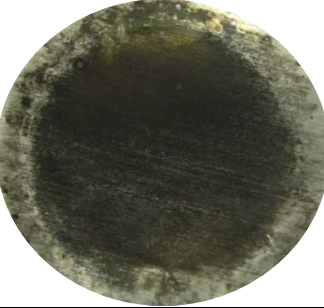
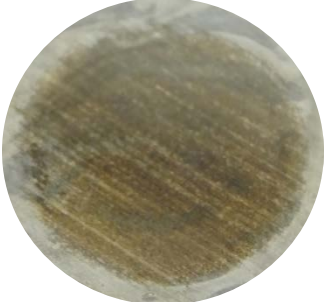| Conc of potassium bicarbonate (replicate 1)	Proton-sensing film placed at cathode (P′) site in contact with potassium salt solution.	Proton-sensing film placed at anode (P) site in contact with pure deionized water.	Middle piece placed inside the center Teflon chamber
0 mM			
10 mM			
25 mM			
50 mM			

Table S11. Continued**.**
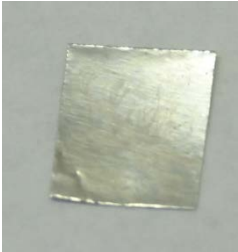
Conc of potassium bicarbonate (replicate 1)	Proton-sensing film placed at cathode (P′) site in contact with potassium salt solution.	Proton-sensing film placed at anode (P) site in contact with pure deionized water.	Middle piece placed inside the center Teflon chamber
75 mM			
100 mM			
200 mM			
500 mM			

Table S12. Observation of proton-sensing films after 10 hours electrolysis (200V) for the "cathode water Al-Tf-Al- **Potassium bicarbonate** - Al-Tf-Al water anode" experiment. Images show proton-sensing films that were placed at P, P′ sites (Second replication).
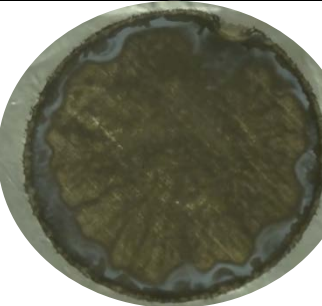
Conc of potassium bicarbonate (replicate 2)	Proton-sensing film placed at cathode (P′) site in contact with potassium salt solution.	Proton-sensing film placed at anode (P) site in contact with pure deionized water.	Middle piece placed inside the center Teflon chamber
0 mM			
10 mM			
25 mM			
50 mM			

Table S12. Continued
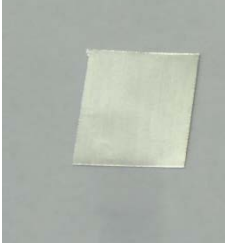
Conc of potassium bicarbonate (replicate 2)	Proton-sensing film placed at cathode (P′) site in contact with potassium salt solution.	Proton-sensing film placed at anode (P) site in contact with pure deionized water.	Middle piece placed inside the center Teflon chamber
75 mM			
100 mM			
200 mM			
500 mM			

Table S13. Images show proton-sensing films that were placed at P′ and P sites for 75 mM sodium bicarbonate solutions that led to the reduction of electrostatically localized protons populations at the P′ site by about 50%.
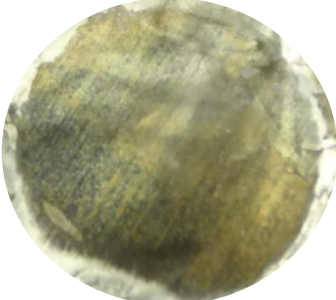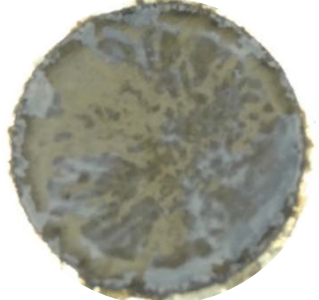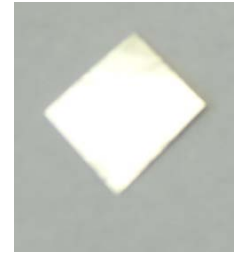
75mM sodium bicarbonate replications	Proton-sensing film placed at cathode (P′) site in contact with sodium salt solution.	Proton-sensing film placed at anode (P) site in contact with pure deionized water.	Middle piece placed inside the center Teflon chamber
Replicate 1			
Replicate 2			
Replicate 3			
Replicate 4			

Table S14. Images show proton-sensing films that were placed at P′ and P sites for 50 mM potassium bicarbonate solutions that led to the reduction of electrostatically localized protons populations at the P′ site by about 50%.
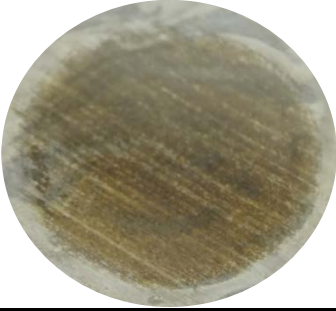
50 mM potassium bicarbonate replications	Proton-sensing film placed at cathode (P′) site in contact with potassium salt solution.	Proton-sensing film placed at anode (P) site in contact with pure deionized water.	Middle piece placed inside the center Teflon chamber
Replicate 1			
Replicate 2			
Replicate 3			
Replicate 4			

Table S15. Raw data for final conductivities and pH measurements for experiments with arrangement "cathode water-Al-Tf-Al-**Sodium bicarbonate**- Al-Tf-Al- water anode" after 10 hours electrolysis (First replication).

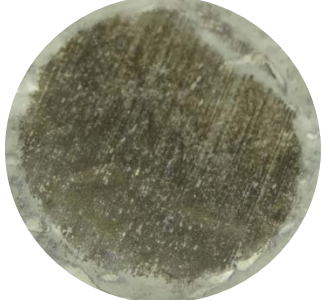| Concentration of Sodium salt solutions (mM)	Experiment (200v)			Experiment (0v) control		
	Conductivity of Cathode Water (µS)	Inner salt solution pH	Conductivity of Anode Water (µS)	Conductivity of Cathode Water (µS)	Inner salt solution pH	Conductivity of Anode Water (µS)
0 mM	1.409	7.52	1.400	1.431	6.35	1.402
	1.420	7.51	1.399	1.440	6.40	1.409
	1.419	7.53	1.410	1.445	6.41	1.409
	1.418	7.51	1.411	1.450	6.44	1.410
	1.421	7.50	1.413	1.459	6.42	1.410
	1.422	7.55	1.414	1.461	6.43	1.415
Average	*1.418 ±0.005*	*7.52 ±0.02*	*1.408 ±0.007*	*1.448 ±0.011*	*6.41 ±0.03*	*1.409 ±0.004*
	Experiment (200v)			Experiment (0v) control		
	Conductivity of Cathode Water (µS)	Inner salt solution pH	Conductivity of Anode Water (µS)	Conductivity of Cathode Water (µS)	Inner salt solution pH	Conductivity of Anode Water (µS)
10 mM	0.999	8.86	0.998	0.989	8.43	1.050
	1.010	8.86	0.967	0.956	8.43	1.051
	1.020	8.86	0.989	0.989	8.43	1.052
	1.028	8.85	0.989	0.979	8.43	1.054
	1.029	8.87	0.969	0.985	8.44	1.067
	1.029	8.86	0.979	1.006	8.43	1.084
Average	*1.019 ± 0.012*	*8.86 ± 0.01*	*0.982 ± 0.012*	*0.984 ± 0.016*	*8.43 ± 0.00*	*1.060 ± 0.013*
	Experiment (200v)			Experiment (0v) control		
	Conductivity of Cathode Water (µS)	Inner salt solution pH	Conductivity of Anode Water (µS)	Conductivity of Cathode Water (µS)	Inner salt solution pH	Conductivity of Anode Water (µS)
25 mM	1.77	8.62	1.392	1.774	8.84	1.641
	1.812	8.53	1.363	1.773	8.85	1.624
	1.814	8.65	1.349	1.821	8.86	1.638
	1.837	8.87	1.429	1.831	8.82	1.558
	1.82	8.88	1.539	1.852	8.84	1.568
	1.75	8.89	1.548	1.836	8.85	1.588
Average	*1.801 ± 0.033*	*8.74 ± 0.16*	*1.437 ± 0.087*	*1.815 ± 0.033*	*8.84 ± 0.01*	*1.603 ± 0.036*

Table S15. Continued

Concentration of sodium salt solutions (mM)	Experiment (200v)			Experiment (0v) control		
	Conductivity of Cathode Water (µS)	Inner salt solution pH	Conductivity of Anode Water (µS)	Conductivity of Cathode Water (µS)	Inner salt solution pH	Conductivity of Anode Water (µS)
50 mM	1.998	8.46	1.321	1.562	8.39	1.421
	1.999	8.47	1.322	1.532	8.38	1.422
	2.01	8.48	1.334	1.544	8.39	1.433
	2.02	8.47	1.338	1.532	8.40	1.423
	1.997	8.47	1.341	1.532	8.41	1.452
	1.996	8.48	1.345	1.526	8.40	1.488
Average	*2.003 ± 0.010*	*8.47 ± 0.01*	*1.334 ± 0.010*	*1.538 ± 0.013*	*8.40 ± 0.01*	*1.440 ± 0.026*
	Experiment (200v)			Experiment (0v) control		
	Conductivity of Cathode Water (µS)	Inner salt solution pH	Conductivity of Anode Water (µS)	Conductivity of Cathode Water (µS)	Inner salt solution pH	Conductivity of Anode Water (µS)
75 mM	1.542	8.40	1.346	1.632	8.45	1.663
	1.556	8.43	1.344	1.645	8.43	1.665
	1.567	8.37	1.346	1.632	8.44	1.688
	1.587	8.38	1.344	1.599	8.46	1.7
	1.588	8.40	1.345	1.623	8.46	1.732
	1.598	8.39	1.346	1.678	8.45	1.752
Average	*1.573 ± 0.022*	*8.40 ± 0.02*	*1.345 ± 0.001*	*1.635 ± 0.026*	*8.45 ± 0.01*	*1.700 ± 0.036*
	Experiment (200v)			Experiment (0v) control		
	Conductivity of Cathode Water (µS)	Inner salt solution pH	Conductivity of Anode Water (µS)	Conductivity of Cathode Water (µS)	Inner salt solution pH	Conductivity of Anode Water (µS)
100 mM	1.321	8.31	0.981	1.056	8.25	0.815
	1.209	8.32	0.982	1.057	8.24	0.820
	1.221	8.29	0.987	1.061	8.24	0.830
	1.208	8.31	0.991	1.068	8.25	0.835
	1.209	8.31	1.020	1.067	8.25	0.835
	1.209	8.31	1.023	1.069	8.24	0.836
Average	*1.230 ± 0.045*	*8.31 ± 0.01*	*0.997 ± 0.019*	*1.063 ± 0.006*	*8.25 ± 0.01*	*0.829 ± 0.009*

Table S15. Continued

Concentration of sodium salt solutions (mM)	Experiment (200v)			Experiment (0v) control		
	Conductivity of Cathode Water (µS)	Inner salt solution pH	Conductivity of Anode Water (µS)	Conductivity of Cathode Water (µS)	Inner salt solution pH	Conductivity of Anode Water (µS)
200 mM	1.898	8.16	1.798	1.523	8.14	1.491
	1.872	8.17	1.781	1.533	8.15	1.492
	1.852	8.16	1.783	1.532	8.15	1.493
	1.881	8.17	1.769	1.581	8.15	1.491
	1.882	8.18	1.779	1.569	8.14	1.489
	1.883	8.17	1.781	1.566	8.16	1.481
Average	*1.878 ± 0.015*	*8.17 ± 0.01*	*1.782 ± 0.009*	*1.551 ± 0.024*	*8.15 ± 0.01*	*1.490 ± 0.004*
	Experiment (200v)			Experiment (0v) control		
	Conductivity of Cathode Water (µS)	Inner salt solution pH	Conductivity of Anode Water (µS)	Conductivity of Cathode Water (µS)	Inner salt solution pH	Conductivity of Anode Water (µS)
500 mM	1.798	8.15	1.654	1.231	8.120	1.211
	1.777	8.15	1.674	1.233	8.130	1.222
	1.789	8.15	1.678	1.211	8.120	1.223
	1.769	8.15	1.674	1.209	8.120	1.220
	1.799	8.15	1.675	1.208	8.130	1.220
	1.795	8.15	1.677	1.208	8.120	1.221
Average	*1.788 ± 0.012*	*8.15 ± 0.00*	*1.672 ± 0.009*	*1.217 ± 0.012*	*8.12 ± 0.01*	*1.220 ± 0.004*

Table S16. Raw data final conductivities and pH measurements for experiments with arrangement "cathode water-Al-Tf-Al-**Sodium bicarbonate**- Al-Tf-Al- water anode" after 10 hours electrolysis (Second replication).

Concentration of Sodium salt solutions (mM)	Experiment (200v)			Experiment (0v) control		
	Conductivity of Cathode Water (µS)	Inner salt solution pH	Conductivity of Anode Water (µS)	Conductivity of Cathode Water (µS)	Inner salt solution pH	Conductivity of Anode Water (µS)
0 mM	1.409	7.52	1.400	1.431	6.35	1.402
	1.420	7.51	1.399	1.440	6.40	1.409
	1.419	7.53	1.410	1.445	6.41	1.409
	1.418	7.51	1.411	1.450	6.44	1.410
	1.421	7.50	1.413	1.459	6.42	1.410
	1.422	7.55	1.414	1.461	6.43	1.415
Average	*1.418 ±0.005*	*7.52 ±0.02*	*1.408 ±0.007*	*1.448 ±0.011*	*6.41 ±0.03*	*1.409 ±0.004*
	Experiment (200v)			Experiment (0v) control		
	Conductivity of Cathode Water (µS)	Inner salt solution pH	Conductivity of Anode Water (µS)	Conductivity of Cathode Water (µS)	Inner salt solution pH	Conductivity of Anode Water (µS)
10 mM	1.213	8.72	1.121	1.011	8.41	0.989
	1.221	8.75	1.132	1.020	8.40	0.988
	1.229	8.76	1.133	1.023	8.41	0.991
	1.258	8.76	1.134	1.015	8.41	0.992
	1.249	8.77	1.135	1.018	8.40	0.995
	1.229	8.77	1.133	1.019	8.40	0.999
Average	*1.233 ± 0.017*	*8.76 ± 0.02*	*1.131 ± 0.005*	*1.018 ± 0.004*	*8.41 ± 0.01*	*0.992 ± 0.004*
	Experiment (200v)			Experiment (0v) control		
	Conductivity of Cathode Water (µS)	Inner salt solution pH	Conductivity of Anode Water (µS)	Conductivity of Cathode Water (µS)	Inner salt solution pH	Conductivity of Anode Water (µS)
25 mM	1.898	8.78	1.509	1.231	8.38	1.233
	1.898	8.79	1.606	1.246	8.38	1.241
	1.951	8.78	1.619	1.251	8.38	1.231
	1.952	8.76	1.620	1.256	8.38	1.235
	1.991	8.80	1.640	1.259	8.38	1.236
	1.991	8.78	1.754	1.259	8.38	1.237
Average	*1.947 ± 0.023*	*8.78 ± 0.02*	*1.625 ± 0.047*	*1.250 ± 0.011*	*8.38 ± 0.00*	*1.236 ± 0.003*

Table S16. Continued

Concentration of Sodium salt solutions (mM)	Experiment (200v)			Experiment (0v) control		
	Conductivity of Cathode Water (µS)	Inner salt solution pH	Conductivity of Anode Water (µS)	Conductivity of Cathode Water (µS)	Inner salt solution pH	Conductivity of Anode Water (µS)
50 mM	1.562	8.44	1.568	1.855	8.41	1.325
	1.566	8.42	1.459	1.845	8.43	1.352
	1.554	8.41	1.469	1.842	8.39	1.332
	1.523	8.45	1.449	1.853	8.38	1.356
	1.523	8.44	1.449	1.845	8.38	1.365
	1.577	8.44	1.448	1.851	8.39	1.366
Average	*1.551 ± 0.023*	*8.43 ± 0.02*	*1.474 ± 0.047*	*1.849 ± 0.005*	*8.39 ± 0.02*	*1.349 ± 0.017*
	Experiment (200v)			Experiment (0v) control		
	Conductivity of Cathode Water (µS)	Inner salt solution	Conductivity of Anode Water (µS)	Conductivity of Cathode Water (µS)	Inner salt solution	Conductivity of Anode Water (µS)
75 mM	1.352	8.45	1.818	1.431	8.30	1.321
	1.341	8.43	1.82	1.445	8.31	1.32
	1.323	8.42	1.821	1.442	8.32	1.319
	1.356	8.41	1.825	1.449	8.33	1.312
	1.366	8.43	1.826	1.446	8.32	1.31
	1.356	8.44	1.827	1.45	8.32	1.319
Average	*1.349 ± 0.015*	*8.43 ± 0.01*	*1.823 ± 0.004*	*1.444 ± 0.007*	*8.32 ± 0.01*	*1.317 ± 0.005*
	Experiment (200v)			Experiment (0v) control		
	Conductivity of Cathode Water (µS)	Inner salt solution pH	Conductivity of Anode Water (µS)	Conductivity of Cathode Water (µS)	Inner salt solution pH	Conductivity of Anode Water (µS)
100 mM	1.231	8.29	1.067	1.001	8.19	1.167
	1.323	8.29	1.077	1.008	8.20	1.166
	1.321	8.29	1.078	1.011	8.20	1.168
	1.331	8.29	1.081	1.109	8.20	1.170
	1.341	8.29	1.082	1.108	8.20	1.171
	1.351	8.29	1.083	1.109	8.21	1.170
Average	*1.316 ± 0.043*	*8.29 ± 0.00*	*1.078 ± 0.006*	*1.058 ± 0.056*	*8.20 ± 0.01*	*1.169 ± 0.002*

Table S16. Continued

Concentration of Sodium salt solutions (mM)	Experiment (200v)			Experiment (0v) control		
	Conductivity of Cathode Water (µS)	**Inner salt solution pH**	**Conductivity of Anode Water (µS)**	**Conductivity of Cathode Water (µS)**	**Inner salt solution pH**	**Conductivity of Anode Water (µS)**
200 mM	1.001	8.20	0.807	1.321	8.16	1.022
	1.002	8.19	0.808	1.235	8.16	1.030
	1.003	8.26	0.810	1.324	8.16	1.023
	1.004	8.20	0.811	1.324	8.17	1.028
	1.009	8.19	0.811	1.423	8.16	1.029
	1.010	8.20	0.812	1.215	8.16	1.035
Average	*1.005 ± 0.004*	*8.21 ± 0.03*	*0.81 ± 0.002*	*1.310 ± 0.075*	*8.16 ± 0.00*	*1.028 ± 0.005*
	Experiment (200v)			Experiment (0v) control		
	Conductivity of Cathode Water (µS)	**Inner salt solution pH**	**Conductivity of Anode Water (µS)**	**Conductivity of Cathode Water (µS)**	**Inner salt solution pH**	**Conductivity of Anode Water (µS)**
500 mM	2.040	8.13	1.015	2.010	8.08	1.019
	2.100	8.13	1.016	1.998	8.09	0.998
	2.110	8.12	1.020	1.991	8.09	0.997
	2.130	8.12	1.031	1.998	8.09	0.996
	2.140	8.12	1.032	1.998	8.10	0.997
	2.130	8.12	1.036	2.050	8.10	0.997
Average	*2.108 ± 0.037*	*8.12 ± 0.01*	*1.025 ± 0.009*	*2.008 ± 0.022*	*8.09 ± 0.01*	*1.001 ± 0.009*

Table S17. Conductivities and pH measurements after 10 hours **open-circuit electrolysis at 200V** for the three water chambers by changing the concentration of **sodium bicarbonate** inside the Teflon sample chamber (average of 2 replicates presented in Tables S15 and S16)**.**

Concentrations of Sodium bicarbonate solutions (mM)	Conductivity of Cathode Water (µS)	Inner salt solution pH	Conductivity of Anode Water (µS)
0 mM	1.418 ±0.005	7.52 ±0.02	1.408 ±0.007
10 mM	1.419 ± 0.090	8.85 ± 0.06	1.909 ± 0.250
25 mM	1.874 ± 0.025	8.78 ± 0.15	1.531 ± 0.065
50 mM	1.777 ± 0.016	8.45 ± 0.02	1.404 ± 0.028
75 mM	1.461 ± 0.018	8.41 ± 0.02	1.584 ± 0.0025
100 mM	3.492 ± 0.235	8.27 ± 0.04	1.728 ± 0.105
200 mM	1.880 ± 0.02	8.17 ± 0.01	1.780 ± 0.01
500 mM	1.788 ± 0.01	8.15 ± 0.00	1.672 ± 0.01

Table S18. Conductivities and pH measurements of **control experiments (0V)** after 10 hours for the three water chambers by changing the concentration of **sodium bicarbonate** inside the Teflon sample chamber (average of 2 replicates presented in Tables S15 and S16).

Concentrations of Sodium bicarbonate solutions (mM)	Conductivity of Cathode Water (µS)	Inner salt solution pH	Conductivity of Anode Water (µS)
0 mM	1.448 ±0.011	6.41 ± 0.03	1.409 ±0.004
10 mM	1.126 ± 0.113	8.42 ± 0.01	1.026 ± 0.036
25 mM	1.532 ± 0.296	8.61 ± 0.24	1.419 ± 0.193
50 mM	1.693 ± 0.162	8.39 ± 0.02	1.395 ± 0.052
75 mM	1.314 ± 0.248	8.37 ± 0.09	1.234 ± 0.314
100 mM	1.060 ± 0.038	8.22 ± 0.02	0.999 ± 0.178
200 mM	1.429 ± 0.138	8.16 ± 0.01	1.259 ± 0.241
500 mM	1.612 ± 0.413	8.11 ± 0.02	1.114 ± 0.114

Table S19. Raw data final conductivities and pH measurements for experiments with arrangement "cathode water-Al-Tf-Al-**Potassium bicarbonate**- Al-Tf-Al- water anode" after 10 hours electrolysis (First replication).

Concentration of potassium salt solutions (mM)	Experiment (200v)			Experiment (0v) control		
	Conductivity of Cathode Water (µS)	Inner salt solution pH	Conductivity of Anode Water (µS)	Conductivity of Cathode Water (µS)	Inner salt solution pH	Conductivity of Anode Water (µS)
0 mM	1.884	7.93	1.524	1.777	6.88	1.873
	1.884	7.93	1.547	1.779	6.68	1.873
	1.889	7.93	1.462	1.789	6.79	1.873
	1.89	7.53	1.749	1.798	6.76	1.873
	1.893	7.93	1.841	1.799	6.79	1.873
	1.893	7.89	1.848	1.789	6.81	1.873
Average	*1.889 ±0.009*	*7.86 ± 0.16*	*1.662 ±0.171*	*1.789 ±0.009*	*6.79 ± 0.07*	*1.873 ±0.000*
	Experiment (200v)			**Experiment (0v) control**		
	Conductivity of Cathode Water (µS)	Inner salt solution pH	Conductivity of Anode Water (µS)	Conductivity of Cathode Water (µS)	Inner salt solution pH	Conductivity of Anode Water (µS)
10 mM	1.195	8.88	1.407	1.333	8.42	1.242
	1.125	8.89	1.353	1.281	8.41	1.194
	1.235	8.61	1.134	0.999	8.41	1.159
	1.331	8.89	1.155	0.989	8.41	1.133
	1.309	8.88	1.184	1.288	8.42	1.015
	1.289	8.89	1.208	1.24	8.41	1.279
Average	*1.247 ±0.153*	*8.84 ± 0.11*	*1.240 ±0.112*	*1.188 ±0.153*	*8.41 ± 0.01*	*1.170 ±0.093*
	Experiment (200v)			**Experiment (0v) control**		
	Conductivity of Cathode Water (µS)	Inner salt solution pH	Conductivity of Anode Water (µS)	Conductivity of Cathode Water (µS)	Inner salt solution pH	Conductivity of Anode Water (µS)
25 mM	1.899	8.51	1.721	1.723	8.39	1.666
	1.989	8.51	1.719	1.733	8.39	1.658
	1.988	8.51	1.72	1.745	8.39	1.659
	1.987	8.51	1.715	1.753	8.39	1.681
	1.987	8.51	1.735	1.742	8.38	1.692
	1.989	8.51	1.733	1.745	8.39	1.697
Average	*1.973 ±0.036*	*8.51 ± 0.00*	*1.724 ±0.008*	*1.740 ±0.011*	*8.39 ± 0.00*	*1.676 ±0.017*

Table S19. Continued

Concentration of potassium salt solutions (mM)	Experiment (200v)			Experiment (0v) control		
	Conductivity of Cathode Water (µS)	Inner salt solution pH	Conductivity of Anode Water (µS)	Conductivity of Cathode Water (µS)	Inner salt solution pH	Conductivity of Anode Water (µS)
50 mM	2.030	8.55	1.171	1.199	8.48	1.201
	2.030	8.52	1.162	1.198	8.48	1.205
	2.050	8.55	1.165	1.199	8.48	1.2
	2.050	8.55	1.167	1.189	8.47	1.2
	2.050	8.55	1.165	1.191	8.47	1.199
	2.050	8.55	1.18	1.198	8.47	1.198
Average	*2.043 ± 0.010*	*8.55 ± 0.01*	*1.168 ± 0.006*	*1.196 ± 0.00*	*8.48 ± 0.01*	*1.201 ± 0.002*
	Experiment (200v)			Experiment (0v) control		
	Conductivity of Cathode Water (µS)	Inner salt solution pH	Conductivity of Anode Water (µS)	Conductivity of Cathode Water (µS)	Inner salt solution pH	Conductivity of Anode Water (µS)
75 mM	4.030	8.51	0.998	1.026	8.39	0.985
	4.035	8.52	1.002	1.165	8.39	0.988
	4.040	8.52	0.996	1.185	8.40	0.980
	4.060	8.53	1.045	1.186	8.40	0.970
	4.048	8.53	1.050	1.189	8.39	0.975
	4.047	8.53	1.050	1.201	8.40	0.975
Average	*4.043 ± 0.011*	*8.52 ± 0.01*	*1.024 ± 0.027*	*1.159 ± 0.066*	*8.40 ± 0.01*	*0.979 ± 0.007*
	Experiment (200v)			Experiment (0v) control		
	Conductivity of Cathode Water (µS)	Inner salt solution pH	Conductivity of Anode Water (µS)	Conductivity of Cathode Water (µS)	Inner salt solution pH	Conductivity of Anode Water (µS)
100 mM	1.285	8.29	1.078	1.125	8.30	0.889
	1.285	8.29	1.088	1.135	8.30	0.899
	1.288	8.29	1.089	1.136	8.30	0.995
	1.285	8.29	1.078	1.137	8.31	0.996
	1.288	8.30	1.090	1.138	8.31	0.994
	1.289	8.29	1.099	1.140	8.31	0.997
Average	*1.287 ± 0.002*	*8.29 ± 0.00*	*1.087 ± 0.008*	*1.135 ± 0.005*	*8.31 ± 0.01*	*0.962 ± 0.053*

Table S19. Continued

Concentration of potassium salt solutions (mM)	Experiment (200v)			Experiment (0v) control		
	Conductivity of Cathode Water (μS)	Inner salt solution pH	Conductivity of Anode Water (μS)	Conductivity of Cathode Water (μS)	Inner salt solution pH	Conductivity of Anode Water (μS)
200 mM	1.050	8.34	0.998	1.056	8.25	0.856
	1.065	8.35	0.995	1.023	8.26	0.859
	1.068	8.35	1.002	1.006	8.26	0.874
	1.080	8.35	1.003	1.023	8.26	0.888
	1.085	8.34	1.005	1.025	8.26	0.884
	1.085	8.34	1.006	1.056	8.26	0.895
Average	*1.072 ± 0.014*	*8.35 ± 0.01*	*1.002 ± 0.004*	*1.032 ± 0.020*	*8.26 ± 0.00*	*0.876 ± 0.016*
	Experiment (200v)			Experiment (0v) control		
	Conductivity of Cathode Water (μS)	Inner salt solution pH	Conductivity of Anode Water (μS)	Conductivity of Cathode Water (μS)	Inner salt solution pH	Conductivity of Anode Water (μS)
500 mM	3.05	8.19	1.231	1.123	8.20	1.025
	3.02	8.19	1.233	1.156	8.20	1.060
	3.06	8.19	1.242	1.154	8.20	1.025
	3.10	8.19	1.245	1.158	8.20	1.089
	3.21	8.21	1.246	1.145	8.20	1.030
	3.24	8.21	1.259	1.170	8.20	1.045
Average	*3.113 ± 0.091*	*8.20 ± 0.01*	*1.243 ± 0.010*	*3.113 ± 0.016*	*8.20 ± 0.00*	*1.243 ± 0.025*

Table S20. Raw data final conductivities and pH measurements for experiments with arrangement "cathode water-Al-Tf-Al-**Potassium bicarbonate**- Al-Tf-Al- water anode" after 10 hours electrolysis (Second replication).

Concentration of potassium bicarbonate solutions (mM)	Experiment (200v)			Experiment (0v) control		
	Conductivity of Cathode Water (µS)	**Inner salt solution pH**	**Conductivity of Anode Water (µS)**	**Conductivity of Cathode Water (µS)**	**Inner salt solution pH**	**Conductivity of Anode Water (µS)**
0 mM	1.884	7.93	1.524	1.777	6.88	1.873
	1.884	7.93	1.547	1.779	6.68	1.873
	1.889	7.93	1.462	1.789	6.79	1.873
	1.890	7.53	1.749	1.798	6.76	1.873
	1.893	7.93	1.841	1.799	6.79	1.873
	1.893	7.89	1.848	1.789	6.81	1.873
Average	1.889 ± 0.011	7.86 ± 0.16	1.662 ± 0.17	1.789 ± 0.012	6.79 ± 0.07	1.873 ± 0.000
10 mM	**Conductivity of Cathode Water (µS)**	**Inner salt solution pH**	**Conductivity of Anode Water (µS)**	**Conductivity of Cathode Water (µS)**	**Inner salt solution pH**	**Conductivity of Anode Water (µS)**
	1.855	8.87	1.234	1.232	8.51	1.123
	1.856	8.88	1.235	1.255	8.50	1.124
	1.877	8.87	1.245	1.239	8.52	1.132
	1.879	8.87	1.246	1.240	8.52	1.209
	1.865	8.86	1.255	1.248	8.53	1.156
	1.875	8.86	1.286	1.245	8.52	1.169
Average	1.868 ± 0.011	8.87 ± 0.01	1.250 ± 0.019	1.243 ± 0.008	8.52 ± 0.01	1.152 ± 0.033
	Experiment (200v)			Experiment (0v) control		
25 mM	**Conductivity of Cathode Water (µS)**	**Inner salt solution pH**	**Conductivity of Anode Water (µS)**	**Conductivity of Cathode Water (µS)**	**Inner salt solution pH**	**Conductivity of Anode Water (µS)**
	2.23	8.71	1.789	1.324	8.45	1.231
	2.24	8.72	1.788	1.321	8.43	1.241
	2.42	8.73	1.831	1.332	8.45	1.245
	2.45	8.72	1.822	1.321	8.44	1.255
	2.49	8.71	1.824	1.326	8.45	1.256
	2.48	8.71	1.829	1.321	8.44	1.266
Average	2.385 ± 0.119	8.72 ± 0.01	1.814 ± 0.020	1.324 ± 0.004	8.44 ± 0.01	1.249 ± 0.012

Table S20. Continued

Concentration of potassium bicarbonate solutions (mM)	Experiment (200v)			Experiment (0v) control		
	Conductivity of Cathode Water (µS)	Inner salt solution pH	Conductivity of Anode Water (µS)	Conductivity of Cathode Water (µS)	Inner salt solution pH	Conductivity of Anode Water (µS)
50 mM	2.400	8.65	1.175	0.975	8.37	0.959
	2.400	8.66	0.995	0.97	8.38	0.96
	2.400	8.66	1.183	0.971	8.39	0.961
	2.410	8.68	1.186	0.972	8.40	0.966
	4.390	8.68	1.188	0.973	8.40	0.968
	2.390	8.70	1.190	0.975	8.40	0.969
Average	*2.732 ± 0.812*	*8.67 ± 0.02*	*1.153 ± 0.077*	*0.973 ± 0.002*	*8.39 ± 0.01*	*0.964 ± 0.004*
	Experiment (200v)			Experiment (0v) control		
	Conductivity of Cathode Water (µS)	Inner salt solution pH	Conductivity of Anode Water (µS)	Conductivity of Cathode Water (µS)	Inner salt solution pH	Conductivity of Anode Water (µS)
75 mM	1.825	8.60	1.755	1.858	8.33	1.878
	1.884	8.58	1.744	1.856	8.33	1.851
	1.888	8.58	1.765	1.858	8.33	1.85
	1.889	8.59	1.746	1.863	8.34	1.84
	1.892	8.59	1.765	1.873	8.34	1.87
	1.899	8.59	1.778	1.883	8.35	1.89
Average	*1.880 ± 0.027*	*8.59 ± 0.01*	*1.759 ± 0.013*	*1.865 ± 0.011*	*8.34 ± 0.01*	*1.863 ± 0.019*
	Experiment (200v)			Experiment (0v) control		
	Conductivity of Cathode Water (µS)	Inner salt solution pH	Conductivity of Anode Water (µS)	Conductivity of Cathode Water (µS)	Inner salt solution pH	Conductivity of Anode Water (µS)
100 mM	2.140	8.23	1.135	1.091	8.29	1.020
	2.150	8.23	1.135	1.100	8.29	1.046
	2.200	8.23	1.163	1.123	8.30	1.049
	2.230	8.24	1.175	1.125	8.30	1.048
	2.235	8.25	1.182	1.129	8.33	1.056
	2.290	8.24	1.191	1.160	8.29	1.058
Average	*2.208 ± 0.057*	*8.24 ± 0.01*	*1.164 ± 0.024*	*1.121 ± 0.024*	*8.30 ± 0.01*	*1.046 ± 0.014*

Table S20. Continued

Concentration of potassium bicarbonate solutions (mM)	Experiment (200v)			Experiment (0v) control		
	Conductivity of Cathode Water (µS)	Inner salt solution pH	Conductivity of Anode Water (µS)	Conductivity of Cathode Water (µS)	Inner salt solution pH	Conductivity of Anode Water (µS)
200 mM	1.566	8.38	1.234	1.231	8.27	1.123
	1.533	8.37	1.234	1.256	8.28	1.123
	1.523	8.37	1.239	1.659	8.27	1.230
	1.554	8.37	1.300	1.654	8.28	1.203
	1.556	8.36	1.301	1.701	8.26	1.236
	1.557	8.37	1.302	1.699	8.26	1.229
Average	*1.548 ± 0.016*	*8.37 ± 0.01*	*1.268 ± 0.036*	*1.533 ± 0.225*	*8.27 ± 0.01*	*1.191 ± 0.054*
	Experiment (200v)			Experiment (0v) control		
	Conductivity of Cathode Water (µS)	Inner salt solution pH	Conductivity of Anode Water (µS)	Conductivity of Cathode Water (µS)	Inner salt solution pH	Conductivity of Anode Water (µS)
500 mM	0.845	8.25	1.020	0.985	8.19	1.001
	0.877	8.26	1.025	0.992	8.18	1.020
	0.892	8.26	1.040	0.996	8.19	1.032
	0.904	8.26	1.045	0.995	8.19	1.032
	0.938	8.26	1.048	0.969	8.19	1.045
	0.950	8.25	1.051	0.970	8.19	1.050
Average	*0.901 ± 0.039*	*8.26 ± 0.01*	*1.038 ± 0.013*	*0.985 ± 0.012*	*8.19 ± 0.00*	*1.030 ± 0.018*

Table S21. Conductivities and pH measurements after 10 hours **open-circuit electrolysis at 200V** for the three water chambers by changing the concentration of **potassium bicarbonate** inside the Teflon sample chamber (average of 2 replicates that were presented in Tables S19 and S20).

Concentration of Sodium bicarbonate solutions (mM)	Conductivity of Cathode Water (μS)	Inner salt solution pH	Conductivity of Anode Water (μS)
0 mM	1.889 ± 0.011	7.86 ± 0.16	1.662 ± 0.171
10 mM	1.558 ± 0.328	8.85 ± 0.08	1.245 ± 0.077
25 mM	2.179 ± 0.231	8.61 ± 0.11	1.769 ± 0.049
50 mM	2.076 ± 0.616	8.48 ± 0.13	1.387 ± 0.282
75 mM	2.961 ± 1.130	8.56 ± 0.03	1.391 ± 0.385
100 mM	1.747 ± 0.482	8.26 ± 0.03	1.125 ± 0.043
200 mM	1.310 ± 0.249	8.36 ± 0.01	1.135 ± 0.141
500 mM	2.007 ± 1.157	8.23 ± 0.03	1.140 ± 0.107

Table S22. Conductivities and pH measurements of **control experiments (0 V)** after 10 hours for the three water chambers by changing the concentration of **potassium bicarbonate** inside the Teflon sample chamber (average of 2 replicates that were presented in Tables S19 and S20).

Concentrations of Sodium bicarbonate solutions (mM)	Conductivity of Cathode Water (μS)	Inner salt solution pH	Conductivity of Anode Water (μS)
0 mM	1.789 ± 0.012	6.79 ± 0.07	1.873 ± 0.000
10 mM	1.216 ± 0.107	8.47 ± 0.05	1.161 ± 0.067
25 mM	1.532 ± 0.217	8.42 ± 0.03	1.462 ± 0.223
50 mM	1.423 ± 0.366	8.45 ± 0.03	1.358 ± 0.300
75 mM	1.512 ± 0.372	8.37 ± 0.03	1.421 ± 0.462
100 mM	1.128 ± 0.018	8.30 ± 0.01	1.004 ± 0.057
200 mM	1.282 ± 0.303	8.26 ± 0.01	1.033 ± 0.169
500 mM	1.068 ± 0.088	8.19 ± 0.01	1.038 ± 0.022

Table S23. pH measurements for **75 mM of sodium salt** solution inside the Teflon center chamber after 10 hours open-circuit electrolysis at 200V.

Replications	pH for 10 hours experiment at 200V	pH for 10 hours control experiment at 0V
Replicate 1	8.40 ± 0.02	8.45 ± 0.01
Replicate 2	8.51 ± 0.01	8.45 ± 0.01
Replicate 3	8.43 ± 0.01	8.32 ± 0.01
Replicate 4	8.57 ± 0.01	8.25 ± 0.00
Average	8.48 ± 0.07	8.37 ± 0.09

Table S24. pH measurements for **50 mM of potassium salt** solution inside the Teflon center chamber after 10 hours open-circuit electrolysis at 200V.

Replications	pH for 10 hours experiment at 200V	pH for 10 hours control experiment at 0V
Replicate 1	8.35 ± 0.01	8.47 ± 0.01
Replicate 2	8.37 ± 0.01	8.45 ± 0.00
Replicate 3	8.54 ± 0.01	8.47 ± 0.01
Replicate 4	8.67 ± 0.02	8.39 ± 0.01
Average	8.48 ± 0.13	8.45 ± 0.03

Table S25. pH measurements for the pure water and sodium bicarbonate solutions inside the anode and the cathode chambers respectively that were placed 30 cm apart after 10 hour open circuit electrolysis at 200V.

Replications	Initial pH of water	Final pH	
		pH of cathode	pH of anode (700mM NaHCO$_3$)
Replicate 1	5.89	5.84	8.31
	5.86	5.84	8.31
	5.85	5.83	8.32
	5.87	5.84	8.32
	5.89	5.83	8.31
	5.85	5.83	8.31
Average	5.87 ± 0.02	5.84 ± 0.01	8.31 ± 0.01
	Initial pH of water	Final pH	
		pH of cathode	pH of anode (700mM NaHCO$_3$)
Replicate 2	7.00	5.81	8.31
	6.98	5.82	8.31
	6.97	5.83	8.31
	6.96	5.81	8.31
	6.94	5.82	8.31
	6.92	5.80	8.31
Average	6.92 ± 0.03	5.82 ± 0.01	8.31 ± 0.00
	Initial pH of water	Final pH	
		pH of cathode	pH of anode (700mM NaHCO$_3$)
Replicate 3	7.00	5.78	8.21
	6.98	5.79	8.21
	6.97	5.80	8.21
	6.93	5.80	8.22
	6.92	5.80	8.21
	6.95	5.81	8.21
Average	6.96 ± 0.03	5.80 ± 0.01	5.80 ± 0.01

APPENDIX D

SUPPLEMENTARY CALCULATIONS

(1) Calculation of capacitance of (Tf-Al-Tf) membrane

$$C = \frac{\kappa \cdot \varepsilon_0 . A}{d}$$

Where κ is the dielectric constant of the membrane; ε_0 is the permittivity; A is the surface area; d is the thickness of the membrane.

$$\frac{Q}{S} = \Delta\psi \cdot \frac{C}{S} = \frac{\Delta\psi \cdot \kappa \cdot \varepsilon_0}{d}$$

$C = \kappa A \varepsilon_0/d = 2.1 \times 8.85 \times 10^{-12}$ (F/m) x (2.5 x 10^{-4} m^2) /175 x10^{-6} m = 2.655 x 10^{-11} F

C/S = 2.655 x 10^{-11} F/ (2.5 x 10^{-4} m^2) = 1.062 x 10^{-7} F/m^2

(2) Experimental calculation of proton density

Experimental Area average below the current versus time curve was 2.88 x 10^{-8} Coulombs

2.88 x 10^{-8} Coulombs / (96485) = 2.98 x 10^{-13} mol H^+

2.98 x 10^{-13} mol H^+ / (2.54 x 10^{-4} m^2) = 1.19 x 10^{-9} mol H^+/ m^2

1.19 x 10^{-9} mol H^+/ m^2 / 10^{-9} m = 1.19 mole.m^{-3}

1.194 mole x 10^{-3} d^{-3} = 1.19 x 10^{-3} M

pH = -log [H^+] = -log (1.19 x 10^{-3} M) = 2.92

(3) Calculation of capacitance of Tf plate (boundary wall between the anode and the cathode chambers)

Teflon plate dimensions: Thickness (d) = 0.772 cm, width = 9.50 cm, length = 5.20 cm.

Area (S) = 49.4 – (area of Teflon center chamber hole) = 49.4 – (Π $(3.10/2)^2$) = 41.852 cm^2 = 4.185 x10^{-3} m

C = κ A ε_0/d = 2.1 x 8.85 x 10^{-12} (F/m) x (4.19 x 10^{-3} m^2) /0.772 x10^{-2} m = 1.007 x 10^{-11} F

APPENDIX E

COPYRIGHT PERMISSIONS

Permissions for Figure 1, 2, 3 and 5 were obtained from Bioenergetics: Open Access

Citation: Lee JW (2015) Proton-Electrostatic Localization: Explaining the Bioenergetic Conundrum in Alkalophilic Bacteria. *Bioenergetics* 4:121. doi:10.4172/2167-7662.1000121

Copyright: © 2015 Lee JW. This is an open-access article distributed under the terms of the Creative Commons Attribution License, which permits unrestricted use, distribution, and reproduction in any medium, provided the original author and source are credited.

Permissions for Figure 4 were obtained from Bioenergetics: Open Access

Citation: Lee JW (2012) Proton-Electrostatics Hypothesis for Localized Proton Coupling Bioenergetics. *Bioenergetics* 1:104. doi:10.4172/2167-7662.1000104

Copyright: © 2012 Lee JW. This is an open-access article distributed under the terms of the Creative Commons Attribution License, which permits unrestricted use, distribution, and reproduction in any medium, provided the original author and source are credited.

Permission for Figure 6 was obtained from Rightslink:

This Agreement between Haitham Saeed ("You") and Elsevier ("Elsevier") consists of your license details and the terms and conditions provided by Elsevier and Copyright Clearance Center.

License Number	3917770272786
License date	Jul 28, 2016
Licensed Content Publisher	Elsevier
Licensed Content Publication	Elsevier Books
Licensed Content Title	Bioenergetics
Licensed Content Author	David G. Nicholls,Stuart J. Ferguson
Licensed Content Date	2013
Licensed Content Pages	10
Start Page	3
End Page	12
Type of Use	reuse in a thesis/dissertation
Portion	figures/tables/illustrations
Number of figures/tables/illustrations	1
Format	both print and electronic
Are you the author of this Elsevier chapter?	No
Will you be translating?	No
Original figure numbers	figure 1.3
Title of your thesis/dissertation	BIOENERGETICS: EXPERIMENTAL DEMONSTRATION OF EXCESS PROTONS AND RELATED FEATURES
Expected completion date	Aug 2016
Estimated size (number of pages)	160
Elsevier VAT number	GB 494 6272 12
Requestor Location	Haitham Saeed Norfolk, VA 23508 United States
Total	0.00 USD

Permission for Figure S2 was obtained from Intech open access:

N. L. Sukiman, X. Zhou, N. Birbilis, A.E. Hughes, J. M. C. Mol, S. J. Garcia, X. Zhou and G. E. Thompson (2012). Durability and Corrosion of Aluminium and Its Alloys: Overview, Property Space, Techniques and Developments, Aluminium Alloys - New Trends in Fabrication and Applications, Prof. Zaki Ahmad (Ed.), InTech, DOI: 10.5772/53752. Available from: http://www.intechopen.com/books/aluminium-alloys-new-trends-in-fabrication-and-applications/durability-and-corrosion-of-aluminium-and-its-alloys-overview-property-space-techniques-and-developm

VITA

Haitham A. Saeed

Department of Chemistry and Biochemistry
Old Dominion University
Norfolk, VA 23529
Email:hytham3adel@gmail.com

EDUCATION

PhD, Chemistry and Biochemistry (12/2016)
Old Dominion University ♦ Norfolk, VA

Master of Science, Chemistry (5/2015)
Old Dominion University ♦ Norfolk, VA

Bachelor of Science, Chemistry (2007)
Alexandria University ♦ Alexandria, Egypt

PUBLICATIONS AND PRESENTATIONS

Saeed HA, Lee JW (2016) Experimental Demonstration of Localized Excess Protons at a Water-Membrane Interface and the Effect of other Cations on Their Stability. *The FASEB Journal* 30(1 Supplement):634.631.

Huff MD, Marshall S, **Saeed HA,** Lee JW "Biochar Surface Modification through the use of Ozone Exposure Treatment" *Journal of Environmental Management* (In review).

Saeed H, Lee J (2015) Experimental Demonstration of Localized Excess Protons at a Water-Membrane Interface. *Bioenergetics* 4(127):2.

Saeed HA, Lee JW "The Effect of Cations (Na^+ and K^+) on Localized and Delocalized Excess Protons at a Water-Membrane Interface" (In preparation for *Physical chemistry B*).

"Bioenergetics: Electrostatically Localized Protons." **Saeed, H.** Old Dominion University, Norfolk, VA Jan-2013.

AWARDS
Graduate Student Travel Award from the Division of Student Engagement & Enrollment Services at Old Dominion University, Spring 2016.
Graduate Student Travel Award from American Society for Biochemistry and Molecular Biology (ASBMB) Graduate Travel Award, Spring 2016.